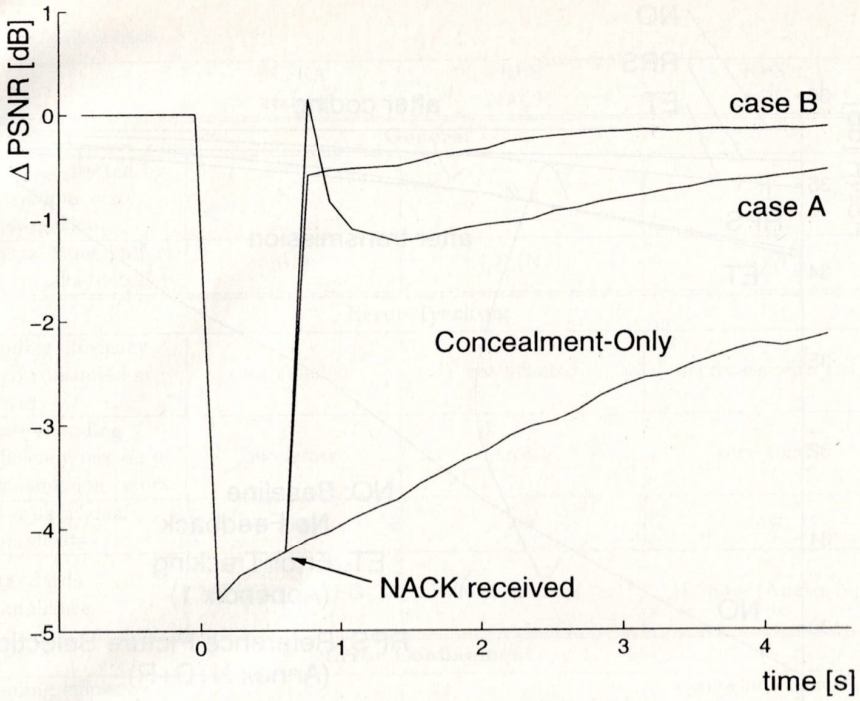


Fig. 11. Loss in PSNR of decoded video signal for inserting I-stream information into a P-stream in a video server application. Case A: I-stream encoded from original sequence. Case B: I-stream encoded from reconstructed P-stream.

advocate the intelligent processing of acknowledgment information by the coding control to adapt the source coder to the channel.

Error tracking allows the encoder to estimate interframe error propagation accurately and adapt its encoding strategy to mitigate the effects of past transmission errors. While error tracking is possible with low complexity, it can be simplified by error confinement techniques, at the expense of compression efficiency. Compression efficiency in case of transmission errors can be improved, however, if multiple previous pictures are kept in an RPS scheme. The simulation of a video transmission over a wireless channel indicates that different channel-adaptive schemes perform very similar but have a significant advantage over schemes that are not feedback-based.

The ITU-T Study Group 16 has adopted feedback-based error control in their effort toward mobile extensions of the successful Recommendation H.263. The first version of H.263 included basic error tracking as described in Section IV-A. The second version, which is informally known as H.263+, was adopted by ITU-T in February 1998. Among many other enhancements, it contains two new options supporting RPS (Annex N) and ISD (Annex R), both discussed in more detail in this article. Future enhancements, e.g., data partitioning, unequal error protection, and reversible variable length coding, are under consideration for future versions of the standard, informally known as H.263++ and H.26L.

Feedback schemes are suitable for interactive, individual communications, but they have inherent limitations outside this domain. They are particularly powerful if the round-trip delay is short. If the round-trip delay increases they become less efficient and ultimately useless. Also, feedback schemes are particularly advantageous for point-to-point communications. For schemes like error tracking that use INTRA updates to stop error propagation, extensions to few users are possible at a loss in performance. In the case of RPS, multipoint communication may even become impossible, because different decoders may require different reference frames. On the other hand, the objection that feedback-based source coding can only be used with real-time encoding is not valid, as shown in Section VI.

While most of the discussed feedback-based error control schemes are pragmatic engineering solutions to a problem at hand, there is an unsolved theoretical problem of fundamental importance underneath. Traditionally, error control has been performed without regard to the contents of the bit stream, e.g., by FEC or transport layer retransmission schemes. Using channel-adaptive source coding for robust transmission is a relatively new idea. In our work, we have learned that well-designed mobile video systems should combine all these techniques, as exemplified in Section V. The tradeoffs in such a system design, however, are not at all well understood, and a general theoretical framework for feedback-based error control is needed.

Appendix
Analysis of Interframe Error Propagation

In the following we derive an analytical model for the distortion that is caused by transmission errors and propa-

gates due to the recursive DPCM structure in the decoder. We are interested in the signal $v[x, y, t]$, which is the frame difference of the reconstructed frames at the encoder and decoder at time step t. We assume that the residual error $u[x, y]$ is introduced at $t = 0$ (after resynchronization and error concealment) such that $v[x, y, 0] = u[x, y]$. In particular, we are interested in the variance $\sigma_v^2[t]$ of the propagated error signal.

A. Two-Dimensional Case

First we consider the two-dimensional case with the discrete spatial and temporal variables x and t. When the decoder is regarded as a linear system $H_t(\omega_x)$ with parameter t, the variance of $v[x, t]$ can be obtained as

$$\sigma_v^2[t] = \frac{1}{2\pi} \int_{-\pi}^{+\pi} |H_t(\omega_x)|^2 \Phi_{uu}(\omega_x)\, d\omega_x \tag{1}$$

where Φ_{uu} is the power spectral density (PSD) of the signal $u[x]$. We assume that a spatial filter $F(\omega_x)$ is applied in each time step. Then the impulse response of the decoder $h_t[x]$ can be defined recursively as $h_t[x] = h_{t-1}[x] * f[x]$, where "$*$" denotes discrete spatial convolution and $f[x]$ is the impulse response of the filter. Based on the central limit theorem we expect $h_t[x]$ to be Gaussian for large t. Therefore, the magnitude of the transfer function of the decoder can be approximated in the base band $|\omega_x| < \pi$ by

$$|\hat{H}_t(\omega_x)| = \exp\left(-\frac{\omega_x^2 t \sigma_f^2}{2}\right) \tag{2}$$

where σ_f^2 is defined as

$$\sigma_f^2 = \sum_x x^2 f[x] - \left(\sum_x x f[x]\right)^2. \tag{3}$$

In the case of linear interpolation, as commonly used for half-pel motion compensation, we obtain $\sigma_f^2 = 1/4$. In addition to the Gaussian approximation for $H_t(\omega_x)$ we also approximate the PSD of the introduced error signal $u[x]$ by

$$\hat{\Phi}_{uu}(\omega_x) = \sigma_u^2 \sqrt{4\pi\sigma_g^2} \exp\left(-\omega_x^2 \sigma_g^2\right) \tag{4}$$

i.e., a Gaussian PSD with the energy σ_u^2. The parameter σ_g^2 determines the shape of the PSD and can be used to match (4) with the true PSD. With the given approximations for $|H_t(\omega_x)|$ and $\Phi_{uu}(\omega_x)$ we can solve (1) directly yielding

$$\hat{\sigma}_v^2[t] = \sigma_u^2 \sqrt{\frac{\sigma_g^2}{\sigma_g^2 + t\sigma_f^2}} = \sigma_u^2 \alpha[t] \tag{5}$$

where $\alpha[t]$ is the power transfer factor after t time steps.

B. Extension to Three-Dimensional Case

In the following we focus on spatial filtering caused by motion compensated prediction with half-pel accuracy and bilinear interpolation. For the extension of the above results to the three-dimensional case with the discrete variables x, y, and t, it has to be considered that individual image regions undergo different filtering operations. For each macroblock a different motion vector is selected, and depending on its sub-pel fractions either no filtering, only horizontal, only vertical, or horizontal and vertical spatial filtering is applied.

In the process of encoding, different combinations of filters are applied to an individual image region after t time steps. The probability that an image region is filtered h times horizontally and v times vertically can be described by a two dimensional probability density function (pdf) $p_t[h, v]$ with parameter t. For $t = 0$ no filter operations have yet been performed, i.e., $p_0[0, 0] = 1$ and otherwise zero. For $t = 1$ the pdf is given by $p_1[0, 0]$, $p_1[1, 0]$, $p_1[0, 1]$, and $p_1[1, 1]$, with all other probabilities being equal to zero. In general, these four probabilities are equal to $1/4$ in moving areas unless specific sub-pel fractions are enforced. For $t > 1$ the pdf can be defined recursively according to

$$p_t[h, v] = p_{t-1}[h, v] * p_1[h, v] \tag{6}$$

under the assumption that the subpel fractions are independent in each frame at a given location. With this assumption and the definition of the power transfer factor $\alpha[\cdot]$ in (5), we obtain the variance of the signal v for the three-dimensional case as

$$\hat{\sigma}_v^2[t] = \sigma_u^2 \sum_h \sum_v \alpha[h]\alpha[v] p_t[h, v]. \tag{7}$$

This equation does not consider INTRA coded macroblocks, which will cause a faster decrease in error energy. If the INTRA mode is selected randomly for n out of N macroblocks per frame, the effect on the variance can be modeled as an additional leakage $\beta = 1 - n/N$ resulting in

$$\hat{\sigma}_v^2[t] = \beta^t \sigma_u^2 \sum_h \sum_v \alpha[h]\alpha[v] p_t[h, v]. \tag{8}$$

REFERENCES

[1] E. Berruto, M. Gudmundson, R. Menolascino, W. Mohr, and M. Pizarroso, "Research activities on UMTS radio interface, network architectures, and planning," *IEEE Commun. Mag.*, vol. 36, pp. 82–95, Feb. 1998.

[2] D. Grillo, Ed., "Special section on third-generation mobile systems in Europe," *IEEE Personal Commun. Mag.*, vol. 5, pp. 5–38, Apr. 1998.

[3] P. Bahl and B. Girod, Eds., "Special section on wireless video," *IEEE Commun. Mag.*, vol. 36, pp. 92–151, June 1998.

[4] S. Lin, D. J. Costello, and M. J. Miller, "Automatic repeat error control schemes," *IEEE Commun. Mag.*, vol. 22, pp. 5–17, Dec. 1984.

[5] A. Heron and N. MacDonald, "Video transmission over a radio link using H.261 and DECT," in *Inst. Elect. Eng. Conf. Publications*, 1992, no. 354, pp. 621–624.

[6] M. Khansari, A. Jalali, E. Dubois, and P. Mermelstein, "Low bit-rate video transmission over fading channels for wireless microcellular systems," *IEEE Trans. Circuits Syst. Video Technol.*, vol. 6, pp. 1–11, Feb. 1996.

[7] P. Cherriman and L. Hanzo, "Programable H.263-based video transceivers for interference-limited environments," *IEEE Trans. Circuits Syst. Video Technol.*, vol. 8, pp. 275–286, June 1998.

[8] Y. Wang and Q.-F. Zhu, "Error control and concealment for video communication: A review," *Proc. IEEE*, vol. 86, pp. 974–997, May 1998.

[9] R. Fischer, P. Mangold, R. M. Pelz, and G. Nitsche, "Combined source and channel coding for very low bitrate mobile visual

communication systems," in *Proc. Int. Picture Coding Symp. (PCS)*, Melbourne, Australia, Mar. 1996, pp. 231–236.
[10] K. Illgner and D. Lappe, "Mobile multimedia communications in a universal telecommunications network," in *Proc. SPIE Conf. Visual Communications and Image Processing (VCIP)*, vol. 2501, Taipei, Taiwan, May 1995, pp. 1034–1043.
[11] B. Girod, U. Horn, and B. Belzer, "Scalable video coding with multiscale motion compensation and unequal error protection," in *Multimedia Communications and Video Coding*, Y. Wang, S. Panwar, S. P. Kim, and H. L. Bertoni, Eds. New York: Plenum, 1996, pp. 475–482.
[12] R. M. Pelz, "An unequal error protected $p \times 8$ kbit/s video transmission for dect," in *Proc. IEEE Vehicular Technology Conf. (VTC)*, Stockholm, Sweden, June 1994, pp. 1020–1024.
[13] R. Talluri, "Error-resilient video coding in the MPEG-4 standard," *IEEE Commun. Mag.*, vol. 36, pp. 112–119, June 1998.
[14] *Video Coding for Low Bitrate Communication*, ITU-T Recommendation H.263, 1996.
[15] A. M. Tekalp, *Digital Video Processing*. Upper Saddle River, NJ: Prentice Hall, 1995.
[16] *Coding of Moving Pictures and Associated Audio for Digital Storage Media at up to About 1.5 Mbit/s (MPEG-1)*, International Standard ISO/IEC 11172-2, 1994.
[17] *Generic Coding of Moving Pictures and Associated Audio, Recommendation H.262 (MPEG-2)*, International Standard ISO/IEC 13818-2, 1995.
[18] *Coding of Audio-Visual Objects: Visual (MPEG-4 Video)*, Committee Draft ISO/IEC 14496-2, Oct. 1997.
[19] *Video Coding for Audiovisual Services at $p \times 64$ kbit/s*, ITU-T Recommendation H.261, 1990.
[20] B. Girod, N. Färber, and E. Steinbach, "Performance of the H.263 video compression standard," *J. VLSI Signal Processing: Syst. Signal, Image, Video Technol.*, vol. 17, pp. 101–111, Nov. 1997.
[21] *Terminal for Low Bitrate Multimedia Communication*, ITU-T Recommendation H.324, 1995.
[22] D. Lindberg, "The H.324 multimedia communication standard," *IEEE Commun. Mag.*, vol. 34, pp. 46–51, Dec. 1996.
[23] *Multiplexing Protocol for Low Bitrate Multimedia Communication*, ITU-T Recommendation H.223, 1996.
[24] N. Färber, B. Girod, and J. Villasenor, "Extensions of ITU-T recommendation H.324 for error-resilient video transmission," *IEEE Commun. Mag.*, vol. 36, pp. 120–128, June 1998.
[25] *Control Protocol for Multimedia Communication*, ITU-T Recommendation H.245, 1996.
[26] *Dual Rate Speech Coder for Multimedia Communications Transmitting at 5.3 and 6.3 kbit/s*, ITU-T Recommendation G.723.1, 1996.
[27] T. J. Ferguson and J. H. Rabinowitz, "Self-synchronizing Huffman codes," *IEEE Trans. Inform. Theory*, vol. IT-30, pp. 687–693, July 1984.
[28] W.-M. Lam and A. R. Reibman, "Self-synchronizing variable length codes for image transmission," in *Proc. IEEE Int. Conf. Acoustics, Speech, and Signal Processing (ICASSP'92)*, vol. 3, San Francisco, CA, Mar. 1992, pp. 477–480.
[29] J. Hagenauer and P. Höher, "A Viterbi algorithm with soft-decision output and its applications," in *Proc. IEEE Global Telecommunications Conf. (GLOBECOM)*, Dallas, TX, Nov. 1989, pp. 47.1.1–47.1.7.
[30] C. Chen, "Error detection and concealment with an unsupervised MPEG2 video decoder," *J. Visual Commun. Image Representation*, vol. 6, no. 3, pp. 265–278, Sept. 1995.
[31] W.-M. Lam and A. R. Reibman, "An error concealment algorithm for images subject to channel errors," *IEEE Trans. Image Processing*, vol. 4, pp. 533–542, May 1995.
[32] J. W. Park, J. W. Kim, and S. U. Lee, "DCT coefficients recovery-based error concealment technique and its application to the MPEG-2 bit stream," *IEEE Trans. Circuits Syst. Video Technol.*, vol. 7, pp. 845–854, Dec. 1997.
[33] J. Wen and J. D. Villasenor, "A class of reversible variable length codes for robust image and video coding," in *Proc. 1997 IEEE Int. Conf. Image Processing (ICIP)*, vol. 2, Santa Barbara, CA, Oct. 1997, pp. 65–68.
[34] J. Wen and J. D. Villasenor, "Reversible variable length codes for efficient and robust image and video coding," in *Proc. IEEE Data Compression Conf. (DCC)*, Mar. 1998, Snowbird, UT, pp. 471–480.
[35] B. Girod, "Bidirectionally decodable streams of prefix code words," *IEEE Commun. Lett.*, to be published.
[36] D. W. Redmill and N. G. Kingsbury, "The EREC: An error-resilient technique for coding variable-length blocks of data," *IEEE Trans. Image Processing*, vol. 5, pp. 565–574, Apr. 1996.
[37] Y. Wang, Q.-F. Zhu, and L. Shaw, "Maximally smooth image recovery in transform coding," *IEEE Trans. Commun.*, vol. 41, pp. 1544–1551, Oct. 1993.
[38] H. Sun and W. Kwok, "Concealment of damaged block transform coded images using projection onto convex sets," *IEEE Trans. Image Processing*, vol. 4, pp. 470–477, Apr. 1995.
[39] H. Sun and J. Zedepski, "Adaptive error concealment algorithm for MPEG compressed video," in *Proc. SPIE Conf. Visual Communications and Image Processing (VCIP)*, vol. 1818, Boston, MA, Nov. 1992, pp. 814–824.
[40] P. Haskell and D. Messerschmitt, "Resynchronization of motion compensated video affected by ATM cell loss," in *Proc. IEEE Int. Conf. Acoustics, Speech, and Signal Processing (ICASSP)*, vol. 3, San Francisco, CA, Mar. 1992, pp. 545–548.
[41] W.-M. Lam, A. R. Reibman, and B. Lin, "Recovery of lost or erroneously received motion vectors," in *Proc. IEEE Int. Conf. Acoustics, Speech, and Signal processing (ICASSP)*, vol. 5, Minneapolis, MN, Apr. 1993, pp. 417–420.
[42] P. Salama, N. Shroff, and E. J. Delp, "A fast suboptimal approach to error concealment in encoded video streams," in *Proc. IEEE Int. Conf. Image Processing (ICIP)*, vol. 2, Santa Barbara, CA, Oct. 1997, pp. 101–104.
[43] N. S. Jayant and P. Noll, *Digital Coding of Waveforms*. Englewood Cliffs, NJ: Prentice Hall, 1984.
[44] B. Girod, "The efficiency of motion-compensating prediction for hybrid coding of video sequences," *IEEE J. Select. Areas Commun.*, vol. SAC-5, pp. 1140–1154, Aug. 1987.
[45] ——, "Motion-compensating prediction with fractional-pel accuracy," *IEEE Trans. Commun.*, vol. 41, pp. 604–612, Apr. 1993.
[46] D. J. Connor, "Techniques for reducing the visibility of transmission errors in digitally encoded video signals," *IEEE Trans. Commun.*, vol. COM-21, pp. 695–706, June 1973.
[47] N. Färber, E. Steinbach, and B. Girod, "Robust H.263 compatible video transmission over wireless channels," in *Proc. Int. Picture Coding Symp. (PCS)*, Melbourne, Australia, Mar. 1996, pp. 575–578.
[48] E. Steinbach, N. Färber, and B. Girod, "Standard compatible extension of H.263 for robust video transmission in mobile environments," *IEEE Trans. Circuits Syst. Video Technol.*, vol. 7, pp. 872–881, Dec. 1997.
[49] B. Girod, N. Färber, and E. Steinbach, "Error-resilient coding for H.263," in *Insights into Mobile Multimedia Communication*, D. Bull, N. Canagarajah, and A. Nix, Eds. New York: Academic, 1999, pp. 445–449.
[50] M. Wada, "Selective recovery of video packet loss using error concealment," *IEEE J. Select. Areas Commun.*, vol. 7, pp. 807–814, June 1989.
[51] S. Fukunaga, T. Nakai, and H. Inoue, "Error resilient video coding by dynamic replacing of reference pictures," in *Proc. IEEE Global Telecommunications Conf. (GLOBECOM)*, London, U.K., Nov. 1996, vol. 3, pp. 1503–1508.
[52] Y. Tomita, T. Kimura, and T. Ichikawa, "Error resilient modified inter-frame coding system for limited reference picture memories," in *Proc. Int. Picture Coding Symp. (PCS)*, Berlin, Germany, Sept. 1997, pp. 743–748.
[53] T. Wiegand, X. Zhang, and B. Girod, "Motion-compensating long-term memory prediction," in *Proc. IEEE Int. Conf. Image Processing (ICIP)*, Santa Barbara, CA, Oct. 1997, pp. 53–56.
[54] T. Wiegand, X. Zhang, and B. Girod, "Long-term memory motion-compensated prediction," *IEEE Trans. Circuits Syst. Video Technol.*, vol. 9, pp. 70–84, Feb. 1999.
[55] B. Girod, T. Wiegand, E. Steinbach, M. Flierl, and X. Zhang, "High-order motion compensation for low bit-rate video," in *Proc. Europ. Signal Processing Conf.*, Rhodes, Greece, Sept. 1998, pp. 253–256.
[56] J. E. Padgett, C. Günther, and T. Hattori, "Overview of wireless personal communications," *IEEE Commun. Mag.*, vol. 33, pp. 28–41, Jan. 1995.
[57] P. Wong and D. Britland, *Mobile Data Communications Systems*. Norwood, MA: Artech House, 1995.
[58] N. Färber, E. Steinbach, and B. Girod, "Robust H.263 compatible transmission for mobile video server access," in *Proc. 1st Int. Workshop Wireless Image/Video Communications*, Lough-

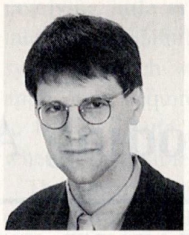
borough, U.K., Sept. 1996, pp. 8–13.
[59] N. Färber and B. Girod, "Robust H.263 compatible video transmission for mobile access to video servers," in *Proc. IEEE Int. Conf. Image Processing (ICIP)*, vol. 2, Santa Barbara, CA, Oct. 1997, pp. 73–76.
[60] B. Girod, N. Färber, and K. Stuhlmüller, "Internet video streaming," in *Multimedia Communications*, F. DeNatale and S. Pupolin, Eds. Berlin, Germany: Springer, 1999, pp. 547–556.



Bernd Girod (Fellow, IEEE) received the M.S. degree in electrical engineering from Georgia Institute of Technology, Atlanta, in 1980 and the Doctoral degree (with highest honors) from the University of Hannover, Germany, in 1987.

He is currently a Chaired Professor of Telecommunications in the Electrical Engineering Department and Head of the Telecommunications Institute I at the University of Erlangen-Nuremberg, Erlangen, Germany. Until 1987, he was a Member of the Research Staff at the Institut für Theoretische Nachrichtentechnik und Informationsverarbeitung, University of Hannover, working on moving image coding, human visual perception, and information theory. In 1988, he joined Massachusetts Institute of Technology, Cambridge, first as a Visiting Scientist with the Research Laboratory of Electronics, then as an Assistant Professor of Media Technology at the Media Laboratory. From 1990 to 1993, he was Professor of Computer Graphics and Technical Director of the Academy of Media Arts in Cologne, Germany, jointly appointed with the Computer Science Section of Cologne University. He was a Visiting Adjunct Professor with the Digital Signal Processing Group at Georgia Institute of Technology in 1993. Since 1997, he has codirected the newly found Telecommunications Laboratory at the University of Erlangen-Nuremberg. He served as the Chairman of the Electrical Engineering Department from 1995 to 1997, and as Director of the Center of Excellence "3-D Image Analysis and Synthesis" since 1995. He was a Visiting Professor with the Information Systems Laboratory of Stanford University, Stanford, CA, in 1997–1998 academic year. His research interests include image communication, video signal compression, human and machine vision, computer graphics and animation, as well as interactive media. For several years, he has served as a consultant to government agencies and companies, with special emphasis on start-up ventures. He has been a founder and Chief Scientist of Vivo Software, Inc., Waltham, MA (1993–1998), Chief Scientist of RealNetworks, Inc., Seattle, WA, (since 1998), and a board member of 8×8, Inc., Santa Clara, CA since 1996.

Dr. Girod was recently elected Fellow of the IEEE "for his contributions to the theory and practice of video communications."



Niko Färber (Member, IEEE) received the Dipl.-Ing. degree in electrical engineering from the Technical University of Munich, Germany, in 1993.

He was then with the Research Laboratory Mannesmann Pilotentwicklung, where he developed system components for satellite based vehicular navigation. In October 1993, he joined the Telecommunications Laboratory at the University of Erlangen-Nuremberg, Erlangen, Germany, where he is now a member of the Image Communication Group. He started his research on robust video transmission as a Visiting Scientist at the Image Processing Laboratory of University of California, Los Angeles, CA. Since then he has published several conference and journal papers on the subject and has contributed successfully to the ITU-T Study Group 16 efforts for robust extensions of the H.263 standard. He has also served as the Publicity Vice Chair for ICASSP-97 in Munich, Germany, and performed research for 8×8, Inc., Santa Clara, CA, and RealNetworks, Inc., Seattle, WA. In cooperation with RealNetworks, he holds a U.S. patent in the area of scalable video coding. His other research interests include combined source and channel coding and software only video coding.

ENGINEERING LIBRARY



APPENDIX SAITO01

screenshot-catalog.libraries.psu.edu-2023.12.05-15_39_10
https://catalog.libraries.psu.edu/catalog/42566942
05.12.2023

MARC View

LEADER 01768nas a2200409 a 4500				
001 42566942				
003 SIRSI				
005 20231114090057.0				
006 m o d				
007 cr n				
008 970512c19939999flubr pss 0 a0eng c				
010				a| sn 97001988
019				a| DO NOT EDIT this 360 MARC RECORD
022				a| 1096-603X l| 1063-5203 y| 1063-5203
035				a| (WaSeSS)ssj0011459
037				b| Academic Press, 6277 Sea Harbor Dr., Orlando, FL 32887-4900
040				a| OH1 b| eng c| OH1 d| NSD d| OCL d| MYG d| OCLCQ d| MYG d| OCLCQ d| MUQ d| OCL d| EEM d| OCLCQ d| OCLCF d| SCB d| OCLCE d| OCLCQ d| DEFHM d| OCLCO d| OCLCA d| VT2 d| OCLCO d| OCLCQ d| UAB d| WaSeSS
042				a| nsdp a| pcc
050	1	4	a| QA403	
082	1	0	a| 515 2| 12	
210	0		a| Appl. comput. harmon. anal. b| (Online)	
222		0	a| Applied and computational harmonic analysis b| (Online)	
245	0	0	a| Applied and computational harmonic analysis h| [electronic resource].	
260			a| Orlando, Fla. : b| Academic Press, c| [©1993]-	
310			a| Bimonthly, b| 1999-	
321			a| Quarterly, b| 1993-1998	
362	0		a| Vol. 1, no. 1 (Dec. 1993)-	
500			a| Title from journal home page (viewed Feb. 28, 2000).	
530			a| Also issued in print.	
538			a| Mode of access: World Wide Web.	
588			a| Latest issue consulted: Vol. 13, issue 3 (Nov. 2002) (ScienceDirect).	
650		0	a| Harmonic analysis v| Periodicals.	
655		0	a| Electronic journals.	
776	0	8	i| Print version: t| Applied and computational harmonic analysis x| 1063-5203 w| (DLC) 94640949 w| (OCoLC)26049297	
856	4	0	u| http://SK8ES4MC2L.search.serialssolutions.com/?V=1.0&L=SK8ES4MC2L&S=JCs&C=APPLANDCOMHA&T=marc	
910			a| CONSER online	
949			a| Electronic resource w| ASIS c| 1 i| 42566942-1001 l| ONLINE m| ONLINE r| Y s| Y t| ONLINE u| 12/2/2023 o| .STAFF. 360 MARC	

PennState

Copyright @2019 The Pennsylvania State University. All rights reserved. Except where otherwise noted, this work is subject to a Creative Commons Attribution 4.0 license. Details and exceptions.

Legal Statements | PSU Hotlines

PENN STATE UNIVERSITY LIBRARIES

Libraries Home (814) 865-6368
Libraries Intranet (Staff Only)
Accessibility Help
Website Feedback
Policies and Guidelines
Staff Directory

screenshot-catalog.libraries.psu.edu-2023.12.05-15_39_10
https://catalog.libraries.psu.edu/catalog/42566942
05.12.2023

Applied and computational harmonic analysis [electronic resource].

Additional Titles: Appl. comput. harmon. anal. (Online)

Published: Orlando, Fla. : Academic Press, [©1993]-

Access Online

serialssolutions.com

Dates of Publication and/or Sequential Designation:
Vol. 1, no. 1 (Dec. 1993)-

Subject(s):
Harmonic analysis—Periodicals

Genre(s):
Electronic journals

ISSN:
1096-603X

Publication Frequency:
Bimonthly, 1999-
Quarterly, 1993-1998

Note:
Title from journal home page (viewed Feb. 28, 2000).

Other Forms:
Also issued in print.

Technical Details:
Mode of access: World Wide Web.

View MARC record | catkey: 42566942

PennState

Copyright @2019 The Pennsylvania State University. All rights reserved. Except where otherwise noted, this work is subject to a Creative Commons Attribution 4.0 license. Details and exceptions.

Legal Statements | PSU Hotlines

PENN STATE UNIVERSITY LIBRARIES

Libraries Home (814) 865-6368
Libraries Intranet (Staff Only)
Accessibility Help
Website Feedback
Policies and Guidelines
Staff Directory

ScienceDirect

Applied and Computational Harmonic Analysis

Supports *open access* • *Open archive*

5.3 CiteScore 2.5 Impact Factor

Submit your article | Guide for authors

Menu Search in this journal

Computational Harmonic Analysis - Part 2

Edited by

- Akram Aldroubi - Vanderbilt University, 1326 Stevenson Center, 13 South Dr., MSC 5766, Building 13/3N17, Nashville, TN 37240
- Charles Chui - Stanford University, Stanford, CA 94305

Volume 20, Issue 1,

Pages 1-158 (January 2006)

Download full issue

Previous vol/issue Next vol/issue

Receive an update when the latest issues in this journal are published

Sign in to set up alerts

Open archive

Editorial Board

Page CO2

View PDF

Editorial *Open archive*

Special issue on computational harmonic analysis, Part II

Akram Aldroubi, Charles Chui

Pages 1-2

FEEDBACK

View PDF

Research article *Open archive*

Robust reprojection methods for the resolution of the Gibbs phenomenon

Anne Gelb, Jared Tanner

Pages 3-25

View PDF Article preview

Research article *Open archive*

Frame expansions for Gabor multipliers

John J. Benedetto, Götz E. Pfander

Pages 26-40

View PDF Article preview

Research article *Open archive*

The polyharmonic local sine transform: A new tool for local image analysis and synthesis without edge effect

Naoki Saito, Jean-François Remy

Pages 41-73

View PDF Article preview

Research article *Open archive*

Affine frame decompositions and shift-invariant spaces

Charles K. Chui, Qiyu Sun

Pages 74-107

View PDF Article preview

Research article *Open archive*

The geometry of sets of parameters of wave packet frames

Wojciech Czaja, Gitta Kutyniok, Darrin Speegle

Pages 108-125

View PDF Article preview

Research article *Open archive*

Second-order Sigma–Delta ($\Sigma\Delta$) quantization of finite frame expansions

John J. Benedetto, Alexander M. Powell, Özgür Yılmaz

Pages 126-148

View PDF Article preview

Correspondence *Open archive*

Some properties of spectral measures

Izabella Łaba, Yang Wang

Pages 149-157

View PDF Article preview

Previous vol/issue Next vol/issue

ISSN: 1063-5203

Copyright © 2023 Elsevier Inc. All rights reserved

ELSEVIER

All content on this site: Copyright © 2023 Elsevier B.V., its licensors, and contributors. All rights are reserved, including those for text and data mining, AI training, and similar technologies. For all open access content, the Creative Commons licensing terms apply.

RELX™

APPENDIX SAITO02

Available online at www.sciencedirect.com
SCIENCE DIRECT®
Appl. Comput. Harmon. Anal. 20 (2006) 41–73
Applied and Computational Harmonic Analysis
www.elsevier.com/locate/acha

The polyharmonic local sine transform: A new tool for local image analysis and synthesis without edge effect ☆

Naoki Saito *, Jean-François Remy [1]

Department of Mathematics, University of California, Davis, CA 95616, USA

Received 9 November 2004; revised 15 January 2005; accepted 25 January 2005

Available online 15 August 2005

Communicated by Charles K. Chui

Abstract

We introduce a new local sine transform that can completely localize image information both in the space domain and in the spatial frequency domain. This transform, which we shall call the *polyharmonic local sine transform* (PHLST), first segments an image into local pieces using the characteristic functions, then decomposes each piece into two components: the *polyharmonic component* and the *residual*. The polyharmonic component is obtained by solving the elliptic boundary value problem associated with the so-called polyharmonic equation (e.g., Laplace's equation, biharmonic equation, etc.) given the boundary values (the pixel values along the boundary created by the characteristic function). Subsequently this component is subtracted from the original local piece to obtain the residual. Since the boundary values of the residual vanish, its Fourier sine series expansion has quickly decaying coefficients. Consequently, PHLST can distinguish *intrinsic* singularities in the data from the artificial discontinuities created by the local windowing. Combining this ability with the quickly decaying coefficients of the residuals, PHLST is also effective for image approximation, which we demonstrate using both synthetic and real images. In addition, we introduce the *polyharmonic local Fourier transform* (PHLFT) by replacing the Fourier sine series above by the complex Fourier series. With a slight sacrifice of the decay rate of the expansion coefficients,

☆ Dedicated to the memory of our fathers, Toshiki Saito and Christian Remy, both of them passed away in 2003. A preliminary version of the material was presented at the SPIE Conference on Wavelets: Applications in Signal and Image Processing X (San Diego, CA, August 2003), and the 2nd International Conference on Computational Harmonic Analysis (Nashville, TN, May 2004).

* Corresponding author.
E-mail addresses: saito@math.ucdavis.edu (N. Saito), jeanfrancois.remy@francetelecom.com (J.-F. Remy).

[1] Present address: France Telecom, Batiment Equinoxe, 4, avenue du 8 mai 1945, 78284 Guyancourt Cedex, France.

1063-5203/$ – see front matter © 2005 Elsevier Inc. All rights reserved.
doi:10.1016/j.acha.2005.01.005

PHLFT allows one to compute local Fourier magnitudes and phases without revealing the edge effect (or Gibbs phenomenon), yet is invertible and useful for various filtering, analysis, and approximation purposes.
© 2005 Elsevier Inc. All rights reserved.

Keywords: Polyharmonic equation; Laplace equation; Local sine transform; Local Fourier transform; Image approximation

1. Introduction

For smooth periodic signals and images, the conventional Fourier series expansion can give us almost everything we need. Simply manipulating the Fourier coefficients, we can shift them, differentiate/integrate them, and filter/attenuate them at our disposal. We can also measure the smoothness class (the Lipschitz/Hölder exponents) of a signal by checking the rate of the decay of its Fourier coefficients, which is related to sparsity since the faster decay of the expansion coefficients leads to a sparser representation. See the standard references on Fourier series [1–3] for the details. It is very important to realize that we lose everything once we have to deal with *nonperiodic* signals. The mismatch caused by the brute-force periodization (i.e., the head and the tail of an input signal do not match) kills every nice property we would have in the case of the smooth periodic signals. For example, the Fourier series expansion coefficients of nonperiodic data decay slowly, i.e., $O(\|\boldsymbol{k}\|^{-1})$, where $\boldsymbol{k}$ is the frequency index vector, and reveal the Gibbs phenomenon. Dealing with nonperiodic signals in a proper manner is of paramount importance in many applications that require analysis of local signal features such as data compression and discrimination. First of all, real signals are often nonperiodic. Second, even if the original signal is perfectly periodic, its locally segmented pieces (for local analysis of such pieces) are almost always not periodic. Thus, what we must do is not to create artificial discontinuities due to the local windowing or the brute-force periodization so that we can focus on the analysis of *intrinsic* discontinuities and singularities in the signal if any. Our goal is to develop a transform that can eliminate the interference of the boundary of a local window imposed by a user with the Fourier analysis of the information inside of such a window as much as possible.

We note that the wavelets/wavelet packets do not really solve this problem because in order to use wavelets or wavelet packets one needs to follow one of the following recipes: (1) periodize a signal and apply the standard wavelets/wavelet packets; or (2) design special wavelets near the boundaries (called "wavelets on the interval") as Cohen, Daubechies, and Vial proposed in [4]; or (3) use the so-called "multiwavelets" developed by Alpert [5], which essentially use segmented orthogonal polynomials. Unfortunately, none of them is really satisfactory for the applications we are interested in. The brute-force periodization (1) again creates the mismatch/discontinuity at the end points, and this generates large wavelet/wavelet packet coefficients. The wavelets on the interval (2) are rather complicated to implement in practice, particularly if one wants to use these in the wavelet packet mode or for images. Finally, the multiwavelets (3) are unfortunately not efficient for oscillatory signals such as textured images.

Coifman and Meyer [6] and Malvar [7,8] independently developed the so-called lapped orthogonal transform (LOT) (also known as local trigonometric transform (LTT) or Malvar wavelets) in an attempt to solve the above problems. However, it turned out that they were not completely satisfactory either, particularly for local signal analysis. The primary reason is the lack of the true localization capability of LTT: it cannot split an input signal into a set of nonoverlapping (disjoint) regions without the influence of their adjacent regions due to its use of the folding operations. (We shall call this a "crosstalk" problem.)

In this respect, the block discrete cosine transform (DCT) used in the JPEG Baseline standard is better because it chops a signal with the characteristic functions, i.e., no influence from the adjacent regions. Chopping the signal with the characteristic functions, however, makes the representation of the signal segment less sparse due to the sharp cutoff at the boundaries of the segment. If the signal segment does not contain any intrinsic discontinuity, the Fourier cosine coefficients decay with the rate $O(\|\boldsymbol{k}\|^{-2})$, which may not be fast enough, although this is better than the complex Fourier series expansion or Fourier sine series expansion, which provide only $O(\|\boldsymbol{k}\|^{-1})$ decay. In the case of LTT, we can tune the width of the overlap in the folding operations to get a faster decay rate, but there is another dilemma. The wider the overlap, the better in terms of sparsity, but the worse in terms of crosstalks (i.e., more statistically dependent). Fang and Séré developed the so-called "multiple folding" local trigonometric transforms (MLTT) [9] to overcome one of the problems. In terms of sparsity, MLTT provides a better representation than the conventional LTT. However, in terms of crosstalk problems, MLTT is definitely worse than LTT because MLTT has wider overlaps, especially in the early stage of the hierarchical split, and that creates more and more crosstalks down in the hierarchy. Villemoes proposed a further improvement in [10], which provides us with a set of local cosines satisfying the uniform bounds on their time–frequency concentrations, which was not possible by LTT and MLTT. However, this method constrains the arrangement of the dyadic blocks: it only allows each block to have adjacent blocks of either the same size or the twice as large or small in each dimension. In other words, around each block, we cannot place its adjacent blocks whose sizes are very different from it. Thus, this method generates a set of blocks similar to the Whitney decomposition [11]. However, this constraint may reduce the efficiency in approximation and compression. In principle, there should not be such a constraint; we should be able to arrange the blocks with different sizes freely. This constraint is due to the specific requirement of the action regions and bell functions which are the essence of the LTT construction.

All these problems essentially boil down to how to treat the boundaries that define those subintervals and regions. To attack this fundamental problem, we developed a new version of the local Fourier transform called "continuous boundary local Fourier transform" (CBLFT) a few years ago [12,13]. CBLFT does not create any crosstalks among the subintervals and any discontinuities in the signal values at the boundaries of those subintervals. For simplicity, let us describe the one-dimensional version of CBLFT here. It first chops a signal into segments with the characteristic functions. Let $I = [0, 1]$ be one of such segments. Then, let us periodize the segmented signal on I, say, $f(x)$ with period 1. Let us assume that f is continuous on I. At this point, the head and tail of f on I does not match, so the periodized signal has two discontinuities at $x = 0$ and $x = 1$. Consider now this periodized function on the extended interval $[-1, 2]$. We add the constant $f(0) - f(1)$ to this periodized signal only over $[-1, 0)$, and similarly $f(1) - f(0)$ only over $(1, 2]$. This makes this extended signal continuous over $[-1, 2]$ although this is not periodic with period 1 anymore. CBLFT then applies the folding operations at $x = 0$ and $x = 1$ and follows the usual LFT recipe of Wickerhauser ([14], [15, Chapter 4]). This procedure guarantees the decay rate of $O(|k|^{-2})$, generates no crosstalk since it only uses the signal information over I, and moreover, allows us to use the complex exponentials instead of real-valued cosine functions, which may be advantageous for certain applications such as computing locally analytic signals. However, CBLFT is not yet satisfactory: it does not deal with discontinuities in the derivatives at $x = 0$ and 1 so that the speed of the decay of the expansion coefficients is not fast enough. Moreover, due to its use of the folding operators, CBLFT is not too effective for analyzing very short segments of a signal.

We shall propose the *polyharmonic local sine transform* (PHLST) in the next section, which is a fundamentally better transform in the sense that it does not suffer from any of these problems compared to

the other methods mentioned above. It can also be generalized easily and hierarchically to higher dimensions. In essence, PHLST first segments an image into local pieces using the characteristic functions, then decomposes each piece into two components: the *polyharmonic component* and the *residual*. The polyharmonic component is obtained by solving the elliptic boundary value problem associated with the so-called polyharmonic equation (e.g., Laplace's equation, biharmonic equation, etc.) given the boundary values (the pixel values along the boundary created by the characteristic function) possibly with the estimates of normal derivatives at the boundary. Subsequently, this component is subtracted from the original local piece to obtain the residual. Because the boundary values of the residual (possibly with their normal derivatives) vanish, its Fourier sine series expansion has quickly decaying coefficients i.e., $O(\|\boldsymbol{k}\|^{-3})$ or faster. Using this transform, we can distinguish *intrinsic* singularities in the data from the artificial discontinuities created by the local windowing using the characteristic functions.

The organization of this paper is as follows. We describe the basic idea of PHLST in the next section. Section 3 describes important practical information, in particular, implementation issues. Section 4 reports the results of our simple image approximation experiments using DCT, local cosine transform (LCT; one version of LTT), discrete wavelet transform (DWT), and PHLST. In Section 5, we introduce the polyharmonic local Fourier transform (PHLFT) by replacing the Fourier sine series expansion of the residuals by the ordinary Fourier series expansion using the complex exponentials. With a slight sacrifice in the decay rate of the expansion coefficients, we gain many nice properties of the complex Fourier series such as the ability to represent local image patches by its Fourier magnitudes and phases without suffering from the Gibbs phenomenon. Finally, we conclude this paper in Section 6 where we discuss the open issues and our future plans, as well as the relation of PHLST to the previous works done by other scientists.

2. Our proposed method: polyharmonic local sine transform

Instead of constructing an orthonormal basis, we first segment a signal $f(\boldsymbol{x})$, $\boldsymbol{x} \in \mathbb{R}^d$ into local pieces using the characteristic functions, then split each piece into two components: the polyharmonic component and the residual. Let $\Omega \in \mathbb{R}^d$ be the overall domain where the signal is supported, and let $\bar{\Omega} = \bigcup_{j=1}^{J} \bar{\Omega}_j$ be a decomposition of the domain Ω into a set of disjoint subdomains $\{\Omega_j\}$. Note that Ω_j's are open and disjoint whereas $\bar{\Omega}_j$'s are closed and may share the boundaries. Let f_j be the restriction of f to $\bar{\Omega}_j$, i.e., $f_j = \chi_{\bar{\Omega}_j} f$. Let us now consider the local decomposition $f_j = u_j + v_j$ on Ω_j. We shall call u_j the *polyharmonic component* of f_j and v_j the *residual*. Let Δ be the Laplace operator in $\mathbb{R}^d$. Then the polyharmonic component is obtained by solving the following polyharmonic equation:

$$\Delta^m u_j = 0 \quad \text{in } \Omega_j, \quad m = 1, 2, \ldots, \tag{1}$$

with given boundary values and normal derivatives

$$\frac{\partial^{q_\ell} u_j}{\partial \nu^{q_\ell}} = \frac{\partial^{q_\ell} f}{\partial \nu^{q_\ell}} \quad \text{on } \partial\Omega_j, \quad \ell = 0, \ldots, m-1, \tag{2}$$

where q_ℓ is the order of the normal derivatives yet to be specified. The parameter q_0 is normally set to 0, which means that $u_j = f$ on the boundary $\partial\Omega_j$. These boundary conditions enforce the function values and the normal derivatives of orders $q_1, \ldots, q_{m-1}$ of the solution u_j along the boundary $\partial\Omega_j$ to match those of the original signal f over there. If the Ω_j's are all rectangles (of possibly different sizes),

then we take $q_\ell = 2\ell$, i.e., the *even order* normal derivatives. It is not necessary to match the odd order normal derivatives for the rectangular domain case because the Fourier sine series of v_j is equivalent to the Fourier series expansion of the extension of v_j by odd reflection with respect to the boundary $\partial\Omega_j$ and *the continuity of the odd order normal derivatives* (*up to order* $2m-1$) *is automatically guaranteed*. For $m = 1$, Eq. (1) becomes the following familiar form:

$$\begin{cases} \Delta u_j = 0 & \text{in } \Omega_j, \\ u_j = f & \text{on } \partial\Omega_j, \end{cases} \tag{3}$$

which is the *Laplace equation with the Dirichlet boundary condition*. For $m = 2$, we have the following *biharmonic equation with the mixed boundary condition*:

$$\begin{cases} \Delta^2 u_j = 0 & \text{in } \Omega_j, \\ u_j = f,\ \frac{\partial^\ell u_j}{\partial \nu^\ell} = \frac{\partial^\ell f}{\partial \nu^\ell} & \text{on } \partial\Omega_j, \end{cases} \tag{4}$$

where $\ell = 1$ or 2 depending on the shape of Ω_j. For the rectangular-shaped Ω_j, we take $\ell = 2$ as explained above. Note that in 1D ($d = 1$), the solution of (3) is simply a straight line connecting two boundary points of an interval $\bar{\Omega}_j$ whereas that of (4) is a cubic polynomial. However, in higher dimensions ($d \geqslant 2$), the solutions of (3), (4), and more generally (1) with (2) are not a tensor product of algebraic polynomials in general.

Subtracting such u_j from f_j gives us the residual $v_j = f_j - u_j$ satisfying:

$$\frac{\partial^{q_\ell} v_j}{\partial \nu^{q_\ell}} = 0 \quad \text{on } \partial\Omega_j, \quad \ell = 0, \ldots, m-1. \tag{5}$$

Since the values and the normal derivatives of v_j on $\partial\Omega_j$ vanish, its Fourier sine expansion coefficients decay rapidly, i.e., $O(\|\boldsymbol{k}\|^{-2m-1})$, if there is no other intrinsic singularity in Ω_j. In fact, we have the following theorem.

Theorem 1. *Let Ω_j be a bounded rectangular domain in $\mathbb{R}^d$, and let $f_j \in C^{2m}(\bar{\Omega}_j)$, but nonperiodic. Assume further that $(\partial/\partial x_i)^{2m+1} f,\ i = 1, \ldots, d$, exist and are of bounded variation. Furthermore, let $f_j = u_j + v_j$ be the PHLST representation, i.e., the polyharmonic component u_j is the solution of the polyharmonic equation* (1) *of degree m with the boundary condition* (2) *with $q_\ell = 2\ell,\ \ell = 0, 1, \ldots, m-1$, and $v_j = f_j - u_j$ is the residual component. Then, the Fourier sine coefficient $b_{\boldsymbol{k}}$ of the residual v_j is of $O(\|\boldsymbol{k}\|^{-2m-1})$ for all $\boldsymbol{k} \neq \boldsymbol{0}$, where $\boldsymbol{k} = (k_1, \ldots, k_d) \in \mathbb{Z}_+^d$, and $\|\boldsymbol{k}\|$ is the usual Euclidean (i.e., ℓ^2) norm of $\boldsymbol{k}$.*

The proof of this theorem is in Appendix A. Note that if we employ the straightforward Fourier series expansion of nonperiodic f_j by brute-force periodization, the decay rate becomes only $O(\|\boldsymbol{k}\|^{-1})$ even if $f_j \in C^{2m}(\bar{\Omega}_j)$. If we use the Fourier cosine series expansion of f_j, we can get $O(\|\boldsymbol{k}\|^{-2})$.

We call this new way of decomposing a function f into a set of functions $\{f_j = u_j + v_j\}_{j=1}^J$ the *polyharmonic local sine transform* (PHLST) of polyharmonicity m. For $m = 1$ and 2, we use the special abbreviations, LLST (Laplace LST) and BLST (biharmonic LST).

Remark 2. The polyharmonic component u_j is smooth particularly in the middle of the region Ω_j and as $\boldsymbol{x}$ approaches the boundary $\partial\Omega_j$, $u_j(\boldsymbol{x})$ approaches $f(\boldsymbol{x})$. In fact, u_j is also the minimizer of the following optimization problem (see, e.g., [16]):

$$\min_{u\in H^m(\Omega_j)} \sum_{|\alpha|=m} \binom{m}{\alpha} \int_{\Omega_j} \left|D^\alpha u\right|^2 \mathrm{d}\boldsymbol{x} \quad \text{subject to the boundary condition (2)}, \tag{6}$$

where $H^m(\Omega_j)$ is an L^2-Sobolev space of order m over Ω_j, $\alpha = (\alpha_1, \ldots, \alpha_d)$ is a multi-index of a d-dimensional variable with the following definitions: $|\alpha| = \alpha_1 + \cdots + \alpha_d$, $\binom{m}{\alpha} = m!/(\alpha_1! \cdots \alpha_d!)$, and $D^\alpha = \partial_1^{\alpha_1} \cdots \partial_d^{\alpha_d}$, where $\partial_i = \partial/\partial x_i$. This means that the polyharmonic component minimizes the *roughness* measured by the objective function in (6) while satisfying the boundary condition (2). The larger the polyharmonicity m is, the smoother the solution u_j gets.

Remark 3. Because the u_j component becomes very smooth away from the boundary and only carries the low frequency information in the middle of the region as discussed in Remark 2, the frequency content of the v_j component is close to that of f_j, particularly, around the mid to higher frequency band, where textures are well represented. Therefore, the v_j component retains the original texture information almost intact and is more suitable for texture analysis than the original image patch f_j.

Remark 4. Our PHLST belongs to a larger class of models, to which Yves Meyer refers as the $u + v$ models [17]. In a $u + v$ model, the original data f is assumed to be a sum of the two components u and v. The first component u is aimed at modeling the objects present in the data (often they are assumed to be in some specific function spaces such as the Besov spaces or the functions of bounded variation BV) whereas the v term is responsible for texture and noise in the data. In our PHLST model, one can also interpret u as "trend" and v as "fluctuation" of the original data f, which are commonly-used terms in the wavelet literature [18]. Yet another interpretation of this decomposition is the following: the polyharmonic component u represents the part of f that is *predictable from the boundary data only*, whereas the residual v represents the *unpredictable* part of f.

3. Practical aspects of PHLST

If Ω and Ω_j's are rectangular regions in $\mathbb{R}^d$ and the functions defined over there are sampled on a regular lattice (which is the most efficient case in terms of numerical implementation), we can employ the discrete sine transform (DST) based on the FFT algorithm to rapidly compute both the polyharmonic components and the Fourier sine series expansion of the residual components. In particular, we use the algorithm proposed by Averbuch and co-workers [19,20], which seems to us the most natural and practical Laplace/Poisson equation solver on rectangles. This ABIV method gives us more accurate solutions (in fact an arbitrary order of accuracy in principle) than those based on the finite difference (FD) approximation of the Laplace operator followed by FFT, which only gives us the solutions with accuracy $O(h^2)$ or $O(h^4)$, depending on the 5-point FD scheme or the modified 9-point FD scheme is used ([21, Section 7.1], [22, Chapter 12]) (h is, of course, the grid spacing here). Yet, the computational cost of the ABIV algorithm is still $O(N^d \log N)$, where N is the number of grid points in each direction of a rectangular domain. We also note that we use the $(d-1)$-dimensional version of PHLST to represent the

boundary function $f(\boldsymbol{x})$ for $\boldsymbol{x} \in \partial\Omega_j$, which can be recursively computed starting from the 1D version. To describe the ABIV method more simply and precisely, let us now consider the LLST decomposition $f(x, y) = u(x, y) + v(x, y)$ on the unit square $\bar{\Omega} = [0, 1]^2 \subset \mathbb{R}^2$. There are several options in the ABIV method, but the simplest and most practical version to compute the solution to (3) that does not require any derivative estimate can be written as follows.

$$u(x, y) = p(x, y) + \sum_{k \geqslant 1} \left\{ b_k^{(1)} h_k(x, 1-y) + b_k^{(2)} h_k(y, 1-x) + b_k^{(3)} h_k(x, y) + b_k^{(4)} h_k(y, x) \right\}, \tag{7}$$

where $p(x, y)$ is a harmonic polynomial that agrees with $f(x, y)$ at the four corner points of the domain, and its simplest form is:

$$p(x, y) = a_3 xy + a_2 x + a_1 y + a_0, \tag{8}$$

where the parameters a_j's can be easily and uniquely determined using the function values at the four corners. The function $h_k(x, y)$ is defined as

$$h_k(x, y) \stackrel{\Delta}{=} \sin(\pi k x) \frac{\sinh(\pi k y)}{\sinh(\pi k)}, \tag{9}$$

and $b_k^{(j)}$, $j = 1, 2, 3, 4$, are the kth 1D Fourier sine coefficients of the boundary functions $f(x, 0) - p(x, 0)$, $f(0, y) - p(0, y)$, $f(x, 1) - p(x, 1)$, and $f(1, y) - p(1, y)$, respectively, where $0 \leqslant x \leqslant 1$, $0 \leqslant y \leqslant 1$. One can easily verify that each sum involving h_k functions in (7) is a solution of the Laplace equation with the nonzero boundary values on only one side of the square. For example, $u^{(1)}(x, y) = \sum_{k \geqslant 1} b_k^{(1)} h_k(x, 1-y)$ satisfies the boundary condition:

$$u^{(1)}(x, 0) = f(x, 0) - p(x, 0), \quad u^{(1)}(x, 1) = 0, \quad u^{(1)}(0, y) = 0, \quad u^{(1)}(1, y) = 0.$$

One the other hand, the v component can be written as

$$v(x, y) = \sum_{m \geqslant 1} \sum_{n \geqslant 1} \beta_{mn} \sin(m\pi x) \sin(n\pi y), \tag{10}$$

where β_{mn} is the 2D Fourier sine coefficients of $v(x, y) = f(x, y) - u(x, y)$. We also note that we use the gridpoint formulation rather than the midpoint formulation for our discretization. Therefore, we use DST-I rather than the DST-II/III combination in this paper. See, e.g., [15, Chapter 4], [23] for the details of gridpoint vs midpoint formulations.

Let us show a simple example of the effect of removing the polyharmonic component. Figure 1 demonstrates this. We first use the global version of LLST, i.e., no further split of the image. One may wonder what is the difference between the original and the residual v component in this case because they look very similar. We would like to point out that the v component is displayed in a shifted dynamic range (i.e., $[-127, 127]$ instead of $[0, 255]$) to see the details. Moreover, if we examine them carefully, we can observe that the overall shading is gone in the v component. The bottom row of Fig. 1 clarifies this by displaying them as 3D perspective plots.

Figure 2 shows the results of LLST decomposition by splitting the original into a set of homogeneous square regions each of which has 17×17 pixels.

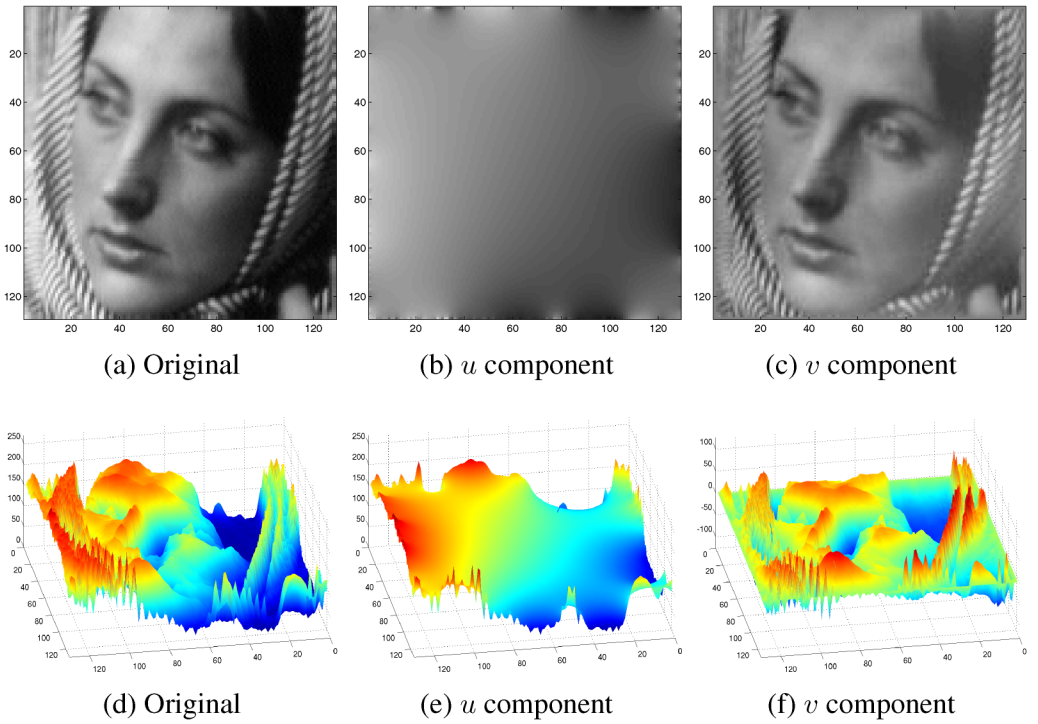


Fig. 1. The global version of LLST applied to the face part (129×129 pixels) of the Barbara image. Note that the display dynamic range of (a) and (b) are set to $[0, 255]$ whereas that of (c) is set to $[-127, 127]$. Figures (d)–(f) are the 3D perspective plots of the top row. It is easier to see in (f) that the overall shading of the face is removed in the v component.

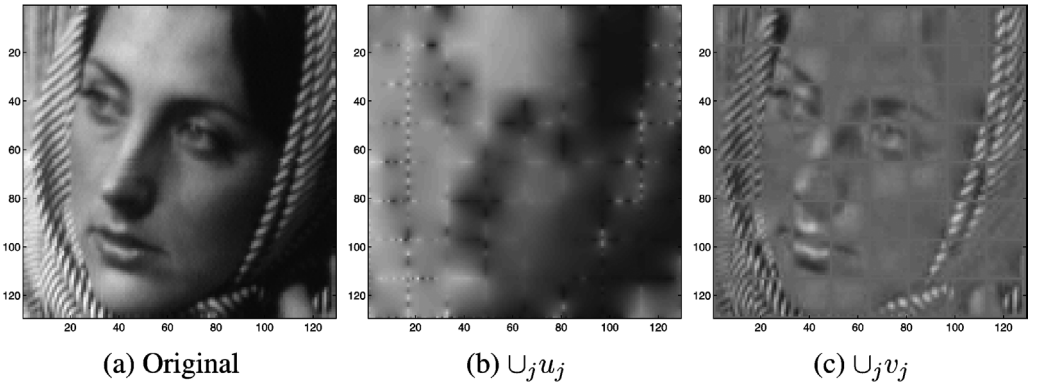


Fig. 2. The hierarchical LLST decomposition of the Barbara face image: (a) Original image; (b) the union of the u_j components $\bigcup_j u_j$ where each $\bar{\Omega}_j$ is a square of 17×17 pixels; (c) the union of the v_j components $\bigcup_j v_j$.

4. Image approximation using PHLST

Since PHLST can represent smooth regions of an image very efficiently (i.e., faster decay of the DST coefficients of the residual components), image approximation and compression are immediate

and important applications of PHLST. In the field of image approximation, a great theoretical progress and understanding has been made. Nonlinear approximation of functions belonging to various function spaces, in particular, using the orthonormal wavelet bases or splines are now well understood [24]. However, as we shall discuss in Section 6.1.3, obtaining precise nonlinear approximation results for PHLST remains elusive. Therefore, in this paper, we shall report the results of our numerical experiments using PHLST and demonstrate its superiority over the other representative transforms such as DCT, LCT, and wavelets, which will hopefully illuminate our theoretical investigation.

In the rest of the paper, the dimension is set to $d = 2$, and the domain Ω and its subdomains Ω_j are all rectangles. We shall also limit our investigation to the specific version of PHLST with $m = 1$, i.e., LLST, rather than the PHLST of a higher polyharmonicity. We shall report the other settings (e.g., on more general domains, PHLST with $m > 1$, and investigation on PHLST-based image compression with quantization) at a later date. In our experiments, we shall examine how the intrinsic discontinuities and the smoothness and oscillation of the data away from the discontinuities affect the approximation performance.

Let us first describe the details of the LLST representation of a given image for a given split of the domain $\bar{\Omega} = \bigcup_j \bar{\Omega}_j$. In each subdomain Ω_j, we have an image patch f_j, which is decomposed into u_j and v_j components. Recall that each harmonic component u_j can be completely represented by the boundary values $f_j|_{\partial\Omega_j}$ that in turn can be represented by 1D version of LLST. As (7) shows, the u_j can be further decomposed into the harmonic polynomial p_j (8) and the rest using the h_k functions (9). The p_j component can be completely represented by (or recovered from) the four corner values of $\bar{\Omega}_j$. The rest of the u_j component is completely determined by 1D DST coefficients of the four boundary functions. Therefore, we represent the u_j component as the four corner values and the four sets of the 1D DST coefficients of the boundary values. We note that these four corner points and four sets of the 1D DST coefficients are shared by the adjacent blocks, so we should not duplicate them for storage efficiency. For example, if we split an image of size $(2^M + 1) \times (2^N + 1)$ pixels into a set of homogeneous blocks of size $(2^m + 1) \times (2^n + 1)$ pixels, then the total number of the corner points without duplication is $(2^{M-m} + 1) \times (2^{N-n} + 1)$. Another thing to note here is about the values of these corner points. The range of the corner pixel values are between 0 and 255 for a typical 8 bit gray scale image, which is quite different from that of the DST coefficients. This difference should be taken into account when the image compression including quantization is considered. Once the u_j component is taken care of, the v_j component is simply obtained by 2D DST (more precisely, 2D DST-I) in a straightforward manner.

As for the performance comparison, we compare LLST with: (1) the block DCT-II (abbreviated as "BDCT" below), which is used in the JPEG Baseline standard [23]; (2) LCT, which uses DCT-IV after the folding operations [15, Chapter 4]; and (3) C6 discrete wavelet transform (C6DWT), which is based on the 'Coiflet' 6-tap conjugate quadrature filter [25], [26, Chapter 8]. Note that the C6 wavelet functions has two vanishing moments, which means that any locally linear part of an input image generates negligible coefficients. Thus, we believe that it is a fair comparison with LLST since the u_j components of LLST also take care of locally linear parts.

Note also that if the size of an original image is $(2^M + 1) \times (2^N + 1)$, which is suitable for LLST, then we remove its last column and row to make it suitable for BDCT, LCT, and C6DWT. On the other hand, if an original image is of size $2^M \times 2^N$ pixels, then we duplicate the last column and row to make it suitable for LLST. Note also that the block size $(2^m + 1) \times (2^n + 1)$ pixels used for LLST correspond to $2^m \times 2^n$ pixels for BDCT and LCT.

Now let us describe our approximation strategy. We first retain all the corner pixel values for LLST, all the "DC" components for BDCT and LCT, and all the coefficients of the coarsest scaling function (i.e., the lowest frequency band) for C6DWT. Starting from those number of retained coefficients, we do the "nonlinear approximation," i.e., we select the coefficient with the largest energy among all the coefficients not yet used, add it to the retained set of coefficients, reconstruct an approximation from this set, and evaluate its quality of approximation. We repeat this process until we use up all the coefficients. The quality of approximation in this paper is measured by *PSNR* (or *peak signal-to-noise ratio*), which is normally considered as a better metric for evaluating image quality than SNR (signal-to-noise ratio) and defined as

$$20\log_{10}\Big(\max_{\boldsymbol{x}\in\bar{\Omega}}\big|f(\boldsymbol{x})\big|\big/\mathrm{RMSE}\Big),$$

where RMSE (the root mean square error) is the absolute ℓ^2 error between the original and the approximation divided by the square root of the number of pixels. The unit of PSNR is decibel (dB). Thus, PSNR $= 0$ dB corresponds to RMSE $= \max|f(\boldsymbol{x})|$, and PSNR $= 350$ dB corresponds to RMSE $\approx 10^{-17.5}\times\max|f(\boldsymbol{x})|$, which is essentially the machine precision, i.e., no error in practice. In our experiments, PSNR is computed as a function of the ratio R of the number of the retained coefficients to the total number of pixels of the input image.

4.1. Approximation of synthetic smooth images with and without discontinuity

In order to demonstrate the power of LLST, we shall conduct simple approximation experiments using synthetic data. We shall first examine the effect of intrinsic discontinuity in otherwise smooth data to the transforms under consideration.

4.1.1. A case without discontinuity

We first synthesize the 2D Gaussian function $\exp(-(x+1/3)^2-(y+1/3)^2)$ over the region $\bar{\Omega}=[-1,1]\times[-1,1]$, which does not have any intrinsic discontinuity. We sample this function with rate $\Delta x=\Delta y=1/128$, yielding discrete data of 257×257 pixels. If $\Omega=\mathbb{R}^2$, then this Gaussian function is in $C^\infty(\Omega)$. However, once we restrict this on a finite rectangle such as $[-1,1]\times[-1,1]$, its periodic extension is not in $C^\infty(\mathbb{R}^2)$ anymore, in fact, not even in $C(\mathbb{R}^2)$! This is due to the domain boundary we discussed in Introduction and by all means we need to remove this boundary effect in order to efficiently represent and characterize this dataset. On the other hand, we really do not need to split Ω into a set of smaller segments in this case since there is no intrinsic discontinuities in the data and it is homogeneous and isotropic. In order to confirm this, we also segment Ω into a set of homogeneous blocks of $2^j\times 2^j$ pixels for BDCT and LCT and $(2^j+1)\times(2^j+1)$ pixels for LLST where $j=7,6,5$, and check their approximation performance. We can view them as the quadtree-structured splits with the original image as the root node and those homogeneous blocks as the leaf nodes. Then, the maximum depth (or level) J of the quadtree is $J=1,2,3$, respectively. Note that $J=0$ implies no split of the domain Ω. For C6DWT, to match the number of the coefficients in the lowest frequency band with that of the DC components in the BDCT/LCT representations, the maximum depth of decomposition needs to be $J=7,6,5$, respectively. In general, for an image of $2^N\times 2^N$ pixels, the maximum depth J in the BDCT/LCT tree corresponds to the maximum depth $N-J$ in the wavelet tree.

Figure 3 shows these approximation results. As we have expected, LLST with no segmentation ($J=0$) outperforms all the other transforms with various depths of decomposition except that it is defeated

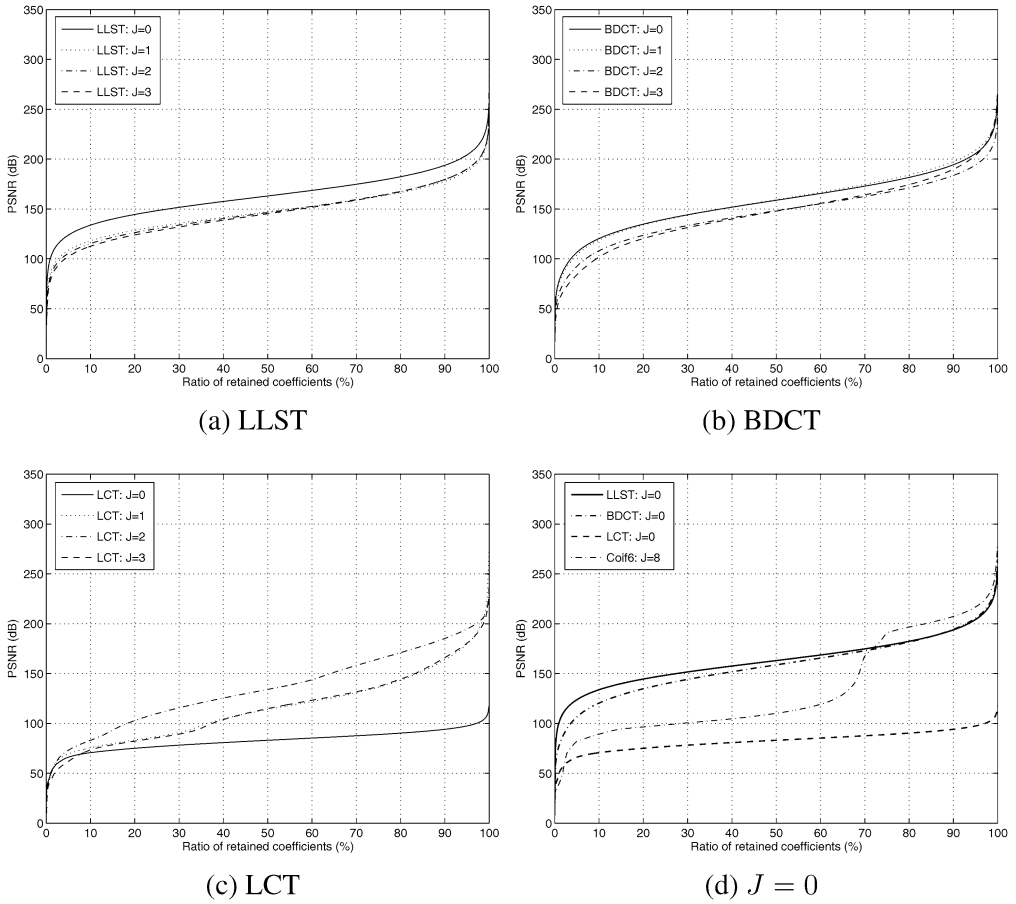


Fig. 3. Quality of approximation of the 2D Gaussian data measured by PSNR values. The index J represents the depth of the quadtree decomposition. Note that $J = 0$ means no splitting (i.e., the original domain is used).

by C6DWT if the ratio of the retained coefficients R is higher than about 72%. However, such a high ratio range is of no interest for the purpose of efficient approximation. We also observe that the more we subdivide the original domain, the more the performance of LLST and that of BDCT degrade. This superior performance of LLST with $J = 0$ over BDCT with $J = 0$ demonstrates the importance of having the coefficients decaying with $O(\|\boldsymbol{k}\|^{-3})$ rather than $O(\|\boldsymbol{k}\|^{-2})$.

The behavior of LCT is markedly different from that of LLST and BDCT. This is due to the folding operations and the use of DCT-IV as the underlying base transform in LCT [15, Chapter 4]. In essence, the folding operations split the data on the original domain into blocks smoothly using the appropriate bell function so that the data on each block become suitable for DCT-IV. In fact, the folding operations make the data locally even at the upper and left boundary and locally odd at the lower and right boundary of each block since each DCT-IV basis function behaves like cosines at the upper and left boundary and like sines at the lower and right boundary. These folding operations, however, need the data outside of the blocks. This means that we have a trouble at the blocks that share the boundary of the original domain because we do not know the data outside of the original domain. In particular, we cannot apply

the folding operation with $J = 0$, unless we can estimate a smooth extension of the data from the original domain. Note also that extending the input data by the brute-force periodization and then performing the folding do not solve the problem at all: such an operation does not match the polarity of the data at the domain boundary to what DCT-IV prefers. For simplicity, we use the so-called "free" boundary condition in our experiments. We do not assume any data outside of the domain, and do not perform any folding at the boundaries of the original domain. Therefore, LCT with $J = 0$ is equivalent to applying DCT-IV to the original image. Consequently, it senses the discontinuity at the lower and right boundaries unlike the simple DCT-II that views the data outside as the even-reflected version of the data inside. Thus, the LCT coefficients for $J = 0$ only decay as $O(\|\boldsymbol{k}\|^{-1})$, and that is the reason why LCT with $J = 0$ performs poorly. This is clearly worse than simply using DCT-II, and that is the main reason why DCT-IV is not used in the JPEG Baseline standard. On the other hand, if we use the smaller blocks such as the $J = 3$ case, then the influence of the boundary effect of the original domain is localized to the out-most blocks sharing the boundary of the original domain. However, the width of the bell function gets too short and the decay rate of the LCT coefficients becomes slow. That is the reason why LCT with $J = 2$ performs better than that with $J = 3$. See also [12,13] for the details of the boundary effects due to the folding operations.

As for the performance of C6DWT, we only plot $J = 8$ case in Fig. 3 (d) because the PSNR curves for the other values $J = 7, 6, 5$ are almost identical to that for $J = 8$ with very small differences in the low ratio region. This is due to the fact that the higher frequency finer scale coefficients are identical for these values of J. C6DWT performs reasonable for this dataset, but it is beaten by LLST and BDCT except at the very high ratios such as the region of $R \geqslant 72\%$ as mentioned above. Note also that this implementation of C6DWT assumes the periodic boundary condition at the domain boundary. Therefore, it too views the domain boundary as discontinuity in general.

Remark 5. The above observations on LCT and C6DWT suggest that removing the u component for $J = 0$ from the original data would help these transforms. In fact, if we remove the boundary by subtracting the u component, the performance of both LCT and C6DWT improves. In particular, for wavelets, this can be an alternative to "wavelets on the intervals" [4] provided that the pixels along the domain boundary (or their transformed version) are retained.

4.1.2. A case with discontinuity

Let us now introduce simple discontinuity in this dataset, and examine how the approximation performance changes by that. We multiply a scalar factor 2 to the circular region satisfying $\{(x, y) \mid (x + 1/3)^2 + (y + 1/3)^2 < 0.2\} \subset \Omega$.

Figure 4 shows these approximation results. Due to the discontinuity, the global methods ($J = 0$) are now inferior to the segmented cases for LLST, BDCT, and LCT. In fact, from Fig. 4 (a) and (b), we can see that the performance steadily improves as J increases. This is obvious since the discontinuity affects all the coefficients for $J = 0$ and makes their decay as $O(\|\boldsymbol{k}\|^{-1})$. On the other hand, for $J = 3$, the effect of the discontinuity is localized to the blocks where the discontinuity passes through. Note that in the continuum, whether covering the discontinuity by a large block or by a set of small or narrow blocks does not matter since the discontinuity results in the countable number of slowly decaying coefficients anyway. However, we are dealing with the finite dimensional sampled data. Consequently, localizing the discontinuity with a set of small size blocks reduces the number of slowly decaying coefficients.

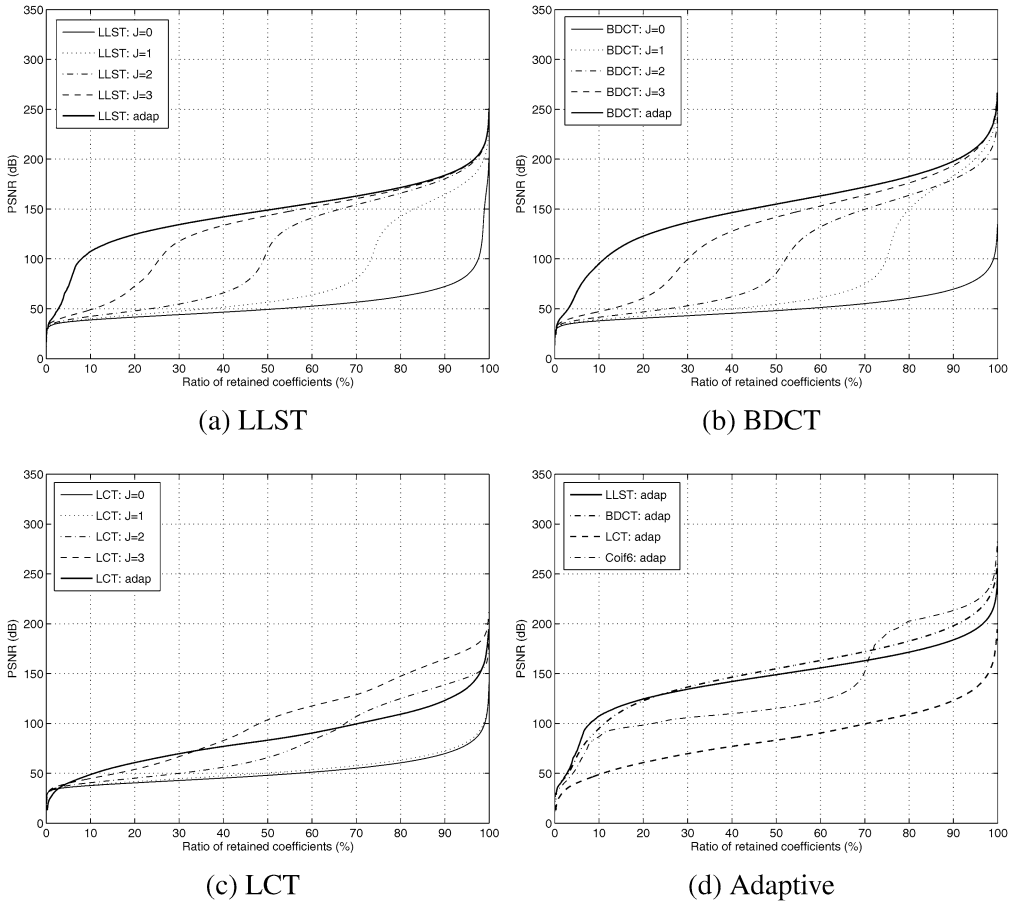


Fig. 4. Quality of approximation of the Gaussian data with circular discontinuity measured by PSNR values.

This observation leads us to the following expectation: grabbing smooth regions by largest possible blocks and using narrow blocks around the singularity should give us more efficient approximation than splitting the domain into a set of homogeneous blocks. There is no need to divide a smooth region into a set of smaller blocks, and in fact, that is wasteful due to the storage of the corner and boundary information in each block as demonstrated earlier. Therefore, we examine the power of the adaptive split of the domain honoring the geometry of (or the singularity in) the data. Figure 5 shows such an adaptive segmentation: smaller blocks around the singularity and progressively larger blocks away from the singularity, which is somewhat similar to the Whitney decomposition [11]. This particular segmentation has been done manually using our Java-based "Interactive Picture Partition" (IPP) program developed by Gary Zhong. We are currently developing an automatic adaptive segmentation algorithm using PHLST, and will report the details at a later date. Figure 4 also shows the performance of the approximations based on this adaptive segmentation. Of course, we use the same segmentation for LLST, BDCT, and LCT. As for adaptive version of C6DWT, we compute the so-called *best sparsifying basis* (BSB) via ℓ^1 norm minimization [27,28] from the C6 wavelet packet tree, and approximate by sorting out the BSB coefficients. However, our numerical computation shows that the BSB for this dataset turns out to be the

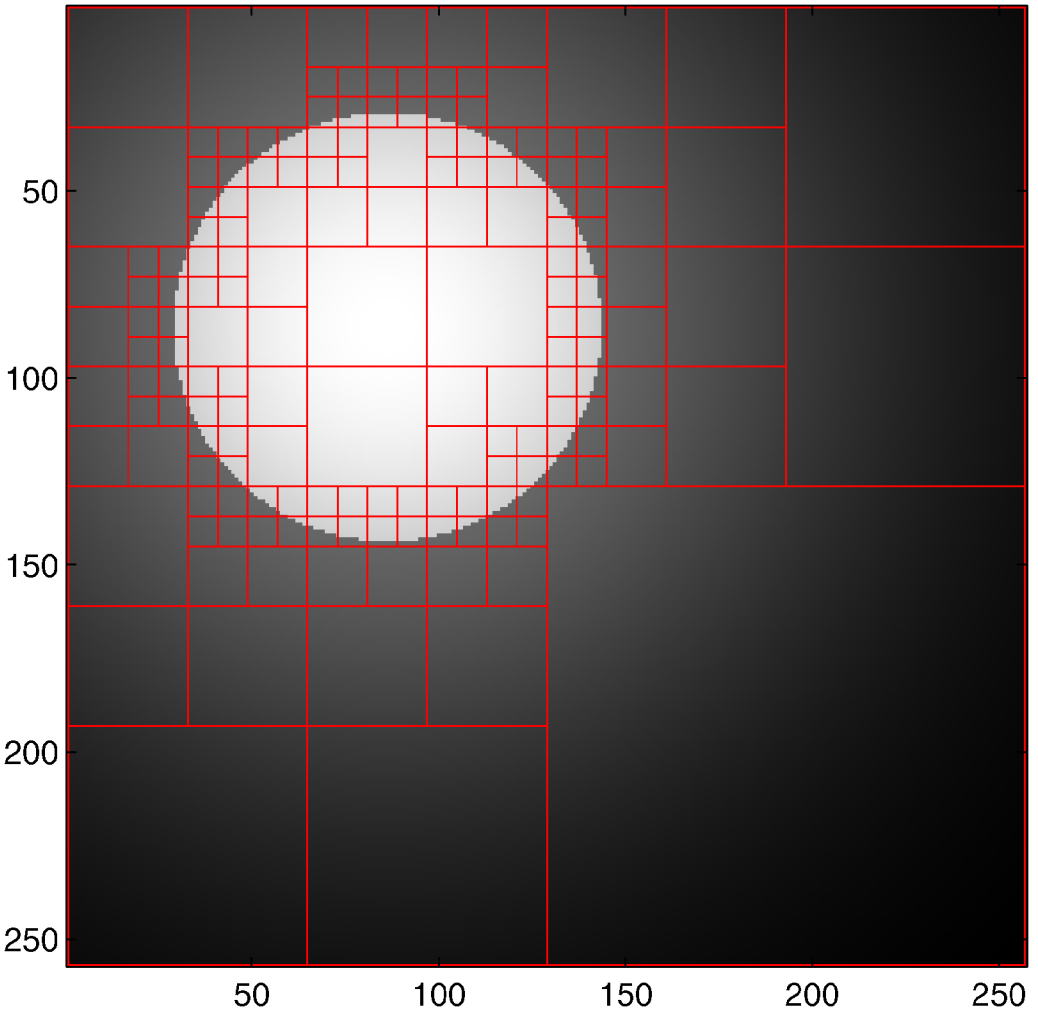


Fig. 5. Adaptive dyadic segmentation of the 2D Gaussian data with circular discontinuity, which honors the geometry of the discontinuity.

standard wavelet decomposition. This confirms the well-known fact that the wavelet transform performs well on piecewise smooth data. As we can easily see, the adaptive segmentation improves the performance of LLST and BDCT. Without adaptive segmentation, C6DWT performed best for $R \leqslant 25\%$ and $R \geqslant 72\%$, which can be seen by comparing the curve of LLST with $J = 3$ in subplot (a) with that of C6BSB ('Coif6: adap') in subplot (d) in Fig. 4.

With adaptive segmentation, however, LLST outperformed both BDCT and C6BSB for $R \leqslant 25\%$, which is the range of our interest.

Interestingly enough, the adaptive segmentation does not improve the performance of LCT so much from that of nonadaptive homogeneous split; it is slightly better only in the range $R \in [0, 30]$. The reason is that the adaptive segmentation uses many small blocks of size 8×8 pixels, as shown in Fig. 5. The version of LCT in our experiments uses the so-called "fixed" folding whose bell function width is com-

pletely determined by the smallest block size [15, Chapter 4]. Since the same bell function is also used for processing larger blocks, LCT loses its effectiveness as we discussed in Introduction and Section 4.1.1. To avoid such a problem, one needs to use multiple folding LCT of Fang and Séré [9], or better yet, the time–frequency LCT of Villemoes [10], which unfortunately constrains possible segmentation patterns as we discussed in Introduction. We shall not pursue these alternative versions of LCT here.

4.2. Approximation of synthetic oscillatory images with and without discontinuity

We shall now examine the performance of these transforms on an oscillatory function, in fact, a Gabor (i.e., a modulated Gaussian) function, with and without discontinuity as in the simple Gaussian case.

4.2.1. A case without discontinuity

We generate the data according to the formula: $f(x, y) = \exp(-(x+1/3)^2 - (y+1/3)^2) \cdot \sin(5\pi(2x + 3y))$, where $(x, y) \in [0, 1]^2$, and sample this with the same rate as before.

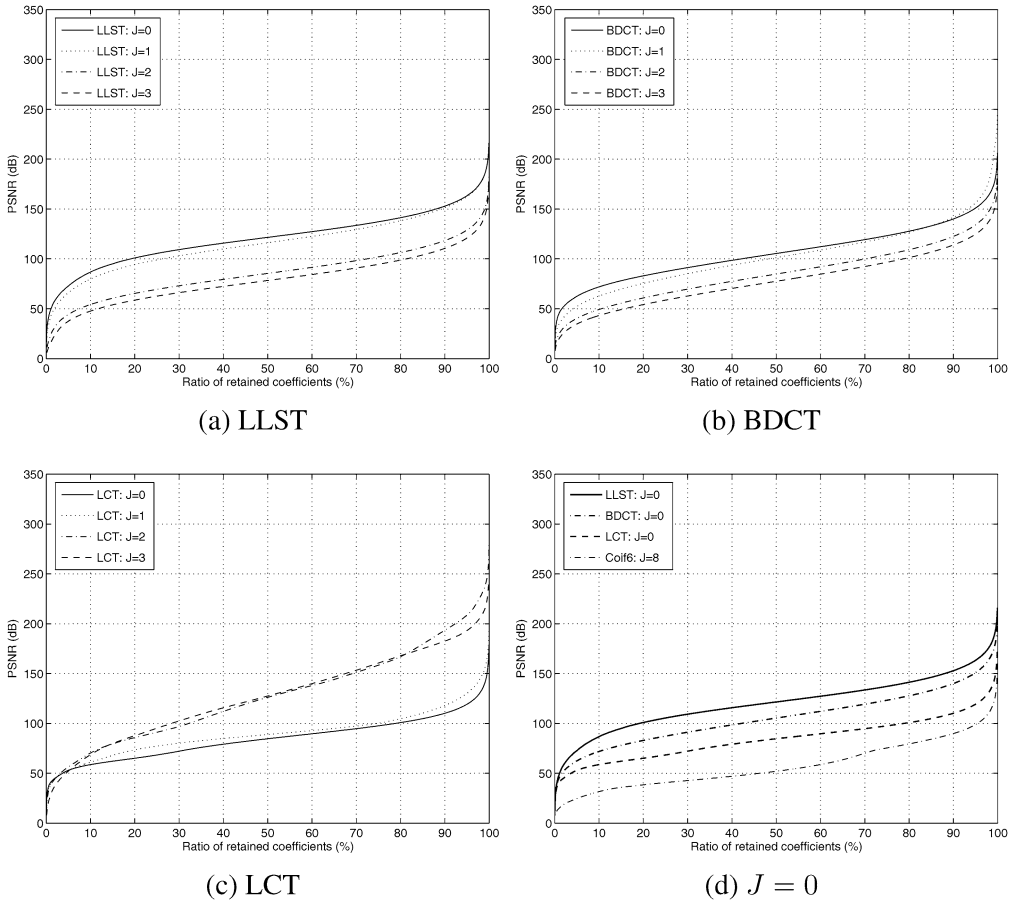
Figure 6 shows the approximation results. Again, in principle, there should not be any gain by splitting the data into a set of smaller blocks because the data do not have any intrinsic singularity. In fact, both LLST and BDCT, the $J = 0$ case outperforms the other values of J, and LLST with $J = 0$ remains as the best performer. Most obvious difference from the simple Gaussian case is the degradation of the performance of C6DWT, which confirms the well-know fact that the wavelet is not efficient for handling oscillatory data and textures. Another interesting observation is that LCT with $J = 2, 3$ performs quite well for this dataset. In fact, LCT with $J = 2, 3$ defeats LLST with $J = 0$ for the range $R > 42\%$; compare Fig. 6 (a) and (c). However, the range of our interest for efficient approximation, LLST with $J = 0$ still performs the best.

4.2.2. A case with discontinuity

Finally, we shall examine the toughest scenario so far: the Gabor function with the same circular discontinuity as the one used in Section 4.1.2. We shall not only use the homogeneous splits, but also the same segmentation pattern shown in Fig. 5 for the adaptive segmentation. We shall also compute the BSB from the C6 wavelet packet tree.

Figure 7 shows the approximation results. The performance of the approximation are degraded for all the transforms compared to the other scenarios considered so far, as expected. However, the overall best performer is LLST with adaptive segmentation, except for the range $R < 6\%$ where BDCT with adaptive segmentation performs slightly better. LCT with adaptive segmentation does not perform better than LCT with $J = 3$ as in the case of the Gaussian with discontinuity for the same reason: the width of the bell function is too narrow due to the smallest block size in this adaptive segmentation. We note that C6BSB in this case tries to subdivide the high frequency bands and performs better than the standard wavelet transform C6DWT unlike the case of Section 4.1.2 where C6BSB is in fact C6DWT.

In summary, our experiments with these synthetic images have shown that LLST is: (1) the best overall performer in the low ratio region of our interest; and (2) most effective if the adaptive segmentation of the domain honoring the geometry of the singularity in the data is used.



(a) LLST (b) BDCT

(c) LCT (d) $J = 0$

Fig. 6. Quality of approximation of the 2D Gabor (i.e., modulated Gaussian) data measured by PSNR values.

4.3. Barbara face image

Finally, we shall examine the approximation performance of various transforms using a real image. We shall use a face part of the famous image "Barbara," shown in Fig. 1 (a), which has been frequently used for image approximation and compression tests. The size of this face part of the Barbara image is 129×129 pixels. This is much more difficult to approximate than the simple Gaussian/Gabor datasets in the previous subsections because it contains a variety of regions: smooth regions (forehead and cheeks); more complicated regions (eyes, nose, mouth); and regions with oscillatory patterns (scarf). In this experiment, we shall use five different homogeneous splits $J = 0, 1, 2, 3, 4$. Note that the $J = 4$ case corresponds to the block size of 8×8 pixels, i.e., the standard JPEG-DCT scenario. We shall also examine the adaptive segmentation.

Figure 8 shows our results. The zoomed-up versions in the range $R \in [0, 20]$ are shown in Fig. 9. We use the IPP program as before to generate the adaptive segmentation for LLST, BDCT, and LCT, which is shown in Fig. 10.

From these figures, we observe the following:

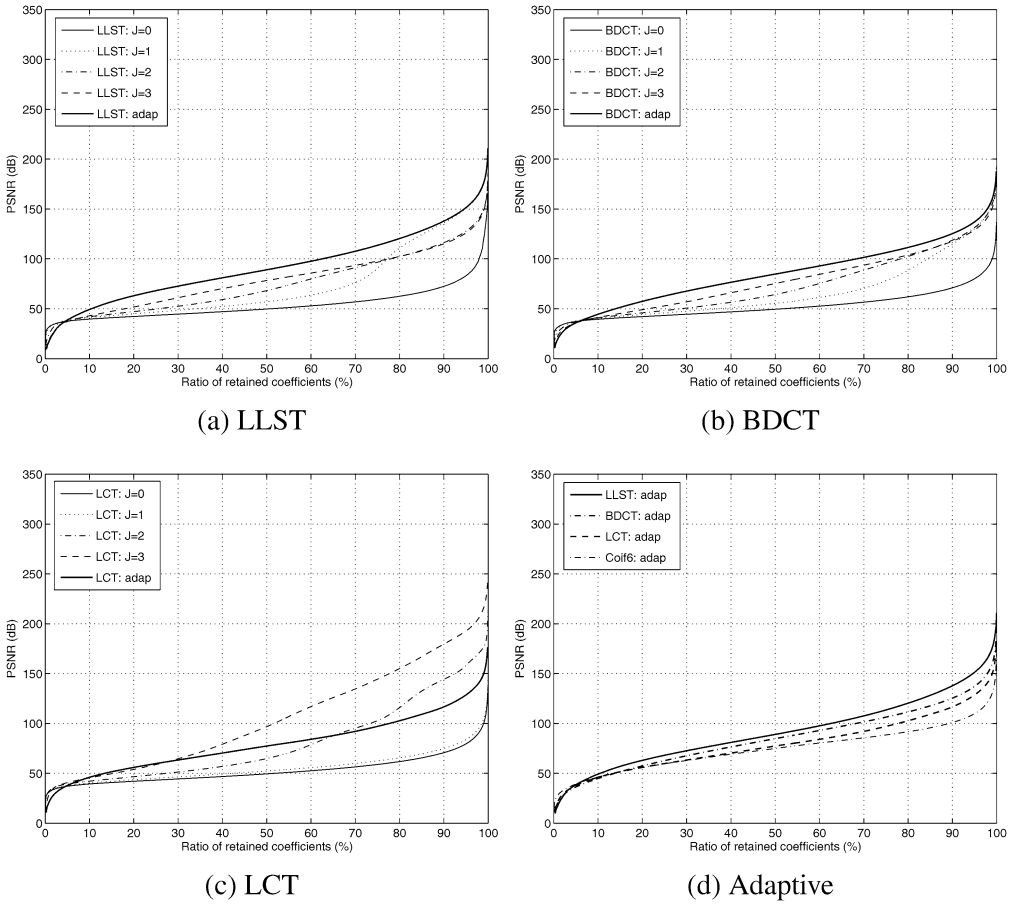


Fig. 7. Quality of approximation of the 2D Gabor data with circular discontinuity measured by PSNR values.

- The performance of LLST and BDCT with the adaptive segmentation and that of the homogeneous splits with $J = 2, 3$ are virtually the same.
- LLST and BDCT (with the adaptive segmentation or the homogeneous splits with $J = 2, 3$) outperform C6BSB except in the range $R \in [0, 5]$.
- The PSNR values of C6BSB in the range of $R \in [2, 20]$ are 1 dB higher than those of C6DWT with $J = 7$ (but not shown in the plots).
- LCT with adaptive segmentation is defeated by LCT with $J = 2, 3$, especially in the low range $R \leqslant 20\%$, by exactly the same reason as the Gaussian/Gabor cases.
- BDCT with $J = 4$ is defeated by BDCT with $J = 3$. This shows the nonoptimality (at least for this image) of the strategy of homogeneously splitting a target image into a set of blocks of size 8×8 pixels, which is adopted in the JPEG Baseline standard.
- Advantage of the adaptive segmentation is less obvious except the C6BSB case for this particular image.

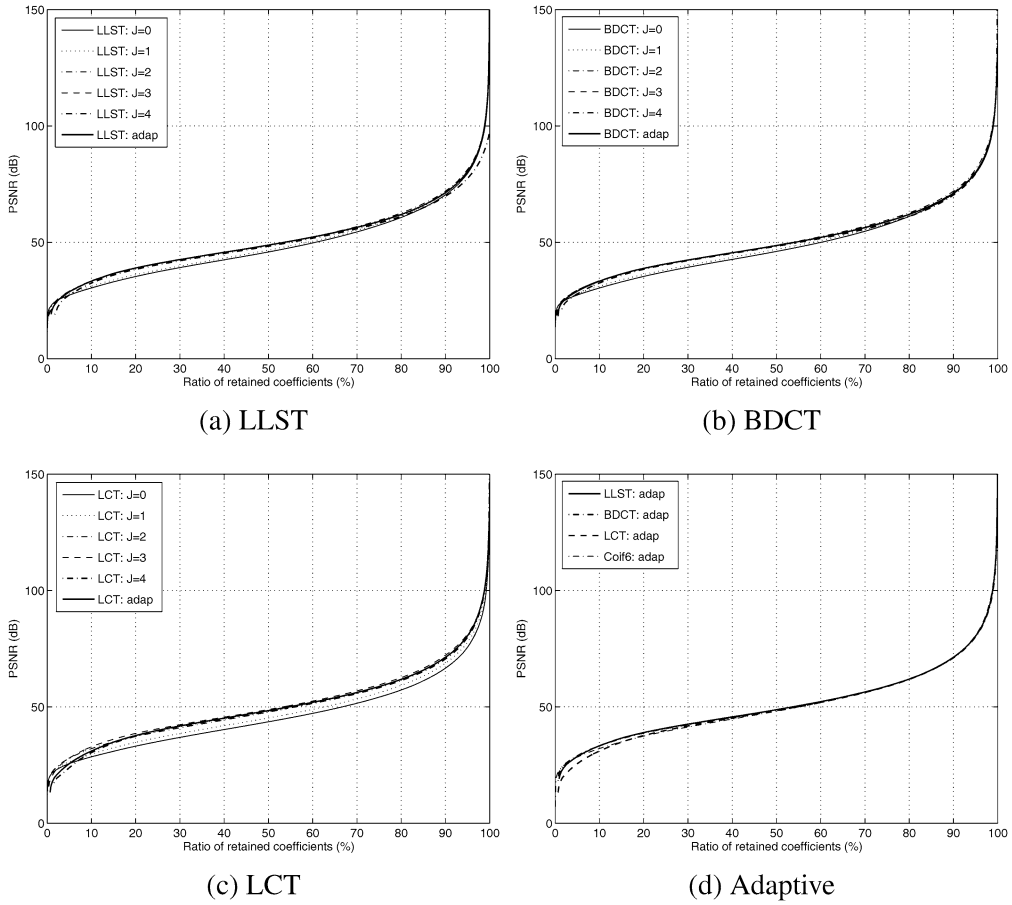
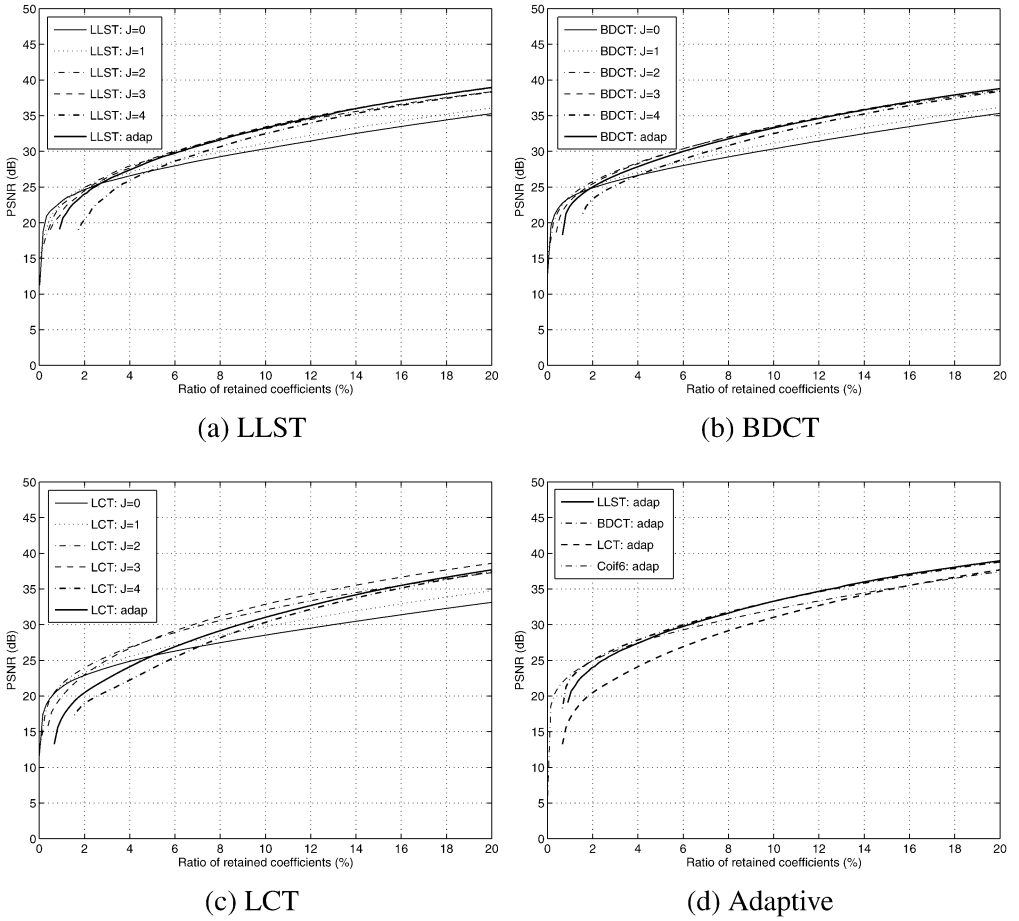


Fig. 8. Quality of approximation of the Barbara face image measured by PSNR values.

From these observations, unlike the synthetic datasets in Sections 4.1 and 4.2, we can claim neither the superiority of the adaptive segmentation over the homogeneous splits nor that of LLST over the other transforms, in particular, over BDCT *for this particular image and in terms of the PSNR values*. We shall therefore compare the perceptual quality of these approximations further by displaying the reconstructed images. Figure 11 shows the approximations using the top 5% of the coefficients by these transforms with the adaptive segmentation. Figure 12 shows the zoomed-up versions to see the quality of those approximations in details. It is clear that the visual quality of the LLST approximation is closest to the original among these transforms. The BDCT approximation reveals the annoying blocking artifact. The LCT approximation is the worst due to the artifact generated by the folding procedure. The C6BSB approximation is perhaps the next best, but the forehead and cheek portions are less smooth than the LLST approximation, and the stripes of the scarf, especially those in the right-hand side, are not well approximated. These experiments suggest that PSNR is not necessarily the best metric for judging the quality of displayed images. In the near future, we plan to use the more perceptually correct metric such as *mean structural similarity index* (MSSIM) [29], which is based on the comparison of the local patterns of pixel intensities normalized for luminance and contrast.



(a) LLST (b) BDCT

(c) LCT (d) Adaptive

Fig. 9. Zoomed up versions of Fig. 8 when 0% to 20% of the original coefficients are retained.

5. Polyharmonic local Fourier transform: use of the complex exponentials

As we discussed in Section 2, the Fourier sine coefficients of the v_j component of the PHLST decomposition posed as (1), (2), and (5) have the good decay rate, i.e., $O(\|\boldsymbol{k}\|^{-2m-1})$, $m = 1, 2, \ldots$. The main motivation of using the sine functions was the extra gain in the decay speed of the expansion coefficients via odd reflection at the boundary of the domain, which in turn is the consequence of the vanishing boundary values of v_j. However, it is well understood now that the *oriented patterns* are not efficiently captured and represented by using only sines (or only cosines). It is much more efficient to use *complex exponentials* for representing oriented patterns than sines alone. Because the boundary values of v_j vanish, it is possible to use the *complex exponentials* instead of sines, i.e., the ordinary Fourier series expansion instead of the Fourier sine series expansion, if one can tolerate slower decay rate of the coefficients. This slower decay is due to the periodization of the v_j component without the odd reflection. We shall call this the *polyharmonic local Fourier transform* (PHLFT). More precisely, let Ω_j be a box of the form $\Omega_j = \boldsymbol{x}_0^j + \prod_{k=1}^d (a_k^j, b_k^j)$, where $\boldsymbol{x}_0^j$ is the vertex of the box closest to the origin (i.e., the lower

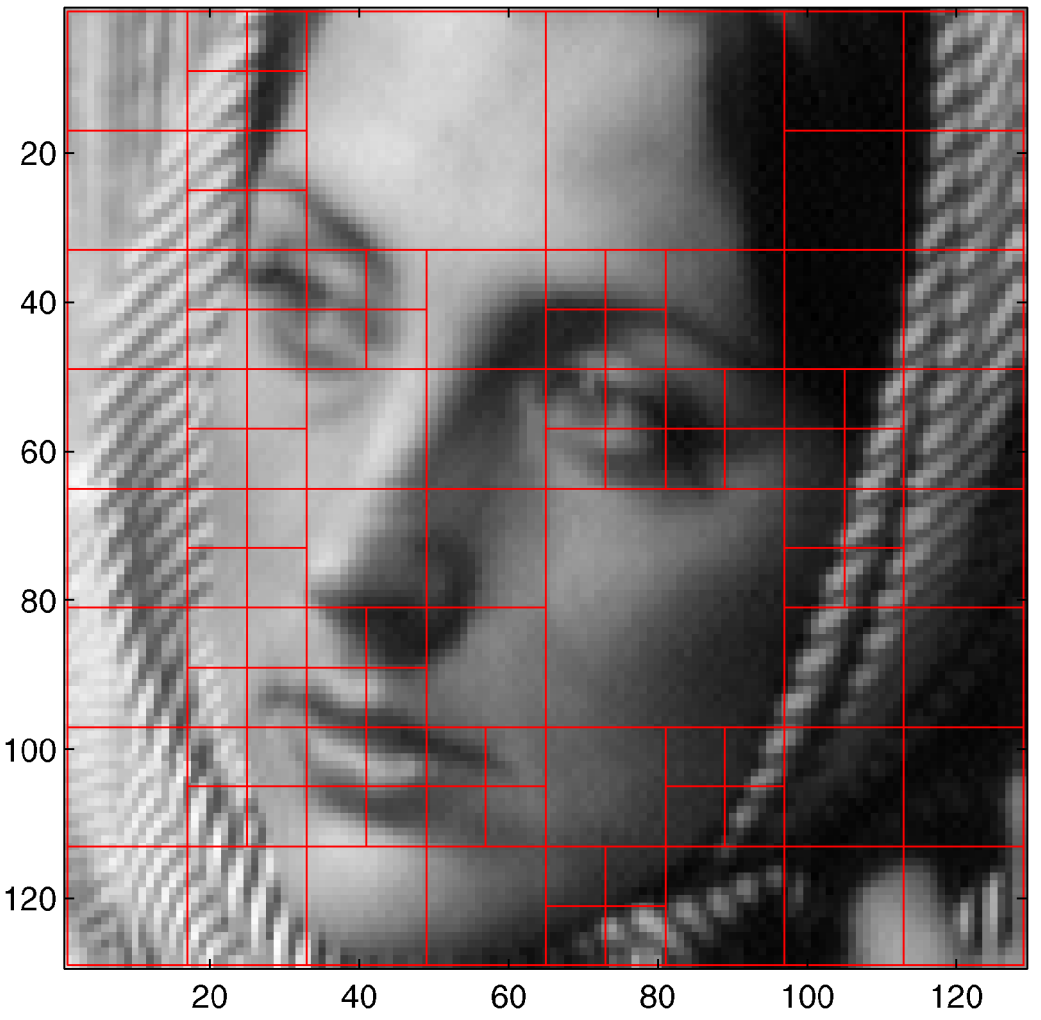


Fig. 10. Adaptive dyadic segmentation of the Barbara face image performed interactively using the Java-based IPP program.

left corner in the case of 2D), and $\ell_k^j \triangleq b_k^j - a_k^j$ is the length of the kth side of this box. Furthermore, let us assume that f is locally C^{2m} on $\bar{\Omega}_j$ with $m \geqslant 1$. If we use the following boundary condition instead of (2) to solve for the u_j component (1):

$$\frac{\partial^\ell u_j}{\partial \nu^\ell} = \frac{\partial^\ell f}{\partial \nu^\ell} \quad \text{on } \partial\Omega_j, \quad \ell = 0, \ldots, m-1, \tag{11}$$

then the resulting v_j component can be extended periodically and becomes $C^{m-1}(\mathbb{R}^d)$. Therefore, we can expand v_j into the Fourier series:

$$v_j(\boldsymbol{x}) \sim \sum_{\boldsymbol{k}\in\mathbb{Z}^d} c_{\boldsymbol{k}} \mathrm{e}^{2\pi \mathrm{i}\langle \boldsymbol{k}, L_{\Omega_j}^{-1}(\boldsymbol{x}-\boldsymbol{x}_0^j)\rangle}, \quad \boldsymbol{x} \in \Omega_j,$$

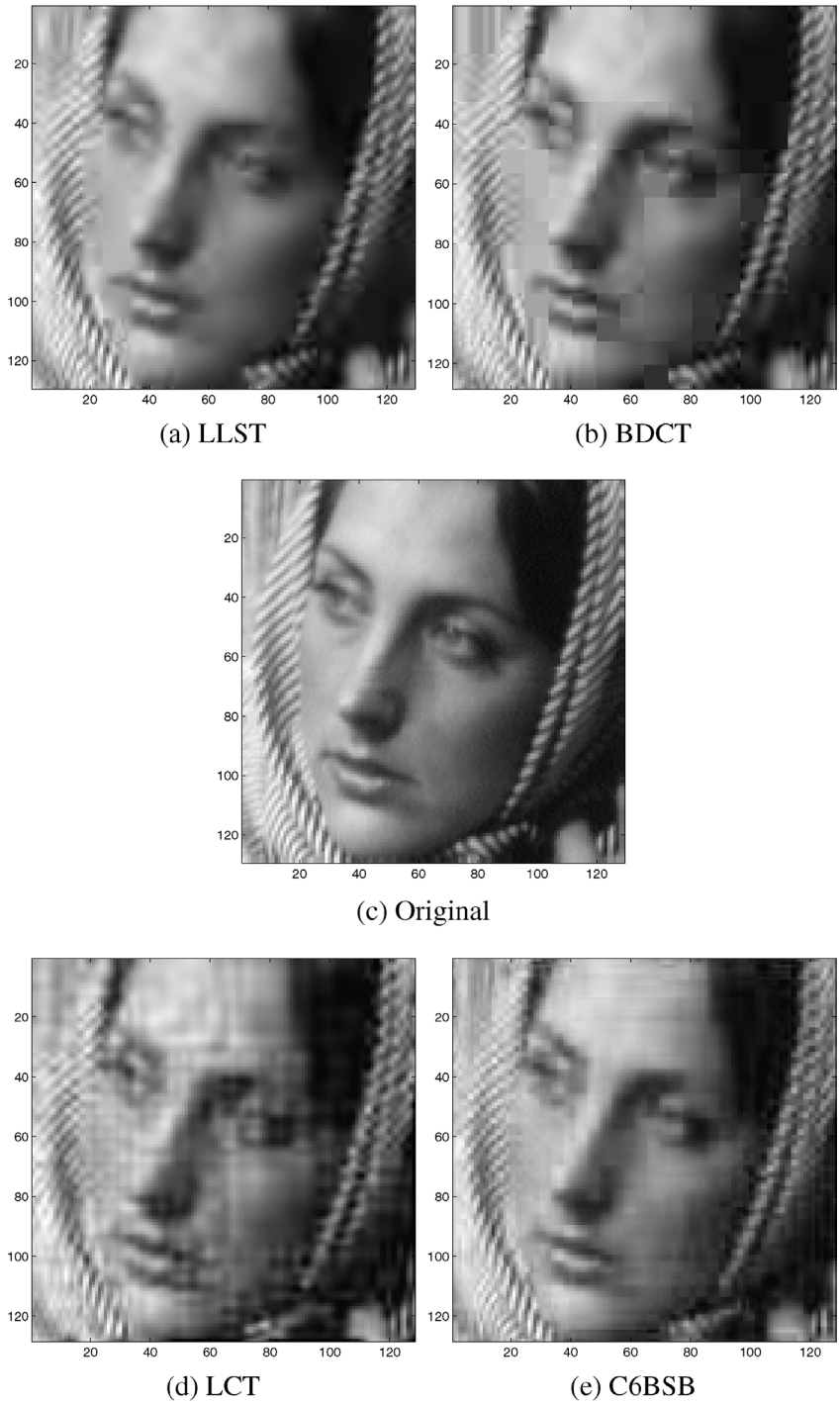


Fig. 11. Approximation of the Barbara face image by LLST, BDCT, LCT, and C6BSB using top 5% of the representations. The adaptive segmentation shown in Fig. 10 was used for LLST, BDCT, and LCT. C6BSB was computed from the C6 wavelet packet tree.

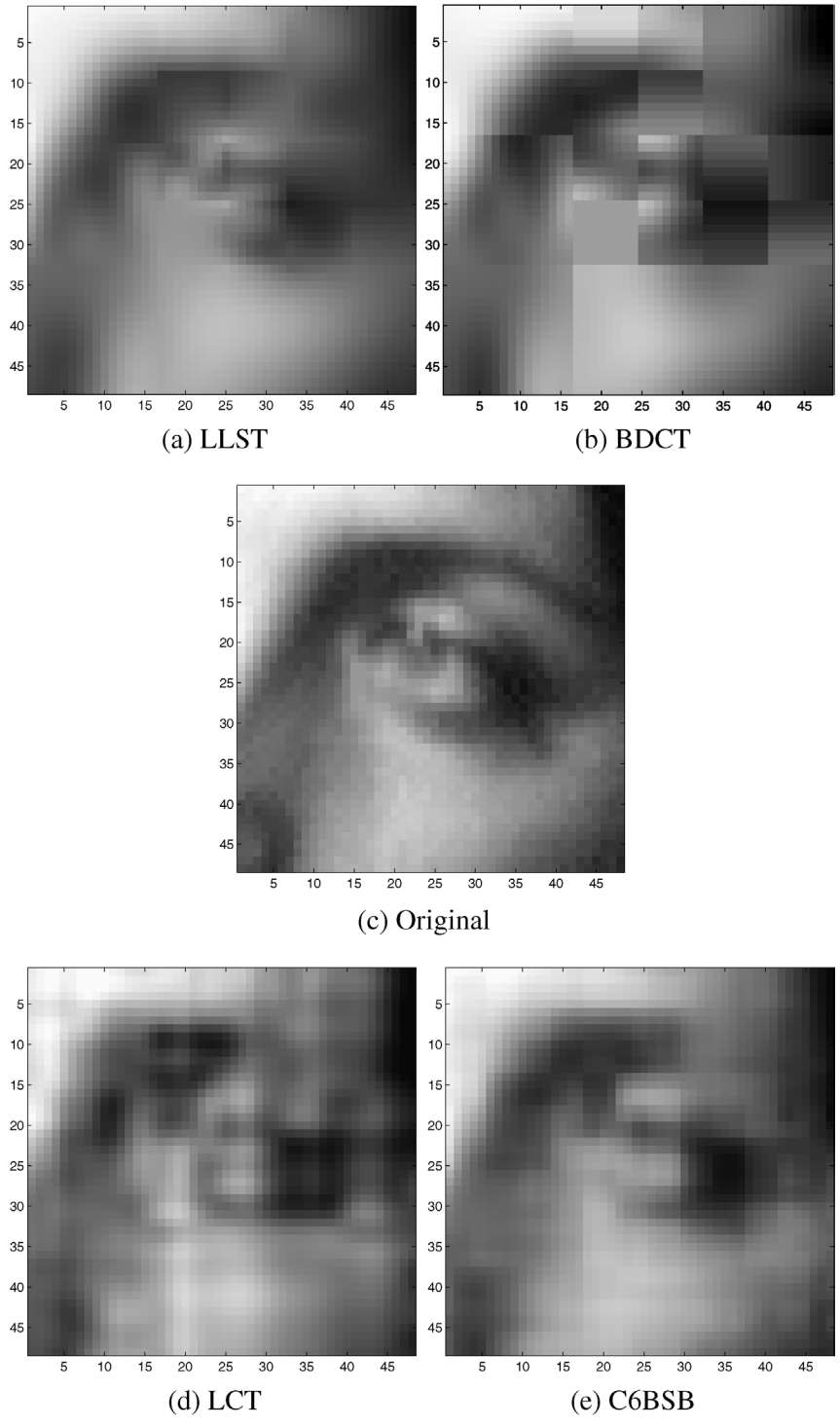


Fig. 12. Zoomed-up versions of Fig. 11.

where $L_{\Omega_j} = \mathrm{diag}(\ell_1^j, \ldots, \ell_d^j)$, with the coefficients $|c_{\boldsymbol{k}}|$ decaying as $O(\|\boldsymbol{k}\|^{-m-1})$; see Theorem A.2 in Appendix A. Accordingly, the case with $m = 1$, which we shall call *Laplace local Fourier transform* (LLFT), has the decay of order $O(\|\boldsymbol{k}\|^{-2})$, which is the same as BDCT. But we gain the ability to easily detect and interpret oriented patterns instead, which is difficult with BDCT or LLST. Figure 13 demonstrates this point. If one uses the block discrete Fourier transform (BDFT) without removing the u_j components, the DFT coefficients are all contaminated by the Gibbs phenomenon due to the block boundaries as shown in Fig. 13 (b). If one uses LLST or BDCT, it is difficult to decipher the orientation information from the coefficients; see Fig. 13 (c), (d). On the other hand, LLFT clearly reveals the ori-

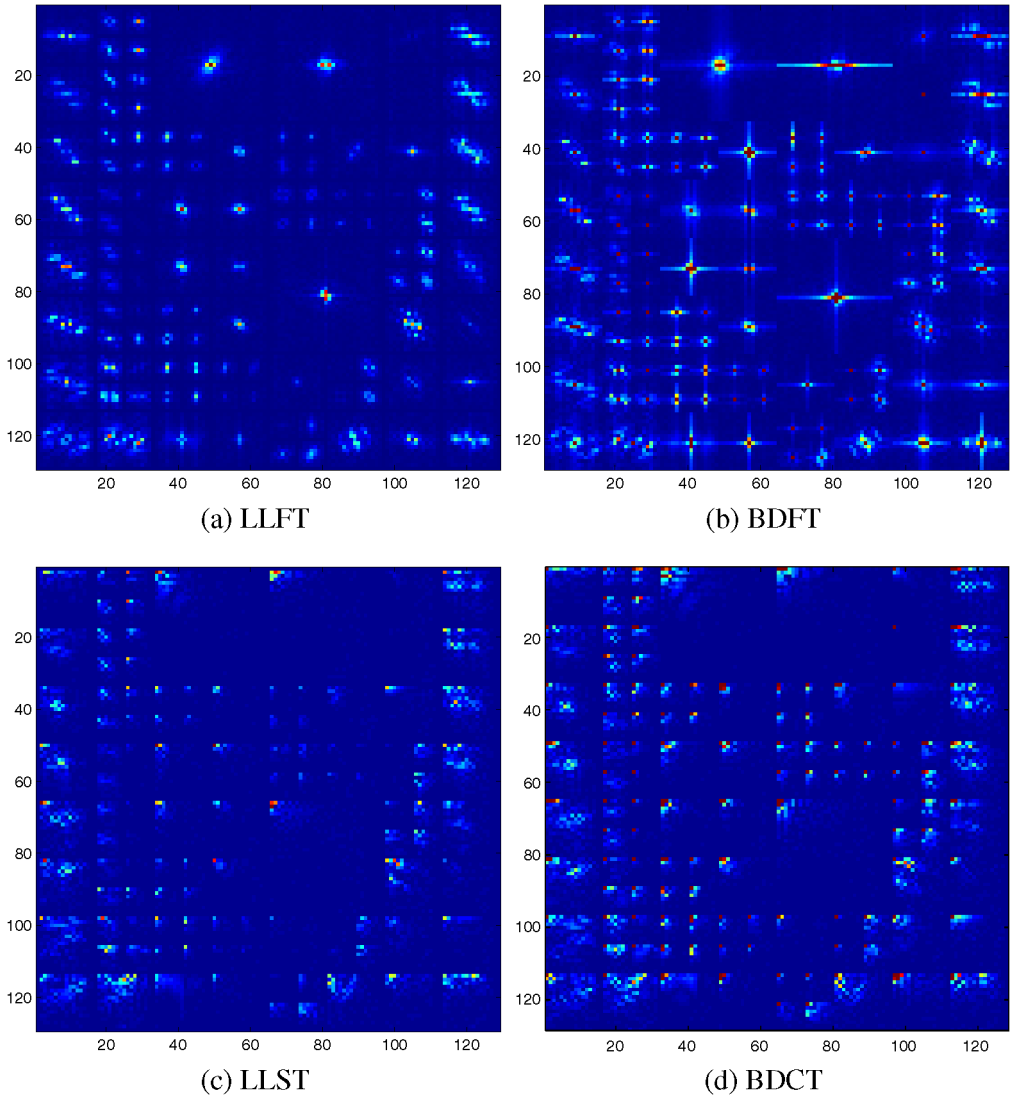


Fig. 13. Magnitude of the coefficients in LLFT, BDFT, LLST, and BDCT of the Barbara face image with the adaptive segmentation of Fig. 10. Note that the corner pixel values and 1D DST coefficients of the boundaries are not shown in LLFT and LLST here.

entation information as shown in Fig. 13 (a). We note that, in practice, one only needs to store the LLFT coefficients in the upper half plane in each block thanks to their symmetry, assuming that an input image is real-valued. LLFT also permits us to compute locally analytic signal, instantaneous frequency, etc., which we will explore at a later date.

6. Discussion

In this section, we shall first discuss issues that are left open in PHLST. Then we shall describe possible extensions and applications using PHLST and its relatives. We shall also discuss the related concepts and methods proposed previously by other researchers and conclude this article by describing the difference of their work from ours.

6.1. Open issues

6.1.1. Compression with quantization

A strategy for lossy image compression using PHLST remains an open issue. Unlike the image approximation, which simply keeps a subset of the exact expansion coefficients and corner pixel values as we discussed in Section 4, lossy image compression truly reduces the number of "bits" required to represent a given image approximately and converts it to a stream of bits via the process of *quantization*. In the JPEG Baseline standard [30,31], the DCT-II coefficients in each block of 8×8 pixels are divided by the entries of the so-called luminance quantization table (LQT) and further rounded into the nearest integers. This quantization process tends to suppress the higher frequency coefficients than the lower frequency coefficients so that this process can result in many zeros (i.e., more compression) without sacrificing visual fidelity too much. In fact, LQT was determined by psychophysical experiments on the visibility of the DCT-II basis vectors [30, Section 4.1.3] for the square block of 8×8 pixels. The Baseline method further uses the zigzag search of the quantized coefficients in each block to record the end of the block position instead of recording all the subsequent zeros in the block. Finally, this quantized sequence (integers) are encoded by some entropy coder (e.g., the Huffman coder or the arithmetic coder) for further compression in a "lossless" manner.

Unfortunately, we cannot directly use this LQT adopted in the JPEG Baseline standard for PHLST because it is optimized only for DCT-II of 8×8 pixel blocks, and not optimal for any other settings. In fact, it is not optimal even for DCT-II if the size of a block is different from 8×8 pixels. Therefore, if we wish to follow this approach, we would need to calibrate the LQT specifically for DST used in PHLST for various pixel sizes such as 9×9, 17×17, 33×33, etc. It would be too costly (in human resources) to conduct such psychophysical experiments. Also, the PHLST representation consists of three different items in each block: four corner pixel values, the 1D DST coefficients of the block boundary; and the 2D DST coefficients of the residual component. We need to examine whether these three components should be quantized separately or not.

We are currently investigating simpler uniform quantizers with "dead zone" (a special bin covering the zero value). This dead zone can get rid of noise in input data if its width is appropriately chosen because any coefficients within this zone are quantized to zero, i.e., killed. Thus, the width of the dead zone plays the role of the threshold in denoising algorithms. The subtle and interesting issue here is how to choose the width of the dead zone as well as that of the uniform bins outside of the dead zone, which determines

the resolution of the quantization. Yet another open issue is that of encoding after quantization. Just like the JPEG Baseline standard, it is possible to use the zigzag search to detect the trailing zeros in each block, and encode the resulting quantized sequences via Huffman coder. However, it still remains to be investigated whether such an approach is most suitable for PHLST.

6.1.2. Segmentation and denoising

Another open problem is how to automatically and adaptively segment a given input image to achieve more efficient approximation and compression. Note that what we mean segmentation here is different from usual image segmentation studied in the image analysis and computer vision literature where one wishes to faithfully segment an image into a set of objects or domains whose boundaries are general smooth curves. What we want to do here is to simply split an image into a set of adaptive dyadic blocks honoring the geometric structure of input data as much as possible. For example, we wish to obtain segmentations like those shown in Figs. 5 and 10 completely automatically rather than manually using an interactive program like IPP. We already demonstrated that such adaptive dyadic splits help image approximation in Section 4. We need to confirm that the same is true for image compression, which necessarily includes the cost of recording the geometry of adaptive splits.

We are currently investigating a hierarchical and recursive split-and-merge strategy similar to the best-basis algorithm of Coifman and Wickerhauser [32] in spirit. Clearly, the key is what criterion we should employ to judge whether smaller blocks should be merged into larger blocks. One of the most promising and natural criteria is the *minimum description length* (MDL) criterion [33–36]. Viewing each split pattern of an image in PHLST as a *model*, the MDL criterion suggests that we should choose among many possible models the one giving the shortest description (counted in bits) of the data *and* the model. This leads to the minimization of the infidelity of the model to the data and the complexity of the model itself in a balanced manner. In the case of PHLST, the MDL criterion is particularly appealing since PHLST does not provide an orthonormal basis. Instead, it provides "nonhomogeneous" representations using the corner pixels, 1D DST coefficients of the boundaries, and the 2D DST coefficients of the residuals, as explained in Section 4. Thus, the sparsity criterion using ℓ^p norm with $0 < p \leqslant 1$ makes less sense contrary to the case of the libraries of orthonormal bases such as local cosines and wavelet packets. It makes more sense to count the description length in bits needed to encode such nonhomogeneous representations.

There are several additional advantages to use the MDL criterion here. First, it forces us to incorporate a quantization procedure to convert the representation into a sequence of bits. Second, it can achieve *simultaneous compression and denoising* of input data. Similarly to the case of wavelets and the libraries of orthonormal bases shown by Saito [36], Chang et al. [37], and Hansen and Yu [38] among others, we expect that the MDL-based method will achieve the desired results for PHLST. Finally, the MDL formulation allows us to incorporate easily various noise models and prior models for distribution of the expansion coefficients: it can automatically select the most suitable noise model and coefficient distribution models out of many competing models. This is advantageous since it is well known that the Laplace (or double exponential) distribution or the generalized Gaussian distribution are more suitable to model the wavelet coefficients [38] and DCT coefficients [39] of natural images than the Gaussian distribution. The DST coefficients in PHLST are expected to behave in a similar manner.

6.1.3. Nonlinear approximation with PHLST

Another open issue is to obtain precise nonlinear approximation results using PHLST. Such a task remains elusive compared to the case of the orthonormal wavelets or splines. Let us briefly explain why

this is so. First, let us introduce some important concepts of the nonlinear approximation. Let X be some function space (e.g., the Besov space) defined on a domain $\Omega \subset \mathbb{R}^d$, and let $\Sigma_n \subset X$ be a nonlinear manifold so that any function belonging to Σ_n can be exactly representable by at most n parameters. Examples of such Σ_n include a set of functions that can be exactly specified by at most n basis functions selected from a basis set for X and a set of piecewise constant functions with n knots or breakpoints for $d = 1$. We now define the n-term approximation error of $f \in X \subset L^p(\Omega)$ as follows:

$$\sigma_n(f)_p \stackrel{\Delta}{=} \inf_{g \in \Sigma_n} \|f - g\|_p,$$

where $1 \leqslant p \leqslant \infty$. In the nonlinear approximation setting, the goodness of Σ_n is measured by the decay rate of the worst case n-term approximation error as n increases:

$$\sigma_n(X)_p \stackrel{\Delta}{=} \sup_{f \in X} \sigma_n(f)_p \leqslant C n^{-\alpha}, \tag{12}$$

where $\alpha > 0$. Clearly, the larger the value of α, the better the manifold Σ_n. The primary difficulty in obtaining n-term approximation results for PHLST lies in the strategy to optimally distribute the resources of n terms (or numbers) to the geometry information $\{\Omega_j\}$, the polyharmonic components $\{u_j\}$, and the residuals $\{v_j\}$. Even with a homogeneous split of Ω, it is challenging to derive an optimal allocation of n terms into the $\{u_j\}$ and $\{v_j\}$ components. Another difficulty, which is clearly related to the primary one above, is to determine a good function space X that allows us to obtain the best possible n-term approximation results, i.e., the largest $\alpha > 0$ in (12). We need to start attacking a simpler case of 1D functions here since DeVore in his plenary lecture [40] pointed out that obtaining nonlinear approximation results for an even simpler "Spline-Fourier" method with $d = 1$ (where a target function is segmented into several pieces brutally and each piece is approximated by the truncated Fourier series) is still open. On the other hand, it is encouraging to know that if $\Omega = [0, 1]^d$ without any further split, then the precise nonlinear approximation results are known [41].

6.2. Extensions and applications

In this section, we shall list possible extensions and applications of PHLST and its relatives.

6.2.1. PHLST/PHLFT in the frequency domain

Nothing prevents us from operating PHLST/PHLFT in the frequency domain. In fact, this strategy may be an excellent alternative to the wavelet packets and the brushlets [42]. The frequency support of each wavelet packet basis function is not completely localized except for the Shannon wavelet packets. On the other hand, each of the Shannon wavelet packets has unbounded support in the spatial domain, which makes them less useful. The frequency support of each brushlet basis functions is more localized than that of the wavelet packets, but still overlaps with that of the adjacent brushlets due to the use of the folding operations in the frequency domain. The PHLST/PHLFT in the frequency domain may overcome these shortcomings of the wavelet packets and the brushlets. We note that it is important to subtract the global u component from the original image f before converting it to the frequency domain. Otherwise, sharp horizontal and vertical lines crossing at the origin (the DC component) are generated due to the Gibbs phenomenon from the domain boundary, which interfere our analysis of the frequency information of the image. This is evident from Fig. 13 (b), which shows the local version of this annoying interference.

6.2.2. Use of the Neumann boundary condition

It is possible to use the *Neumann boundary condition* instead of the Dirichlet condition in (3). This will give us the $O(\|\boldsymbol{k}\|^{-4})$ decay rate of the v_j components instead of $O(\|\boldsymbol{k}\|^{-3})$ in the case of the Dirichlet boundary condition. To do so, we need to modify (3); we shall solve the following *Poisson equation* with the Neumann boundary condition:

$$\begin{cases} \Delta u_j = K_j & \text{in } \Omega_j, \\ \frac{\partial u_j}{\partial \nu} = \frac{\partial f_j}{\partial \nu} & \text{on } \partial\Omega_j, \end{cases} \tag{13}$$

where K_j is a constant that needs to be computed as follows:

$$K_j = \frac{1}{|\Omega_j|} \int_{\partial\Omega_j} \frac{\partial f_j}{\partial \nu}\, \mathrm{d}s,$$

which is the boundary integral of $\partial f_j/\partial\nu$ normalized by $|\Omega_j|$ (the volume of the domain). This constant K_j is necessary for (13) to have a unique solution (modulo an additive constant); see, e.g., [43, p. 84]. The solution u_j is not just a function having the same normal derivative at the boundary with the original function f_j; one can show that it is *the minimizer of the total squared curvature integral* on the domain Ω_j. Once we get the solution u_j, the residual function $v_j = f_j - u_j$ clearly satisfies $\partial v_j/\partial\nu = 0$ on $\partial\Omega_j$. Assuming that $f_j \in C^2(\bar{\Omega}_j)$, we can show that the residual v_j has at least C^2 smoothness across the block boundary when it is extended by the even reflection. Therefore, if we use the Fourier *cosine* series expansion of v_j we get the coefficients with decay rate $O(\|\boldsymbol{k}\|^{-4})$. See also Theorem A.2 in Appendix A. We naturally call this version of the transform the *polyharmonic local cosine transform* (PHLCT). However, this method of course requires to estimate the first order normal derivative of data at the boundary. We are currently investigating this issue with our collaborator, Katsu Yamatani, and getting encouraging results [44].

6.2.3. Extension to higher orders of polyharmonicity

We believe that PHLST of polyharmonicity $m > 2$ is not practical considering the need to estimate $\partial^{2(m-1)} f_j/\partial\nu^{2(m-1)}$ in (2) and the numerical sensitivity to compute these high order derivatives. However, the case of $m = 2$, i.e., BLST (biharmonic local sine transform), remains to be investigated; we are interested in knowing whether BLST is of practical interest for image approximation and compression or not. In theory, the Fourier sine coefficients of the v_j components in BLST should decay as $O(\|\boldsymbol{k}\|^{-5})$ instead of $O(\|\boldsymbol{k}\|^{-3})$ in LLST. However, the effectiveness of BLST still hinges on the accuracy of the second order normal derivative estimates at the boundary. Thus developing a robust method to estimate those derivatives from noisy data will be an challenging but important project. Note that such a method will also be useful for other purposes, for example, edge detection.

6.2.4. Extension to higher dimensions

It is important to realize that the information contained in the boundary becomes more and more meaningful as the dimension increases. For example, in 1D, the boundary of an interval simply consists of two endpoints. In 2D, the boundary of a domain becomes a 1D curve whereas in 3D, this becomes a 2D surface. If the data is supported in a 3D cube, then the boundary consists of six faces of that cube. It is also important to recognize that the boundary structure is *recursively organized*. For example, the boundary of each 2D face of a 3D cube consists of four 1D edges, and the boundary of each 1D edge

in turn consists of two corners. We can take advantage of this recursive structure: we can process each component, i.e., edges, faces, bodies, etc., by PHLST of the corresponding dimensions. The simple, hierarchical, and recursive algorithmic structure of PHLST can be carried over to higher dimensions in a straightforward manner. In particular, PHLST for 3D datasets is promising for efficient approximation, compression, and local feature computation for 3D medical images and 3D geophysical data, which we are currently investigating in collaboration with our graduate student Noel Smith [45].

6.2.5. Other potential applications

Because of its ability to completely localize the analysis of an input image and sparsify its representation equipped with a fast algorithm, there are many potential applications of PHLST. For example, its application to image zooming and interpolation is promising since PHLST does not suffer from the boundary effect/the Gibbs phenomenon, which is often a nuisance in image zooming. Commonly used image zooming/interpolation techniques such as pixel replication, bilinear interpolation, bi-cubic interpolation have all drawbacks, especially with large magnifications. The pixel replication is computationally most efficient, but generates annoying blocky zoomed images. The bilinear interpolation generates superfluous horizontal and vertical artifacts, and this is also true for the bi-cubic interpolation to a lesser extent. One can use DCT for image zooming, but again one may see the artifacts generated by the even reflection at the boundaries. Sinc (or band-limited) interpolation is theoretically ideal but its straightforward implementation does not work well due to the Gibbs phenomenon.

Another important application of PHLST is local feature computation. PHLST allows us to evaluate and compute various attributes (e.g., directional derivatives) at *any point* in the domain Ω_j even if we start from discrete samples. See Eqs. (7)–(10). We are currently investigating the interpolation of image values along a given *curve* as well as directional derivatives along such a curve, which is not easy using the conventional methods.

6.3. Relation to the other works

Retrospectively speaking, our work is related to many previous works done by other scientists. However, we did not find exactly the same strategy as ours in the other works. As early as 1938, Cornelius Lanczos [46] suggested that "denoising" and interpolation of digital signals sampled on an *equispaced* grid over a *finite interval* should be very nicely dealt with by trigonometric polynomials once the edge effect is taken care of. This was only an abstract given at the AMS conference. Somehow, a full version of the paper did not appear until 1952 [47]. He first used the line removal idea [46] corresponding to the 1D LLST in our case, and then proposed to remove a higher order polynomials [47,48]. As far as we know, Lanczos is one of the first scientists who recognized the importance of representing and interpolating data sampled at equispaced grid points using a combination of trigonometric polynomials and algebraic polynomials. He clearly understood that only using algebraic polynomials leads to the infamous Runge phenomenon, and only using trigonometric polynomial leads to the Gibbs phenomenon. Zygmund had a similar idea (i.e., removal of singularities) for different purposes in 1935 or earlier [49, Section 2.13]. See also [2, Section 2.2], [50, Chapter 4], [51, Chapter 2], and [48, Chapter 2]. The book of Kantrovich and V.I. Krylov [52] cites an early attempt of extending a function supported on $[0, 1]$ to $[-1, 1]$ smoothly and periodically (with period 2) by Maliev [53,54]. Smirnov [55] also cites the work of A.N. Krylov for speeding up the decay of Fourier coefficients of a compactly supported function using the line and polynomial removal.

In 1990, Madych and Nelson [56,57] introduced the so-called "polyharmonic cardinal splines," which uses the polyharmonic equations to interpolate the data given on the lattice $\mathbb{Z}^d$ in $\mathbb{R}^d$. Their main concern, however, is the interpolation, and they are not concerned with the residuals at all.

The "polysplines" proposed by Kounchev [58,59] are also related to our PHLST. In his case, though, he used a sequence of decreasing subdomains $\Omega = \Omega_0 \supset \Omega_1 \supset \cdots$ instead of the disjoint subdomains of our case. This led him to develop a new version of multidimensional wavelets. Again, he is not concerned with the residuals.

All of the above scientists except Lanczos only focused on the u component. As far as we know, Lanczos was the only one who seriously considered the residual v, but explored his idea neither for higher dimensions nor for multiscale setting.

Acknowledgments

This research was partially supported by the ONR grant N00014-00-1-0469 and the NSF grant DMS-0410406. We thank Professor Gregory Beylkin, University of Colorado at Boulder for fruitful discussions on the numerical issues of the Laplace equation solvers, Professor Grant Welland, University of Missouri at St. Louis for checking the proof of Theorem A.2, and Professor Raphy Coifman, Yale University for his warm encouragement.

Appendix A. Proof of Theorem 1

First we prove the following auxiliary theorems:

Theorem A.1. *Let $\mathbb{T}$ be a torus (i.e., $[0,1]$), and $f \in C^m(\mathbb{T})$ and periodic. Furthermore, let us assume that $f^{(m+1)}$ exists and in $BV[0,1]$. Then its Fourier coefficient $c_k = \hat{f}(k)$ decays as $O(|k|^{-m-2})$.*

Proof. We use the periodicity of f, i.e., $f^{(\ell)}(0) = f^{(\ell)}(1),\ \ell = 0, 1, \ldots, m$, and integration by parts.

$$\begin{aligned}
\hat{f}(k) &= \int_0^1 f(x)\mathrm{e}^{-2\pi \mathrm{i}kx}\,\mathrm{d}x = \frac{\mathrm{e}^{-2\pi \mathrm{i}kx}}{-2\pi \mathrm{i}k} f(x)\bigg|_0^1 + \frac{1}{2\pi \mathrm{i}k}\int_0^1 f'(x)\mathrm{e}^{-2\pi \mathrm{i}kx}\,\mathrm{d}x \\
&= \frac{\mathrm{e}^{-2\pi \mathrm{i}kx}}{-(2\pi \mathrm{i}k)^2} f'(x)\bigg|_0^1 + \frac{1}{(2\pi \mathrm{i}k)^2}\int_0^1 f''(x)\mathrm{e}^{-2\pi \mathrm{i}kx}\,\mathrm{d}x \\
&= \cdots \\
&= \frac{\mathrm{e}^{-2\pi \mathrm{i}kx}}{-(2\pi \mathrm{i}k)^{m+1}} f^{(m)}(x)\bigg|_0^1 + \frac{1}{(2\pi \mathrm{i}k)^{m+1}}\int_0^1 f^{(m+1)}(x)\mathrm{e}^{-2\pi \mathrm{i}kx}\,\mathrm{d}x \\
&= \frac{1}{(2\pi \mathrm{i}k)^{m+1}}\int_0^1 f^{(m+1)}(x)\mathrm{e}^{-2\pi \mathrm{i}kx}\,\mathrm{d}x.
\end{aligned}$$

By assumption, $f^{(m+1)} \in BV[0,1]$, so we can use the theorem of Taibleson [60] to get:

$$\left|\hat{f}(k)\right| \leqslant \frac{V(f^{(m+1)})}{(2\pi)^{m+1}|k|^{m+2}},$$

where $V(\cdot)$ is the total variation of the argument over $[0,1]$. This implies that $\hat{f}(k) = O(|k|^{-m-2})$. □

Theorem A.2. *Let $\mathbb{T}^d$ be a d-dimensional torus (i.e., $[0,1]^d$), and $f \in C^m(\mathbb{T}^d)$ and periodic. Furthermore, let us assume that $\partial_j^{m+1} f$ exists and in $BV[0,1]$, $j = 1,\ldots,d$. Then its Fourier coefficient $c_{\boldsymbol{k}} = \hat{f}(\boldsymbol{k})$ decays as $O(\|\boldsymbol{k}\|^{-m-2})$.*

Proof. We proceed essentially the same way as Körner [61, p. 409]. We consider each variable x_j in turn. Since f as a function of x_j (with all the other variables fixed) belongs to $C^m(\mathbb{T})$ and $\partial_j^{m+1} f \in BV[0,1]$, we can use Theorem A.1 as:

$$\left| \int_{\mathbb{T}} f(x_1,\ldots,x_j,\ldots,x_d) \mathrm{e}^{-2\pi \mathrm{i} k_j x_j}\,\mathrm{d}x_j \right| \leqslant \frac{C_j}{|k_j|^{m+2}}, \tag{A.1}$$

where $C_j > 0$ is a constant depending on j and k_j is a jth frequency index (nonzero integer). Then,

$$\begin{aligned}
\left|\hat{f}(\boldsymbol{k})\right| &= \left| \int_{\mathbb{T}} \cdots \int_{\mathbb{T}} f(x_1,\ldots,x_d) \mathrm{e}^{-2\pi \mathrm{i} \sum_j k_j x_j}\,\mathrm{d}x_1 \cdots \mathrm{d}x_d \right| \\
&\leqslant \int_{\mathbb{T}} \cdots \int_{\mathbb{T}} \left| \int_{\mathbb{T}} f(x_1,\ldots,x_d) \mathrm{e}^{-2\pi \mathrm{i} k_j x_j}\,\mathrm{d}x_j\, \mathrm{e}^{-2\pi \mathrm{i} \sum_{\ell \neq j} k_\ell x_\ell} \right| \mathrm{d}x_1 \cdots \mathrm{d}x_{j-1}\,\mathrm{d}x_{j+1} \cdots \mathrm{d}x_d \\
&\leqslant \int_{\mathbb{T}} \cdots \int_{\mathbb{T}} \frac{C_j}{|k_j|^{m+2}}\,\mathrm{d}x_1 \cdots \mathrm{d}x_{j-1}\,\mathrm{d}x_{j+1} \cdots \mathrm{d}x_d \\
&= \frac{C_j}{|k_j|^{m+2}}.
\end{aligned}$$

Therefore, we have the following estimate:

$$\left|\hat{f}(\boldsymbol{k})\right| \leqslant \frac{C_j}{|k_j|^{m+2}}, \quad j = 1,\ldots,d,\ k_j \neq 0. \tag{A.2}$$

Thus, if $\boldsymbol{k} \neq 0$, then

$$\begin{aligned}
\left|\hat{f}(\boldsymbol{k})\right| &\leqslant \min_{1\leqslant j\leqslant d} C_j |k_j|^{-m-2} \leqslant \left(\max_{1\leqslant j\leqslant d} C_j\right) \cdot \left(\min_{1\leqslant j\leqslant d} |k_j|^{-m-2}\right) = \left(\max_{1\leqslant j\leqslant d} C_j\right) \cdot \left(\max_{1\leqslant j\leqslant d} |k_j|\right)^{-m-2} \\
&\leqslant \left(\max_{1\leqslant j\leqslant d} C_j\right) \cdot \left(\|\boldsymbol{k}\|/\sqrt{d}\right)^{-m-2} = \frac{C}{\|\boldsymbol{k}\|^{m+2}},
\end{aligned}$$

where $C = \max_{1\leqslant j\leqslant d} C_j \cdot d^{1+m/2} > 0$. This implies the conclusion of the theorem. □

Now, we prove Theorem 1.

Proof. In this proof, for the notational simplicity, we use u, v, Ω instead of u_j, v_j, Ω_j, which will not generate any confusion. Since Ω is a rectangle in $\mathbb{R}^d$, it is easy to convert it to a unit cube $\mathbb{T}^d = [0,1]^d$ by rescaling and translation, which only changes the constants in the following argument. Therefore, we assume that $\Omega = \mathbb{T}^d$ below. Let us now consider the residual $v(\boldsymbol{x})$ over Ω. Let $\boldsymbol{x} = (x_1, \ldots, x_d) \in [0,1]^d$, and $\boldsymbol{\sigma} = (\sigma_1, \ldots, \sigma_d)$ be a d-dimensional vector whose entries consist of only 1 or -1. Now, the odd extension $\tilde{v}(\boldsymbol{x})$ of $v(\boldsymbol{x})$ to the extended cube $\tilde{\Omega} \triangleq [-1,1]^d$ can be defined as follows:

$$\tilde{v}(\sigma_1 \cdot x_1, \ldots, \sigma_d \cdot x_d) \triangleq \left(\prod_{k=1}^{d} \sigma_k \right) \cdot v(x_1, \ldots, x_d), \quad (x_1, \ldots, x_d) \in [0,1]^d.$$

The boundary conditions of $u(\boldsymbol{x})$ are:

$$u|_{\partial\Omega} = f|_{\partial\Omega}, \qquad \left.\frac{\partial^2 u}{\partial \nu^2}\right|_{\partial\Omega} = \left.\frac{\partial^2 f}{\partial \nu^2}\right|_{\partial\Omega}, \qquad \ldots, \qquad \left.\frac{\partial^{2m-2} u}{\partial \nu^{2m-2}}\right|_{\partial\Omega} = \left.\frac{\partial^{2m-2} f}{\partial \nu^{2m-2}}\right|_{\partial\Omega}.$$

Therefore, these imply the following in terms of $\tilde{v}$:

$$\tilde{v}|_{\partial\tilde{\Omega}} = 0, \tag{A.3}$$

$$\partial_j^{2k} \tilde{v}(x_1, \ldots, x_{j-1}, -1, x_{j+1}, \ldots, x_d) = \partial_j^{2k} \tilde{v}(x_1, \ldots, x_{j-1}, 1, x_{j+1}, \ldots, x_d) = 0, \tag{A.4}$$

$$\partial_j^{2k} \tilde{v}(x_1, \ldots, x_{j-1}, 0-, x_{j+1}, \ldots, x_d) = \partial_j^{2k} \tilde{v}(x_1, \ldots, x_{j-1}, 0+, x_{j+1}, \ldots, x_d) = 0, \tag{A.5}$$

$$\partial_j^{2k+1} \tilde{v}(x_1, \ldots, x_{j-1}, -1, x_{j+1}, \ldots, x_d) = \partial_j^{2k+1} \tilde{v}(x_1, \ldots, x_{j-1}, 1, x_{j+1}, \ldots, x_d), \tag{A.6}$$

$$\partial_j^{2k+1} \tilde{v}(x_1, \ldots, x_{j-1}, 0-, x_{j+1}, \ldots, x_d) = \partial_j^{2k+1} \tilde{v}(x_1, \ldots, x_{j-1}, 0+, x_{j+1}, \ldots, x_d), \tag{A.7}$$

where $j = 1, \ldots, d$ and $k = 0, \ldots, m-1$. Note that $k = 0$ in Eq. (A.4) means $\tilde{v}|_{\partial\tilde{\Omega}} = 0$, which is different from (A.3). Equations (A.3)–(A.7) imply that $\tilde{v} \in C^{2m-1}(\tilde{\Omega})$ and *periodic*. Therefore, we can invoke Theorem A.2 with m replaced by $2m-1$ so that we get:

$$\hat{f}(\boldsymbol{k}) = O\left(\|\boldsymbol{k}\|^{-2m-1}\right) \quad \text{for } \boldsymbol{k} \neq \boldsymbol{0}. \qquad \square$$

References

[1] G.H. Hardy, W.W. Rogosinski, Fourier Series, third ed., Cambridge Univ. Press, 1956, republished by Dover Publications, 1999.

[2] A. Zygmund, Trigonometric Series, third ed., Cambridge Mathematical Library/Cambridge Univ. Press, 2003, vols. I and II combined.

[3] M.A. Pinsky, Introduction to Fourier Analysis and Wavelets, Brooks/Cole, 2002.

[4] A. Cohen, I. Daubechies, P. Vial, Wavelets on the interval and fast wavelet transforms, Appl. Comput. Harmon. Anal. 1 (1) (1993) 54–81.

[5] B.K. Alpert, A class of bases in L^2 for the sparse representation of integral operators, SIAM J. Math. Anal. 24 (1) (1993) 246–262.

[6] R.R. Coifman, Y. Meyer, Remarques sur l'analyse de Fourier à fenêtre, C. R. Acad. Sci. Paris, Sér. I 312 (1991) 259–261.

[7] H.S. Malvar, The LOT: Transform coding without blocking effects, IEEE Trans. Acoust. Speech Signal Process. 37 (1989) 553–559.

[8] H.S. Malvar, Lapped transforms for efficient transform/subband coding, IEEE Trans. Acoust. Speech Signal Process. 38 (1990) 969–978.

[9] X. Fang, E. Séré, Adapted multiple folding local trigonometric transforms and wavelet packets, Appl. Comput. Harmon. Anal. 1 (1994) 169–179.

[10] L.F. Villemoes, Adapted bases of time–frequency local cosines, Appl. Comput. Harmon. Anal. 10 (2001) 139–162.
[11] H. Whitney, Analytic extensions of differentiable functions defined in closed sets, Trans. Amer. Math. Soc. 36 (1) (1934) 63–89.
[12] B. Larson, N. Saito, The continuous boundary local Fourier transform, in: A.F. Laine, M.A. Unser, A. Aldroubi (Eds.), Wavelets IX, in: Proc. SPIE, vol. 4478, 2001, pp. 415–426.
[13] B. Larson, The continuous boundary local trigonometric transform, Ph.D. thesis, Department of Mathematics, University of California, Davis, 2002.
[14] M.V. Wickerhauser, Smooth localized orthonormal bases, C. R. Acad. Sci. Paris, Sér. I 316 (1993) 423–427.
[15] M.V. Wickerhauser, Adapted Wavelet Analysis from Theory to Software, A K Peters, Wellesley, MA, 1994, with diskette.
[16] G. Wahba, Spline Models for Observational Data, CBMS-NSF Regional Conference Series in Applied Mathematics, vol. 59, SIAM, Philadelphia, 1990.
[17] Y. Meyer, Oscillating Patterns in Image Processing and Nonlinear Evolution Equations, Univ. Lecture Ser., vol. 22, AMS, Providence, RI, 2001.
[18] S. Jaffard, Y. Meyer, R.D. Ryan, Wavelets: Tools for Science & Technology, SIAM, Philadelphia, 2001.
[19] A. Averbuch, M. Israeli, L. Vozovoi, A fast Poisson solver of arbitrary order accuracy in rectangular regions, SIAM J. Sci. Comput. 19 (3) (1998) 933–952.
[20] E. Braverman, M. Israeli, A. Averbuch, L. Vozovoi, A fast 3D Poisson solver of arbitrary order accuracy, J. Comput. Phys. 144 (1998) 109–136.
[21] W.L. Briggs, V.E. Henson, The DFT: An Owner's Manual for the Discrete Fourier Transform, SIAM, Philadelphia, 1995.
[22] A. Iserles, A First Course in the Numerical Analysis of Differential Equations, Cambridge Texts in Applied Mathematics, Cambridge Univ. Press, New York, 1996.
[23] G. Strang, The discrete cosine transform, SIAM Rev. 41 (1) (1999) 135–147.
[24] R.A. DeVore, Nonlinear approximation, in: Acta Numerica, Cambridge Univ. Press, 1998, pp. 51–150.
[25] I. Daubechies, Orthonormal bases of compactly supported wavelets. II. Variations on a theme, SIAM J. Math. Anal. 24 (2) (1993) 499–519.
[26] I. Daubechies, Ten Lectures on Wavelets, CBMS-NSF Regional Conference Series in Applied Mathematics, vol. 61, SIAM, Philadelphia, 1992.
[27] B. Bénichou, N. Saito, Sparsity vs. statistical independence in adaptive signal representations: A case study of the spike process, in: G.V. Welland (Ed.), Beyond Wavelets, in: Stud. Comput. Math., vol. 10, Academic Press, San Diego, CA, 2003, pp. 225–257, Ch. 9.
[28] N. Saito, The generalized spike process, sparsity, and statistical independence, in: D. Rockmore, J.D. Healy (Eds.), Modern Signal Processing, in: MSRI Publications, vol. 46, Cambridge Univ. Press, 2004, pp. 317–340.
[29] Z. Wang, A.C. Bovik, H.R. Sheikh, E.P. Simoncelli, Image quality assessment: From error measurement to structural similarity, IEEE Trans. Image Process. 13 (4) (2004) 600–613.
[30] W.B. Pennebaker, J.L. Mitchell, JPEG Still Image Data Compression Standard, Van Nostrand Reinhold, New York, 1993.
[31] G.K. Wallace, The JPEG still picture compression standard, IEEE Trans. Consumer Electron. 38 (1) (1992) xviii–xxxiv.
[32] R.R. Coifman, M.V. Wickerhauser, Entropy-based algorithms for best basis selection, IEEE Trans. Inform. Theory 38 (2) (1992) 713–719.
[33] J. Rissanen, Stochastic Complexity in Statistical Inquiry, World Scientific, Singapore, 1989.
[34] M.H. Hansen, B. Yu, Model selection and the principle of minimum description length, J. Amer. Statist. Assoc. 96 (454) (2001) 746–774.
[35] Y.G. Leclerc, Constructing simple stable descriptions for image partitioning, Intern. J. Computer Vision 3 (1989) 73–102.
[36] N. Saito, Simultaneous noise suppression and signal compression using a library of orthonormal bases and the minimum description length criterion, in: E. Foufoula-Georgiou, P. Kumar (Eds.), Wavelets in Geophysics, Academic Press, San Diego, CA, 1994, pp. 299–324, Ch. XI.
[37] S.G. Chang, B. Yu, M. Vetterli, Adaptive wavelet thresholding for image denoising and compression, IEEE Trans. Image Process. 9 (9) (2000) 1532–1546.
[38] M. Hansen, B. Yu, Wavelet thresholding via MDL: Simultaneous denoising and compression, IEEE Trans. Inform. Theory 46 (5) (2000) 1778–1788.
[39] E.Y. Lam, J.W. Goodman, A mathematical analysis of the DCT coefficient distributions for images, IEEE Trans. Image Process. 9 (10) (2000) 1661–1666.
[40] R.A. DeVore, Wavelets and approximation, Presented at the SPIE Conference on Wavelets X, August 2003.

[41] R.A. DeVore, V.N. Temlyakov, Nonlinear approximation by trigonometric sums, J. Fourier Anal. Appl. 2 (1) (1995) 29–48.
[42] F.G. Meyer, R.R. Coifman, Brushlets: A tool for directional image analysis and image compression, Appl. Comput. Harmon. Anal. 4 (1997) 147–187.
[43] G.B. Folland, Introduction to Partial Differential Equations, second ed., Princeton Univ. Press, 1995.
[44] K. Yamatani, N. Saito, Improvement of DCT-based compression algorithms using Poisson's equation, Technical report, Department of Mathematics, University of California, Davis, 2005, in preparation.
[45] N. Smith, The higher dimensional extension of the polyharmonic local trigonometric transforms, Ph.D. thesis, Department of Mathematics, University of California, Davis, 2005, in preparation.
[46] C. Lanczos, A simple interpolation method for the representation of rugged curves, Abstract of contributed paper given at the November Meeting of the AMS in Cleveland, OH, November 25–26, 1938.
[47] C. Lanczos, Smoothing of noisy data by trigonometric truncation, in: National Bureau of Standards Report, No. 1582, 1952, pp. 1–16.
[48] C. Lanczos, Discourse on Fourier Series, Hafner, New York, 1966.
[49] A. Zygmund, Trigonometrical Series, Chelsea, 1952.
[50] C. Lanczos, Applied Analysis, Prentice–Hall, Englewood Cliffs, NJ, 1956, republished by Dover Publications, 1988.
[51] C. Lanczos, Linear Differential Operators, D. Van Nostrand, New York, 1961, republished by Dover Publications, 1997.
[52] L.V. Kantrovich, V.I. Krylov, Approximate Methods of Higher Analysis, Interscience, New York, 1958.
[53] A.S. Maliev, Fourier series of heightened convergence for functions defined in a given interval, Izv. AN SSSR OMEN 10 (1932) 1437–1450.
[54] A.S. Maliev, On the expansion in Fourier series of heightened convergence of functions defined in a given interval, Izv. AN SSSR OMEN 8 (1933) 1113–1120 (in Russian).
[55] V.I. Smirnov, A Course of Higher Mathematics, vol. II, Pergamon Press, New York, 1964, translated by D.E. Brown.
[56] W.R. Madych, S.A. Nelson, Polyharmonic cardinal splines, J. Approx. Theory 60 (2) (1990) 141–156.
[57] W.R. Madych, S.A. Nelson, Polyharmonic cardinal splines: A minimization property, J. Approx. Theory 63 (3) (1990) 303–320.
[58] O.I. Kounchev, Minimizing the Laplacian of a function squared with prescribed values on interior boundaries—Theory of polysplines, Trans. Amer. Math. Soc. 350 (5) (1998) 2105–2128.
[59] O. Kounchev, Multivariate Polysplines: Applications to Numerical and Wavelet Analysis, Academic Press, San Diego, CA, 2001.
[60] M. Taibleson, Fourier coefficients of functions of bounded variation, Proc. Amer. Math. Soc. 18 (4) (1967) 766.
[61] T.W. Körner, Fourier Analysis, Cambridge Univ. Press, 1988.

APPENDIX SHIRANI01

screenshot-catalog.libraries.psu.edu-2023.12.05-15_44_41
https://catalog.libraries.psu.edu/catalog/1181068/marc_view
05.12.2023

MARC View

LEADER 07877nas a22009611a 4500				
001 1181068				
003 SIRSI				
005 20151215050216.0				
008 830531c19839999nyumr 0 0eng d				
010				a| 83643067 z| sn82005410
019				a| MARS
022	0			a| 0733-8716
035				a| LIAS1351817
035				a| (OCoLC)9450566
040				d| UtOrBLW
245	0	0		a| IEEE journal on selected areas in communications : b| a publication of the IEEE Communications Society.
246	3	9		a| IEEE journal on selected areas in communications
246	3	0		a| Selected areas in communications
264		1		a| New York, N.Y. : b| Institute of Electrical and Electronics Engineers, c| [1983-]
264		4		c| ©1983-
300				a| volumes : b| illustrations ; c| 28 cm
310				a| Monthly, b| 2005-
321				a| Frequency varies, b| 1983-2004
336				a| text b| txt 2| rdacontent
337				a| unmediated b| n 2| rdamedia
338				a| volume b| nc 2| rdacarrier
362	0			a| Vol. SAC-1, no. 1 (Jan. 1983)- v.SAC-5, no. 9 (1987) ; Vol. 6, no. 1 (Jan. 1988)-
710	2			a| Institute of Electrical and Electronics Engineers.
710	2			a| IEEE Communications Society.
533				a| Microform. b| [New York, N.Y.? c| IEEE], d| 19__? e| microfiches ; 11 x 15 cm.
949				a| Microfiche w| ASIS c| 1 i| 1181068-1001 d| 3/19/2001 l| MICROS-HB m| HARRISBURG r| Y s| Y t| MICROFORM u| 4/13/2001
949				a| TK5101.A1I16 v.SAC-1 1983 w| LCPER c| 1 i| 000018892062 d| 3/19/2001 e| 3/19/2001 l| ACAD-BLDG m| UP-ANNEX r| Y s| Y t| PERIODICAL u| 4/13/2001 z| 862
949				a| TK5101.A1I16 v.SAC-3 no.4-6 1985 w| LCPER c| 1 i| 000045496486 l| ACAD-BLDG m| UP-ANNEX r| Y s| Y t| PERIODICAL u| 2/12/2002 z| 862
949				a| TK5101.A1I16 v.SAC-2 1984 w| LCPER c| 1 i| 000060038159 l| ACAD-BLDG m| UP-ANNEX r| Y s| Y t| PERIODICAL u| 10/3/2007 z| 862
949				a| TK5101.A1I16 v.SAC-3 no.1-3 1985 w| LCPER c| 1 i| 000060038166 l| ACAD-BLDG m| UP-ANNEX r| Y s| Y t| PERIODICAL u| 10/3/2007 z| 862
949				a| TK5101.A1I16 v.SAC-4 no.1-5 1986 w| LCPER c| 1 i| 000060038067 l| ACAD-BLDG m| UP-ANNEX r| Y s| Y t| PERIODICAL u| 10/3/2007 z| 865
949				a| TK5101.A1I16 v.SAC-4 no.6-9 1986 w| LCPER c| 1 i| 000060038074 l| ACAD-BLDG m| UP-ANNEX r| Y s| Y t| PERIODICAL u| 10/3/2007 z| 865
949				a| TK5101.A1I16 v.SAC-5 no.1-4 1987 w| LCPER c| 1 i| 000060037954 l| ACAD-BLDG m| UP-ANNEX r| Y s| Y t| PERIODICAL u| 10/3/2007 z| 865
949				a| TK5101.A1I16 v.SAC-5 no.5-9 1987 w| LCPER c| 1 i| 000060037961 l| ACAD-BLDG m| UP-ANNEX r| Y s| Y t| PERIODICAL u| 10/3/2007 z| 865
949				a| TK5101.A1I16 v.SAC-6 no.1-5 1988 w| LCPER c| 1 i| 000060037978 l| ACAD-BLDG m| UP-ANNEX r| Y s| Y t| PERIODICAL u| 10/3/2007 z| 865
949				a| TK5101.A1I16 v.6 no.6-9 1988 w| LCPER c| 1 i| 000060037985 l| ACAD-BLDG m| UP-ANNEX r| Y s| Y t| PERIODICAL u| 10/3/2007 z| 865
949				a| TK5101.A1I16 v.7 no.1-5 1989 w| LCPER c| 1 i| 000060037893 l| ACAD-BLDG m| UP-ANNEX r| Y s| Y t| PERIODICAL u| 10/3/2007 z| 865
949				a| TK5101.A1I16 v.7 no.6-9 1989 w| LCPER c| 1 i| 000060037800 l| ACAD-BLDG m| UP-ANNEX r| Y s| Y t| PERIODICAL u| 10/3/2007 z| 865
949				a| TK5101.A1I16 v.8 Jan-Apr 1990 w| LCPER c| 1 i| 000018894073 l| CATO-2 m| UP-ANNEX r| Y s| Y t| PERIODICAL u| 3/5/2003 z| 7769
949				a| TK5101.A1I16 v.8 May-Aug 1990 w| LCPER c| 1 i| 000018894080 l| CATO-2 m| UP-ANNEX r| Y s| Y t| PERIODICAL u| 3/5/2003 z| 7769

949	a| TK5101.A1I16 v.8 Sept-Dec 1990 w| LCPER c| 1 i| 000018894097 l| CATO-2 m| UP-ANNEX r| Y s| Y t| PERIODICAL u| 3/5/2003 z| 7769
949	a| TK5101.A1I16 v.9 Jan-Apr 1991 w| LCPER c| 1 i| 000018894103 l| CATO-2 m| UP-ANNEX r| Y s| Y t| PERIODICAL u| 3/5/2003 z| 7769
949	a| TK5101.A1I16 v.9 May-Aug 1991 w| LCPER c| 1 i| 000018894110 l| CATO-2 m| UP-ANNEX r| Y s| Y t| PERIODICAL u| 3/5/2003 z| 7769
949	a| TK5101.A1I16 v.9 Sept-Dec 1991 w| LCPER c| 1 i| 000018894127 l| CATO-2 m| UP-ANNEX r| Y s| Y t| PERIODICAL u| 3/5/2003 z| 7769
949	a| TK5101.A1I16 v.10 Jan-June 1992 w| LCPER c| 1 i| 000018894134 l| CATO-2 m| UP-ANNEX r| Y s| Y t| PERIODICAL u| 3/5/2003 z| 7769
949	a| TK5101.A1I16 v.10 Aug-Dec 1992 w| LCPER c| 1 i| 000018894141 l| CATO-2 m| UP-ANNEX r| Y s| Y t| PERIODICAL u| 3/5/2003 z| 7769
949	a| TK5101.A1I16 v.11 Jan-June 1993 w| LCPER c| 1 i| 000018894158 d| 10/11/2006 l| CATO-2 m| UP-ANNEX q| 1 r| Y s| Y t| PERIODICAL u| 3/5/2003 z| 7769
949	a| TK5101.A1I16 v.11 Aug-Dec 1993 w| LCPER c| 1 i| 000018894165 d| 10/11/2006 l| CATO-2 m| UP-ANNEX q| 1 r| Y s| Y t| PERIODICAL u| 3/5/2003 z| 7769
949	a| TK5101.A1I16 v.12 Jan-May 1994 w| LCPER c| 1 i| 000018894172 l| CATO-2 m| UP-ANNEX r| Y s| Y t| PERIODICAL u| 3/5/2003 z| 7769
949	a| TK5101.A1I16 v.12 June-Dec 1994 w| LCPER c| 1 i| 000018894189 l| CATO-2 m| UP-ANNEX r| Y s| Y t| PERIODICAL u| 3/5/2003 z| 7769
949	a| TK5101.A1I16 v.13 Jan-June 1995 w| LCPER c| 1 i| 000018894196 l| CATO-2 m| UP-ANNEX r| Y s| Y t| PERIODICAL u| 3/5/2003 z| 7769
949	a| TK5101.A1I16 v.13 Aug-Dec 1995 w| LCPER c| 1 i| 000018894202 d| 9/18/2008 l| CATO-2 m| UP-ANNEX q| 1 r| Y s| Y t| PERIODICAL u| 3/5/2003 z| 7769
949	a| TK5101.A1I16 v.14 Jan-June 1996 w| LCPER c| 1 i| 000018894219 l| CATO-2 m| UP-ANNEX r| Y s| Y t| PERIODICAL u| 3/5/2003 z| 7769
949	a| TK5101.A1I16 v.14 July-Dec 1996 w| LCPER c| 1 i| 000018894226 l| CATO-2 m| UP-ANNEX r| Y s| Y t| PERIODICAL u| 3/5/2003 z| 7769
949	a| TK5101.A1I16 v.15 Jan-June 1997 w| LCPER c| 1 i| 000018894233 l| CATO-2 m| UP-ANNEX r| Y s| Y t| PERIODICAL u| 3/5/2003 z| 7769
949	a| TK5101.A1I16 v.15 July-Dec 1997 w| LCPER c| 1 i| 000018894240 l| CATO-2 m| UP-ANNEX r| Y s| Y t| PERIODICAL u| 3/5/2003 z| 7769
949	a| TK5101.A1I16 v.16 Feb-June 1998 w| LCPER c| 1 i| 000018894257 l| CATO-2 m| UP-ANNEX r| Y s| Y t| PERIODICAL u| 3/5/2003 z| 7769
949	a| TK5101.A1I16 v.16 Aug-Dec 1998 w| LCPER c| 1 i| 000018894264 l| CATO-2 m| UP-ANNEX r| Y s| Y t| PERIODICAL u| 3/5/2003 z| 7769
949	a| TK5101.A1I16 v.17 Jan-June 1999 w| LCPER c| 1 i| 000018894271 l| CATO-2 m| UP-ANNEX r| Y s| Y t| PERIODICAL u| 3/5/2003 z| 7769
949	a| TK5101.A1I16 v.17 July-Dec 1999 w| LCPER c| 1 i| 000018894288 l| CATO-2 m| UP-ANNEX r| Y s| Y t| PERIODICAL u| 3/5/2003 z| 7769
949	a| TK5101.A1I16 v.18 Jan-June 2000 w| LCPER c| 1 i| 000018894295 d| 7/11/2003 l| CATO-2 m| UP-ANNEX q| 1 r| Y s| Y t| PERIODICAL u| 3/5/2003 z| 7769
949	a| TK5101.A1I16 v.18 July-Sept.2000 w| LCPER c| 1 i| 000047609952 l| CATO-2 m| UP-ANNEX r| Y s| Y t| PERIODICAL u| 11/1/2001 z| 7769
949	a| TK5101.A1I16 v.18 Oct.-Dec.2000 w| LCPER c| 1 i| 000047609808 l| CATO-2 m| UP-ANNEX r| Y s| Y t| PERIODICAL u| 11/1/2001 z| 7769
949	a| TK5101.A1I16 v.19 Jan-Mar 2001 w| LCPER c| 1 i| 000048255431 l| CATO-2 m| UP-ANNEX r| Y s| Y t| PERIODICAL u| 11/28/2001 z| 7769
949	a| TK5101.A1I16 v.19 Apr-June 2001 w| LCPER c| 1 i| 000048255424 l| CATO-2 m| UP-ANNEX r| Y s| Y t| PERIODICAL u| 11/28/2001 z| 7769
949	a| TK5101.A1I16 v.19 July-Sept 2001 w| LCPER c| 1 i| 000048424660 l| CATO-2 m| UP-ANNEX r| Y s| Y t| PERIODICAL u| 11/4/2002 z| 7769
949	a| TK5101.A1I16 v.20 Jan-June 2002 w| LCPER c| 1 i| 000051870089 d| 7/7/2004 l| CATO-2 m| UP-ANNEX q| 1 r| Y s| Y t| PERIODICAL u| 5/2/2003 z| 7769
949	a| TK5101.A1I16 v.20 Aug-Dec 2002 w| LCPER c| 1 i| 000051870157 l| CATO-2 m| UP-ANNEX r| Y s| Y t| PERIODICAL u| 5/2/2003 z| 7769
949	a| TK5101.A1I16 v.21 Jan-June 2003 w| LCPER c| 1 i| 000052812422 l| CATO-2 m| UP-ANNEX r| Y s| Y t| PERIODICAL u| 3/17/2004 z| 7769
949	a| TK5101.A1I16 v.21 Aug-Dec 2003 w| LCPER c| 1 i| 000052812415 l| CATO-2 m| UP-ANNEX r| Y s| Y t| PERIODICAL u| 3/17/2004 z| 7769
949	a| TK5101.A1I16 v.22 Jan-June 2004 w| LCPER c| 1 i| 000054847187 l| CATO-2 m| UP-ANNEX r| Y s| Y t| PERIODICAL u| 4/8/2005 z| 7769
949	a| TK5101.A1I16 v.22 Aug-Dec 2004 w| LCPER c| 1 i| 000054847194 l| CATO-2 m| UP-ANNEX r| Y s| Y t| PERIODICAL u| 4/7/2005 z| 7769
949	a| TK5101.A1I16 v.23 Jan-Apr 2005 w| LCPER c| 1 i| 000054976375 l| CATO-2 m| UP-ANNEX r| Y s| Y t| PERIODICAL u| 4/18/2006 z| 7769
949	a| TK5101.A1I16 v.23 May-Aug 2005 w| LCPER c| 1 i| 000054976368 l| CATO-2 m| UP-ANNEX r| Y s| Y t| PERIODICAL u| 4/18/2006 z| 7769
949	a| TK5101.A1I16 v.23 Sept-Dec 2005 w| LCPER c| 1 i| 000054976351 l| CATO-2 m| UP-ANNEX r| Y s| Y t| PERIODICAL u| 4/18/2006

			z| 7769
949			a| TK5101.A1I16 v.24 Jan-Apr 2006 w| LCPER c| 1 i| 000055217415 l| CATO-2 m| UP-ANNEX r| Y s| Y t| PERIODICAL u| 6/12/2007 z| 7769
949			a| TK5101.A1I16 v.24 May-Aug 2006 w| LCPER c| 1 i| 000055217293 l| CATO-2 m| UP-ANNEX r| Y s| Y t| PERIODICAL u| 6/12/2007 z| 7769
949			a| TK5101.A1I16 v.24 Sept-Dec 2006 w| LCPER c| 1 i| 000055217422 l| CATO-2 m| UP-ANNEX r| Y s| Y t| PERIODICAL u| 6/12/2007 z| 7769
852	0	1	a| PSt b| UP-ANNEX c| ANNEX h| TK5101.A1 i| I16
866		0	8| 0 a| v.SAC-1(1983)-v.SAC-6:no.5(1988), v.6:no.6(1988)-v.15(1997), v.16:Feb.(1998)-v.24(2006)
852	8		a| PSt b| HARRISBURG c| MICROS-HB h| Microfiche
866		0	8| 0 a| v.1 1983-v.17 1999

PennState

Copyright @2019 The Pennsylvania State University. All rights reserved. Except where otherwise noted, this work is subject to a Creative Commons Attribution 4.0 license. Details and exceptions.

Legal Statements | PSU Hotlines

PENN STATE UNIVERSITY LIBRARIES

Libraries Home (814) 865-6368
Libraries Intranet (Staff Only)
Accessibility Help
Website Feedback
Policies and Guidelines
Staff Directory

screenshot-catalog.libraries.psu.edu-2023.12.05-15_43_54
https://catalog.libraries.psu.edu/catalog/1181068
05.12.2023

IEEE journal on selected areas in communications : a publication of the IEEE Communications Society

Additional Titles:	IEEE journal on selected areas in communications and Selected areas in communications
Published:	New York, N.Y. : Institute of Electrical and Electronics Engineers, [1983-]
Copyright Date:	©1983-
Physical Description:	volumes : illustrations ; 28 cm
Additional Creators:	Institute of Electrical and Electronics Engineers and IEEE Communications Society

Availability

Browse Nearby on Shelf I Want It

Penn State Harrisburg (1 item)

Call number	Material	Location
Harrisburg - Microforms - 2nd Floor - In-Library Use: Holdings Summary v.1 1983-v.17 1999		
Microfiche	Microfilm, Microfiche, etc.	Harrisburg - Microforms - 2nd Floor - In-Library Use

Library Storage (52 items)

Call number	Material	Location
Annexed Material: Holdings Summary v.SAC-1(1983)-v.SAC-6:no.5(1988), v.6:no.6(1988)-v.15(1997), v.16:Feb.(1998)-v.24(2006)		
TK5101.A1I16 v.6 no.6-9 1988	Bound Journal	Annexed Material
TK5101.A1I16 v.7 no.1-5 1989	Bound Journal	Annexed Material
TK5101.A1I16 v.7 no.6-9 1989	Bound Journal	Annexed Material
TK5101.A1I16 v.8 Jan-Apr 1990	Bound Journal	Annexed Material
TK5101.A1I16 v.8 May-Aug 1990	Bound Journal	Annexed Material
TK5101.A1I16 v.8 Sept-Dec 1990	Bound Journal	Annexed Material
TK5101.A1I16 v.9 Jan-Apr 1991	Bound Journal	Annexed Material
TK5101.A1I16 v.9 May-Aug 1991	Bound Journal	Annexed Material
TK5101.A1I16 v.9 Sept-Dec 1991	Bound Journal	Annexed Material
TK5101.A1I16 v.10 Aug-Dec 1992	Bound Journal	Annexed Material
TK5101.A1I16 v.10 Jan-June 1992	Bound Journal	Annexed Material
TK5101.A1I16 v.11 Aug-Dec 1993	Bound Journal	Annexed Material
TK5101.A1I16 v.11 Jan-June 1993	Bound Journal	Annexed Material
TK5101.A1I16 v.12 Jan-May 1994	Bound Journal	Annexed Material
TK5101.A1I16 v.12 June-Dec 1994	Bound Journal	Annexed Material
TK5101.A1I16 v.13 Aug-Dec 1995	Bound Journal	Annexed Material
TK5101.A1I16 v.13 Jan-June 1995	Bound Journal	Annexed Material
TK5101.A1I16 v.14 Jan-June 1996	Bound Journal	Annexed Material
TK5101.A1I16 v.14 July-Dec 1996	Bound Journal	Annexed Material
TK5101.A1I16 v.15 Jan-June 1997	Bound Journal	Annexed Material
TK5101.A1I16 v.15 July-Dec 1997	Bound Journal	Annexed Material

TK5101.A1I16 v.16 Aug-Dec 1998	Bound Journal	Annexed Material
TK5101.A1I16 v.16 Feb-June 1998	Bound Journal	Annexed Material
TK5101.A1I16 v.17 Jan-June 1999	Bound Journal	Annexed Material
TK5101.A1I16 v.17 July-Dec 1999	Bound Journal	Annexed Material
TK5101.A1I16 v.18 Jan-June 2000	Bound Journal	Checked out
TK5101.A1I16 v.18 July-Sept.2000	Bound Journal	Annexed Material
TK5101.A1I16 v.18 Oct.-Dec.2000	Bound Journal	Annexed Material
TK5101.A1I16 v.19 Apr-June 2001	Bound Journal	Annexed Material
TK5101.A1I16 v.19 Jan-Mar 2001	Bound Journal	Annexed Material
TK5101.A1I16 v.19 July-Sept 2001	Bound Journal	Annexed Material
TK5101.A1I16 v.20 Aug-Dec 2002	Bound Journal	Annexed Material
TK5101.A1I16 v.20 Jan-June 2002	Bound Journal	Annexed Material
TK5101.A1I16 v.21 Aug-Dec 2003	Bound Journal	Annexed Material
TK5101.A1I16 v.21 Jan-June 2003	Bound Journal	Annexed Material
TK5101.A1I16 v.22 Aug-Dec 2004	Bound Journal	Annexed Material
TK5101.A1I16 v.22 Jan-June 2004	Bound Journal	Annexed Material
TK5101.A1I16 v.23 Jan-Apr 2005	Bound Journal	Annexed Material
TK5101.A1I16 v.23 May-Aug 2005	Bound Journal	Annexed Material
TK5101.A1I16 v.23 Sept-Dec 2005	Bound Journal	Annexed Material
TK5101.A1I16 v.24 Jan-Apr 2006	Bound Journal	Annexed Material
TK5101.A1I16 v.24 May-Aug 2006	Bound Journal	Annexed Material
TK5101.A1I16 v.24 Sept-Dec 2006	Bound Journal	Annexed Material
TK5101.A1I16 v.SAC-1 1983	Bound Journal	Annexed Material
TK5101.A1I16 v.SAC-2 1984	Bound Journal	Annexed Material
TK5101.A1I16 v.SAC-3 no.1-3 1985	Bound Journal	Annexed Material
TK5101.A1I16 v.SAC-3 no.4-6 1985	Bound Journal	Annexed Material
TK5101.A1I16 v.SAC-4 no.1-5 1986	Bound Journal	Annexed Material
TK5101.A1I16 v.SAC-4 no.6-9 1986	Bound Journal	Annexed Material
TK5101.A1I16 v.SAC-5 no.1-4 1987	Bound Journal	Annexed Material
TK5101.A1I16 v.SAC-5 no.5-9 1987	Bound Journal	Annexed Material
TK5101.A1I16 v.SAC-6 no.1-5 1988	Bound Journal	Annexed Material

Dates of Publication and/or Sequential Designation:
Vol. SAC-1, no. 1 (Jan. 1983)- v.SAC-5, no. 9 (1987) ; Vol. 6, no. 1 (Jan. 1988)-

ISSN:
0733-8716

Publication Frequency:
Monthly, 2005-
Frequency varies, 1983-2004

Reproduction Note:
Microform. [New York, N.Y.? IEEE], 19__? microfiches ; 11 x 15 cm.

View MARC record | catkey: 1181068

PennState

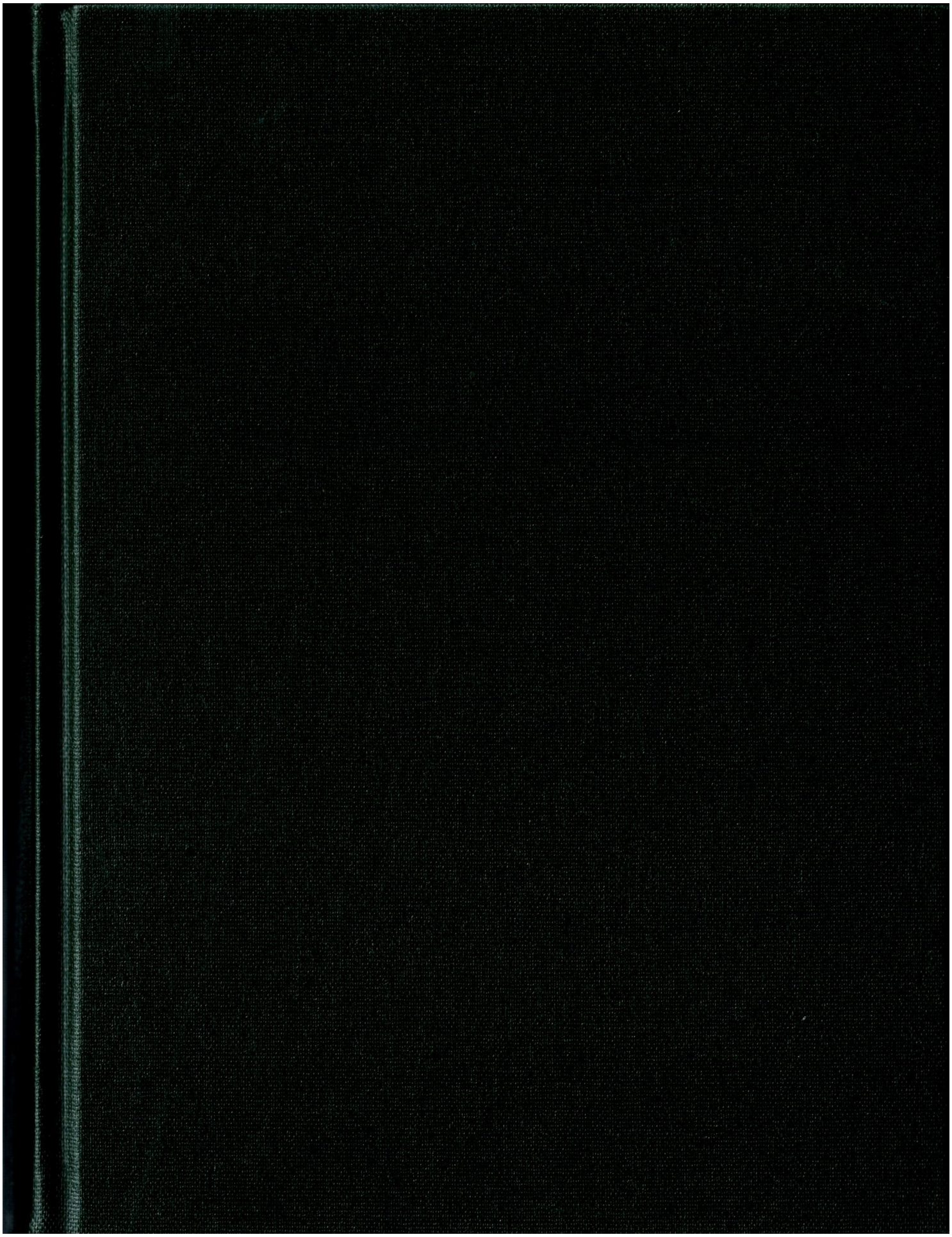
Copyright @2019 The Pennsylvania State University. All rights reserved. Except where otherwise noted, this work is subject to a Creative Commons Attribution 4.0 license. Details and exceptions.

Legal Statements | PSU Hotlines

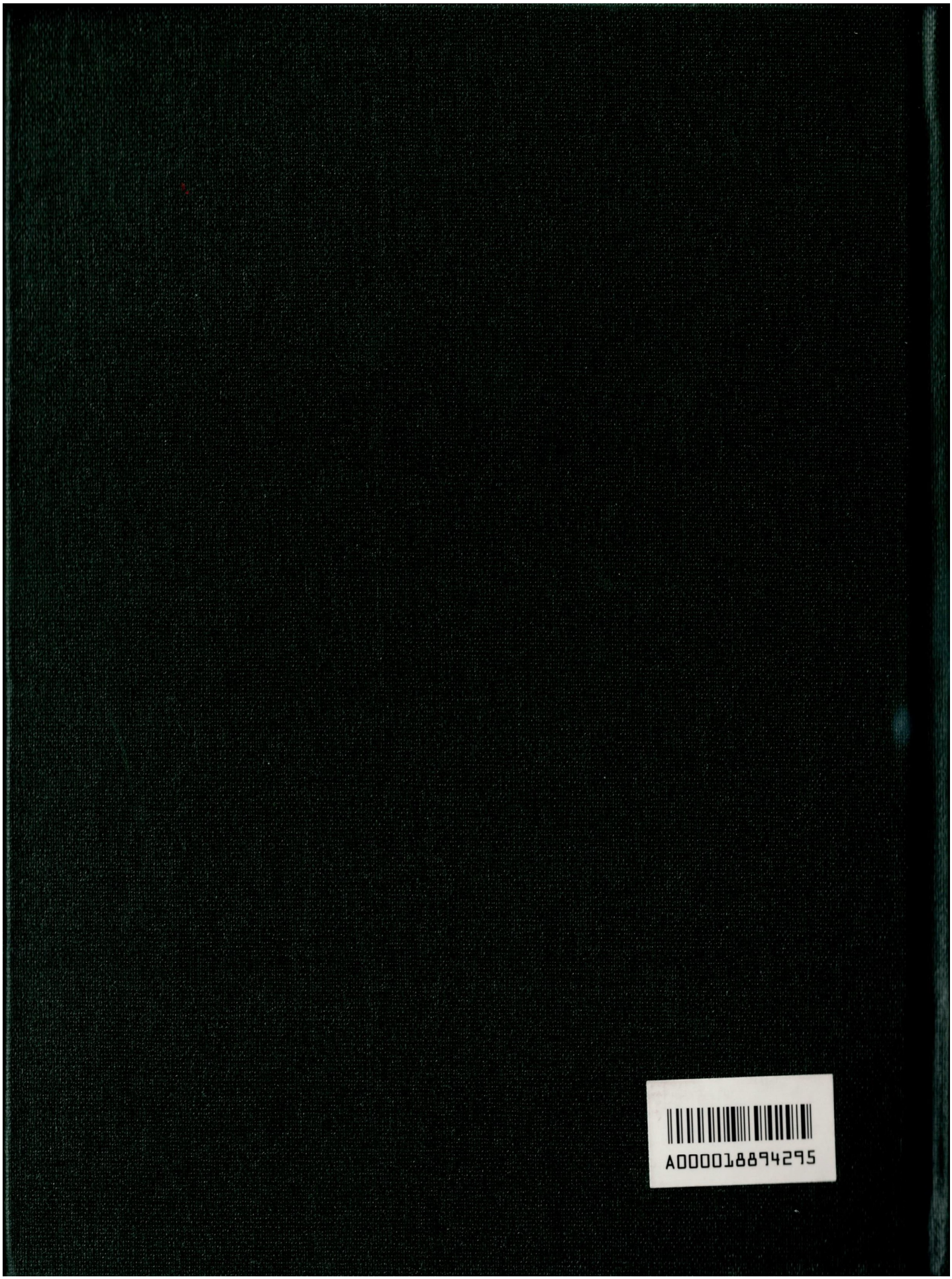
PENN STATE UNIVERSITY LIBRARIES

Libraries Home (814) 865-6368
Libraries Intranet (Staff Only)
Accessibility Help
Website Feedback
Policies and Guidelines
Staff Directory

APPENDIX SHIRANI02




IEEE JOURNAL ON SELECTED AREAS IN COMMUNICATIONS 18 JAN-JUNE 2000 ENGIN TK5101 .A1 I16
126


A000018894295

ENGINEERING LIBRARY

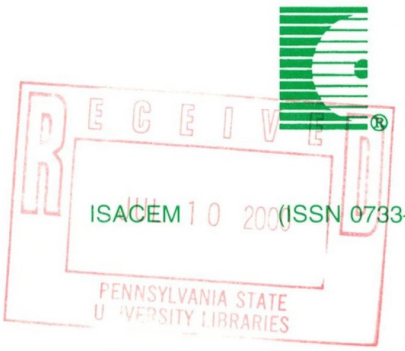
SHELVED IN
BOUND
PERIODICAL
COLLECTION

Engin

IEEE JOURNAL ON

SELECTED AREAS IN COMMUNICATIONS

A PUBLICATION OF THE IEEE COMMUNICATIONS SOCIETY



JUNE 2000 VOLUME 18 NUMBER 6 ISACEM (ISSN 0733–8716)

ERROR-RESILIENT IMAGE AND VIDEO TRANSMISSION

Guest Editors—C. W. Chen, P. Cosman, N. Kingsbury, J. Liang, and J. W. Modestino

Guest Editorial ..... *C. W. Chen, P. Cosman, N. Kingsbury, J. Liang, and J. W. Modestino* 809

PAPERS

Unequal Error Protection of SPIHT Encoded Image Bit Streams ..... *A. A. Alatan, M. Zhao, and A. N. Akansu* 814
Unequal Loss Protection: Graceful Degradation of Image Quality over Packet Erasure Channels Through Forward Error Correction ..... *A. E. Mohr, E. A. Riskin, and R. E. Ladner* 819
A Vector Set Partitioning Noisy Channel Image Coder with Unequal Error Protection ..... *D. Mukherjee and S. K. Mitra* 829
Power Minimization for Delivering Integrated Multimedia Services over Digital Subscriber Line ..... *H. Zheng and K. J. R. Liu* 841
Progressive Transmission of Images over Memoryless Noisy Channels ..... *V. Chande and N. Farvardin* 850
Arithmetic Coding-Based Continuous Error Detection for Efficient ARQ-Based Image Transmission ..... *J. Chou and K. Ramchandran* 861
Turbo Codes for Image Transmission—A Joint Channel and Source Decoding Approach ..... *Z. Peng, Y.-F. Huang, and D. J. Costello, Jr.* 868
Combined Source-Channel Coding Schemes for Video Transmission over an Additive White Gaussian Noise Channel ..... *M. Bystrom and J. W. Modestino* 880
A Wavelet Domain Diversity Method for Transmission of Images over Wireless Channels ..... *L. C. Ramac and P. K. Varshney* 891
Error-Resilient Coding in JPEG-2000 and MPEG-4 ..... *I. Moccagatta, S. Soudagar, J. Liang, and H. Chen* 899
Permuted Smoothed Descriptions and Refinement Coding for Images ..... *J. Ridge, F. W. Ware, and J. D. Gibson* 915
Robust Image Transmission Using Resynchronizing Variable-Length Codes and Error Concealment ..... *S. S. Hemami* 927
Image Coding with Robust Channel-Optimized Trellis-Coded Quantization ..... *T.-T. Lam, G. P. Abousleman, and L. J. Karam* 940

(Contents Continued on Back Cover)

(Contents Continued from Front Cover)

Optimal Mode Selection and Synchronization for Robust Video Communications over Error-Prone Networks ..... *G. Côté, S. Shirani, and F. Kossentini* 952
Video Coding with Optimal Inter/Intra-Mode Switching for Packet Loss Resilience ..... *R. Zhang, S. L. Regunathan, and K. Rose* 966
An End-to-End Approach for Optimal Mode Selection in Internet Video Communication: Theory and Application ..... *D. Wu, Y. T. Hou, B. Li, W. Zhu, Y.-Q. Zhang, and H. J. Chao* 977
Efficient Video Transmission over Correlated Nakagami Fading Channels for IS-95 CDMA Systems ..... *N. H. L. Chan and P. T. Mathiopoulos* 996
Analysis of Video Transmission over Lossy Channels ..... *K. Stuhlmüller, N. Färber, M. Link, and B. Girod* 1012
Error Recovery for Interactive Video Transmission over the Internet ..... *I. Rhee and S. R. Joshi* 1033
Error-Resilient Video Transmission Using Long-Term Memory Motion-Compensated Prediction ..... *T. Wiegand, N. Färber, K. Stuhlmüller, and B. Girod* 1050
Error-Resilient Transcoding for Video over Wireless Channels ..... *G. de los Reyes, A. R. Reibman, S.-F. Chang, and J. C.-I. Chuang* 1063
Loss-Resilient ATM Protocol Architecture for MPEG-2 Video Communications ..... *P. Cuenca, L. Orozco-Barbosa, F. J. Quiles, and A. Garrido* 1075
MPEG-4 Image Transmission Using MAP Source-Controlled Channel Decoding ..... *R. E. Van Dyck* 1087
Zerotree Pattern Coding of Motion Picture Residues for Error-Resilient Transmission of Video Sequences ..... *J. A. Robinson and Y. Shu* 1099
DCT Information Recovery of Erroneous Image Blocks by a Neural Predictor ..... *F. G. B. De Natale, C. Perra, and G. Vernazza* 1111
A Concealment Method for Video Communications in an Error-Prone Environment ..... *S. Shirani, F. Kossentini, and R. Ward* 1122
Error Concealment in MPEG Video Streams over ATM Networks ..... *P. Salama, N. B. Shroff, and E. J. Delp* 1129

Upcoming Issues of the IEEE JOURNAL ON SELECTED AREAS IN COMMUNICATIONS

Topic	Date of Call*
Analysis and Synthesis of MAC Protocols	March 1999
Wideband CDMA	April 1999
Protocols and Architectures for Next Generation Optical WDM Networks	April 1999
Quality of Service (QoS) in the Internet	June 1999
Signal Processing for High Density Storage Channels	September 1999
Active and Programmable Networks	November 1999
The Turbo Principle: From Theory to Practice	December 1999
IEEE J-SAC: Wireless Communications Series	Ongoing

*Issue of J-SAC in which the Call for Papers first appears.

A Concealment Method for Video Communications in an Error-Prone Environment

Shahram Shirani, *Member, IEEE*, Faouzi Kossentini, *Senior Member, IEEE*, and Rabab Ward, *Fellow, IEEE*

***Abstract*—In this paper, we propose a two-stage error-concealment method for block-based compressed video which was transmitted in an error-prone environment. In the first stage, we obtain initial estimates of the missing blocks. If the motion vectors associated with the missing blocks are available, motion compensation is used to provide good estimates. Otherwise, a novel algorithm which preserves image continuity is used to estimate the blocks. In the second stage, a maximum *a posteriori* (MAP) estimator, which employs an adaptive Markov random field (MRF) as the image *a priori* model, is used to improve the video reconstruction quality. The adaptive model enables the estimation to incorporate information embedded not only in the immediate neighborhood pixels but also in a wider neighborhood into the reconstruction procedure without increasing the order of the MRF model. The proposed concealment method achieves very good computation–performance tradeoffs, as demonstrated via experimental results.**

***Index Terms*—Error concealment, image reconstruction, Markov random fields.**

I. Introduction

DIGITAL image and video signals require very high bit rates, thus, compression of such signals before their transmission is necessary. Communication channels are not error free and, consequently, the encoded bit streams are vulnerable to transmission errors—usually causing loss of blocks of data and/or loss of synchronization. Despite the various methods that have been proposed to combat or localize the effects of channel errors, the quality of a decoded video sequence may degrade significantly because of the residual errors. Error concealment intends to conceal the effects of such errors by exploiting redundancies in the video signal and limitations of the human visual system, without requiring additional information.

Temporal concealment methods are usually used for error concealment in inter-coded frames. Data of an inter-coded block are composed of the motion vector and the DCT coefficients of the prediction error. If the motion vectors are received without errors, the missing blocks are set to their corresponding motion compensated blocks. Since in many of the video compression algorithms (e.g., H.263) the coded motion vectors and the DCT coefficients are interleaved, the loss of data of a block usually results in the loss of both the motion vectors and the DCT coefficients.[1] Therefore, most of the proposed temporal concealment methods first estimate the motion vector associated with a missing block using the motion vectors of adjacent blocks [1], [2]. The estimated motion vector is then used to find a block in the previous frame which yields the restoration of the missing block. One problem associated with these methods is that if the adjacent blocks are coded in a nonpredictive way (e.g., intra-coded), there would not be any data available to estimate the missing motion vectors. Thus, ad hoc assumptions for estimating the missing motion vector should be made, and the results may be unreliable. Moreover, if the missing block lies on the boundary of two objects moving in opposite directions, such methods will perform quite poorly.

Spatial error-concealment methods restore the missing blocks using the information in the current frame. In [3], to restore the missing data, a measure of variations (e.g., gradient or Laplacian) between adjacent pixels is minimized. The underlying smoothness assumption of this method limits its ability in restoring image details. In [4], each pixel in a damaged block is interpolated from the corresponding pixels in its four neighboring blocks such that the total squared border error is minimized. In [5] and [6], the missing information is interpolated utilizing spatially correlated edge information from a large local neighborhood. Note that although these edge-based methods are generally more accurate than other approaches, they are computationally more intensive. In [7], a computationally simple, spatial directional interpolation scheme has been proposed. The two nearest surrounding layers of pixels of a missing block are converted into a binary pattern to reveal the local geometrical structure. Then, the missing pixels are interpolated in a way to preserve the local geometrical structures. In the statistical error concealment methods, for example the one proposed in [8], it is assumed that the pixel values in an image or video signal are realizations of an underlying statistical model (e.g., MRF model). The statistical approaches of spatial error concealment are expected to outperform the deterministic ones, as they provide a systematic way for incorporating the *a priori* information about the video signal in the restoration procedure.

Previous spatial error-concealment methods employing the MRF model usually yield blurry images with a significant loss of detail in the high frequency or edge portions of the image. This is due to 1) the type of the MRF selected as the image model, and 2) the fact that the amount of information that is

Manuscript received May 4, 1999; revised November 30, 1999. This work was supported by MDSI, BC ASI, and NSERC.

The authors are with the Department of Electrical and Computer Engineering, University of British Columbia, Vancouver, BC, V6T 1Z4, Canada.

Publisher Item Identifier S 0733-8716(00)04337-7.

[1]Recognizing the need to improve the concealment capabilities, in the new generation of video compression standards (e.g., MPEG 4, H.263++), the motion information is separated from other information through partitioning of the coded data.

0733–8716/00$10.00 © 2000 IEEE

used in the reconstruction process is often restricted to a single-pixel wide region around the erroneous area. Incorporating more pixels in order to enhance restoration of edges and high-frequency parts would usually require a higher order MRF model. However, this is computationally expensive, as the complexity grows exponentially with the order of the MRF model.

In this paper, we propose a two-stage error-concealment method for compressed video. In the first stage, if applicable, we use the information in the previous frame to obtain initial estimates of the missing blocks. If the motion vectors of the missing blocks are available, motion compensation is used to provide the estimates. Otherwise, an algorithm which preserves image continuity is employed to compute the initial estimates. In the second stage, a MAP estimator is used for refinement of the initial estimates. The MAP estimator employs an adaptive MRF as the image *a priori* model. The proposed adaptive MRF takes into account the local image characteristics embedded not only in the immediate neighborhood pixels of the damaged area but also in a wider neighborhood without a dramatic increase in computational complexity. Our concealment method improves on the existing statistical methods in that it yields good reconstruction performance regardless of the content of the missing blocks.

To make the compressed data more error resilient, most of the standard-compliant video compression systems partitioned a video frame into Groups of Blocks (GOB's) or "slices," which are coded independently. Therefore, the output bit stream usually consists of segments separated with markers, where each segment corresponds to the coded data of the blocks in a GOB or a slice. When channel errors occur, the decoder usually discards the erroneous data between two markers surrounding the erroneous data, effectively discarding the GOB or the slice. Then, loss of data of a slice does not affect the rest of the compressed video sequence. In our work, it is assumed that the frames of the coded video sequence are partitioned into GOB's or slices and, thus, the missing data belong to blocks of a GOB or a slice. Moreover, it is assumed that the decoder knows the locations of the missing blocks. This information (e.g., the checksum information) can be obtained from the network or it can be inferred, for example, by detecting the semantic or syntactic violations as a result of errors [9].

The rest of this paper is organized as follows. In Section II, MAP estimation of missing data is briefly reviewed. Section III presents the proposed error concealment method. Section IV discusses the computational complexity of the proposed method. Sections V and VI present our experimental results and conclusions, respectively.

II. MAP Estimation of Missing Data

Let the corrupted image be represented by the vector $\boldsymbol{Y}$, while the decompressed image without errors can be represented by $\boldsymbol{X}$. Using MAP estimation, the decompressed image estimate is given by

$$\hat{\boldsymbol{X}} = \arg\max_{\boldsymbol{X}} \log \Pr(\boldsymbol{X} \mid \boldsymbol{Y}).$$

Using the Bayes' rule we, obtain

$$\begin{aligned}\hat{\boldsymbol{X}} &= \arg\max_{\boldsymbol{X}} \left\{ \log \frac{\Pr(\boldsymbol{Y} \mid \boldsymbol{X}) \Pr(\boldsymbol{X})}{\Pr(\boldsymbol{Y})} \right\} \\ &= \arg\max_{\boldsymbol{X}} \{ \log \Pr(\boldsymbol{Y} \mid \boldsymbol{X}) + \log \Pr(\boldsymbol{X}) \} \end{aligned} \tag{1}$$

where the term $\log \Pr(\boldsymbol{Y})$ has been dropped because it is independent of $\boldsymbol{X}$. The corrupted image can be expressed as $\boldsymbol{Y} = \mathcal{T}\boldsymbol{X}$, where $\mathcal{T}$ is the transform that converts the decompressed image $\boldsymbol{X}$ into the corrupted one $\boldsymbol{Y}$.[2] The conditional probability of the corrupted image can be then written as follows:

$$\Pr(\boldsymbol{Y} \mid \boldsymbol{X}) = \begin{cases} 1: & \boldsymbol{Y} = \mathcal{T}\boldsymbol{x} \\ 0: & \boldsymbol{Y} \neq \mathcal{T}\boldsymbol{x}. \end{cases} \tag{2}$$

Substituting (2) in (1), the MAP estimation becomes

$$\hat{\boldsymbol{X}} = \arg\min_{\boldsymbol{X} \in \mathcal{S}} \{ -\log \Pr(\boldsymbol{X}) \} \tag{3}$$

where $\mathcal{S} = \{\boldsymbol{z}: \boldsymbol{Y} = \mathcal{T}\boldsymbol{z}\}$.

For image *a priori* model $(\Pr(\boldsymbol{X}))$, we use the MRF. According to the Hammersley–Clifford theorem, every MRF should have a Gibbs distribution [10] in the following form:

$$\Pr(\boldsymbol{X} = x) = \frac{1}{Z} \exp\left\{ -\sum_{c \in C} V_c(x) \right\} \tag{4}$$

where Z is a normalizing constant, $V_c(\cdot)$ is called a potential function and is a function of a local group of pixels c called clique, and C denotes the set of all cliques throughout the image. The potential function characterizes the relationship between a group of pixels by assigning larger costs to configurations of pixels which are less likely to occur. The choice of the potential function impacts substantially the performance of the image model. The function $\sum_{c \in C} V_c(x)$ should be convex in order to have an easily obtainable global minimum. Otherwise, local minima will be present, and the function must then be minimized via a computationally expensive technique such as simulated annealing. Commonly, the potential functions are selected to be of the form

$$\sum_{c \in C} V_c(x) = \sum_{c \in C} \rho\left(\boldsymbol{d}_{\boldsymbol{c}}^{\boldsymbol{t}} \boldsymbol{x}\right) \tag{5}$$

where $\boldsymbol{d}_{\boldsymbol{c}}$ is a coefficient vector, $\boldsymbol{x}$ is the vector of pixels in the clique c, and $\rho(\cdot)$ is the cost function. The convexity property of the cost function insures that the $\sum_{c \in C} V_c(x)$ remains convex. The coefficients $\boldsymbol{d}_{\boldsymbol{c}}$ are usually selected such that $\boldsymbol{d}_{\boldsymbol{c}}^{\boldsymbol{t}} \boldsymbol{x}$ provides an approximation of the first or second derivative of the image at each pixel. For the special case of $\rho(x) = x^2$, the model is called a Gauss–Markov random field (GMRF).

III. Proposed Method

As mentioned earlier, our method consists of two stages. The purpose of the first stage of our method is to obtain an initial estimate of the missing block using information from the previous frame. If the missing block has been intra-coded, the initial estimate is set to zero. If the missing block has been inter-coded, and its motion vector is received correctly (e.g., because the encoded

[2]See [8] for a more detailed discussion of the transform.

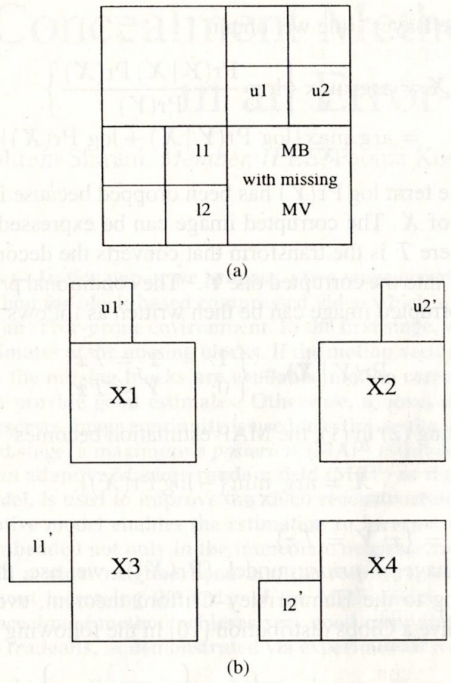


Fig. 1. (a) The four subblocks, (b) their corresponding subblocks in the previous frame, and the blocks connected to them.

data have been partitioned), then the estimate is set to the corresponding motion compensation block. When the motion vector is not available, we find an estimate of the missing block such that image continuity inside the block and across its boundaries is preserved [11]. To do this, subblocks adjacent to the missing block, i.e., $u1, u2, l1$, and $l2$ in Fig. 1(a), are considered. First, for each of these subblocks, a corresponding subblock in the previous frame is determined. The corresponding subblock is found by searching a small area around the point corresponding to the center of each of the subblocks $u1, u2, l1, l2$ in the previous frame. The sum of absolute differences is used as the measure of similarity. The four subblocks $u1, u2, l1, l2$ and their corresponding subblocks $u1', u2', l1', l2'$ in the previous frame are shown in Fig. 1(a) and (b). For example, $u1'$ is the subblock corresponding to $u1$. Then, four blocks, namely $\boldsymbol{X1}, \boldsymbol{X2}, \boldsymbol{X3}$, and $\boldsymbol{X4}$, which are connected to $u1', u2', l1'$, and $l2'$ (respectively), are determined. To obtain an initial estimate of the missing block that smoothly connects to the rest of the image, a block from the above four blocks that minimizes the squared sums of border errors, between the estimated block and its adjacent above and left blocks, is selected. Thus,

$$\hat{\boldsymbol{X}} = \arg \min_{\boldsymbol{X1},\boldsymbol{X2},\boldsymbol{X3},\boldsymbol{X4}} \epsilon^2$$

where

$$\epsilon^2 = \epsilon_T^2 + \epsilon_L^2. \tag{6}$$

Each of the border errors ϵ_T and ϵ_L is defined in terms of pixels by

$$\epsilon_T^2 = \|(\hat{\boldsymbol{x}}_t - \boldsymbol{p}_{\mathrm{Tb}})\|^2 \quad \text{and} \quad \epsilon_L^2 = \|(\hat{\boldsymbol{x}}_l - \boldsymbol{p}_{\mathrm{Lr}})\|^2$$

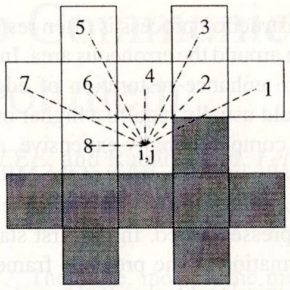


Fig. 2. A pixel, its clique c, and the eight directions. The complement of the clique c' is the dark area.

where the vector $\boldsymbol{p}_{\mathrm{Tb}}$ consists of the bottom line pixels of the block to the top of the missing block, and $\boldsymbol{p}_{\mathrm{Lr}}$ consists of the right column pixels of the block to the left of missing block. The vectors $\hat{\boldsymbol{x}}_t$ and $\hat{\boldsymbol{x}}_l$ are those elements of the estimated block $\hat{\boldsymbol{X}}$ that correspond to the pixels in its top row and left column, respectively. To ensure the online applicability (e.g., concealment while decoding the blocks in raster scan), only subblocks to the left and above the missing block are used. If the condition of online concealment is relaxed, the same method can be extended to include the subblocks of the blocks to the right and below of the missing block.

The estimation of motion of the subblocks has a high computational overhead which can possibly introduce unacceptable requirements on decoder. The computational overhead can be reduced if the search for displacement of each of the subblocks is restricted to a set of candidate motion vectors. This is a decoder option and can be used to trade performance against computational complexity. The set consists of the motion vector of the block corresponding to the missing block in the previous frame, the motion vectors of available neighboring blocks, the median of the motion vectors of available neighboring blocks, the average of the motion vectors of available neighboring blocks, and the zero motion vector [2].

In the second stage of our proposed error-concealment method, the information around each missing block is used to refine the initial estimate. This stage is based on a MAP estimator. We consider a GMRF model with an eight-pixel clique around each pixel as the image *a priori* model (see Fig. 2). The reason for selecting an eight-pixel clique in the manner shown in Fig. 2 will become clear later. The potential function of (5) is selected as

$$\sum_{c \in C} V_c(x) = \sum_i \sum_j \sum_{(k,l) \in c} w_{i,j \to k,l}\, \rho(x_{i,j} - x_{k,l}) \tag{7}$$

where c is the clique, $w_{i,j \to k,l}$ is the weight assigned to the difference between the values of the pixel in position (i, j) and the pixel in its clique at position (k, l) and $\rho(x) = x^2$.

Combining the MAP estimator of (3) with the image model [(4) and (7)], the restoration of missing data eventuates in the following minimization problem:

$$\hat{\boldsymbol{X}} = \min_{x_{i,j}} \sum_{i,j \in \mathcal{M}} \sum_{k,l \in c} w_{i,j \to k,l}\, \rho(x_{i,j} - x_{k,l}) \tag{8}$$

where $\mathcal{M}$ is the set of all missing pixels in the frame. Since $\rho(x) = x^2$ is a convex function, the above minimization problem yields a unique global solution. In fact, the estimated value of a pixel is given by

$$\hat{x}_{i,j} = \sum_{(k,l)\in c\cup c'} w_{i,j\to k,l}\ x_{k,l} \Big/ \sum_{(k,l)\in c\cup c'} w_{i,j\to k,l} \qquad (9)$$

where c is the clique and c' is its complement shown in Fig. 2.

In our adaptive MRF model, the weight corresponding to the difference between a pixel and one of the pixels in its clique [$w_{i,j\to k,l}$ in (9)] is selected adaptively, based on the likelihood of an edge in the direction of the subject pair of pixels. The rationale behind this selection is to weigh more the difference between the pixels in that direction which will cause the values of the pixels in that direction to get closer to each other. The likelihood of edges in each of the eight directions is computed using blocks around the missing block. In this way, the available information in a larger area is exploited without increasing the order of the MRF model (which increases dramatically the computational complexity). To determine the likelihood of edges in each of the eight directions, edges in the blocks surrounding the missing block whose directions imply that they pass through the missing block are determined. That is, we first obtain

$$g_x = x_{i+1,j-1} - x_{i-1,j-1} + 2x_{i+1,j} - 2x_{i-1,j} + x_{i+1,j+1} - x_{i-1,j+1}$$

and

$$g_y = x_{i-1,j+1} - x_{i-1,j-1} + 2x_{i,j+1} - 2x_{i,j-1} + x_{i+1,j+1} - x_{i+1,j-1}$$

for every pixel in the blocks to the left, right, top, and bottom of the missing block. The magnitude and angular direction of the edge at pixel (i,j) are

$$G = \sqrt{g_x^2 + g_y^2} \quad \text{and} \quad \theta = \arctan\left(\frac{g_y}{g_x}\right)$$

where θ determines if the edge at pixel (i,j) passes through the missing block. Since there are eight pixels in the clique, the value of θ is rounded to one of the eight directions equally spaced in the range from 0° to 180°. There is a counter c_m $(m = 1,2,\ldots,8)$ for each of the eight directions. If the extension of an edge at pixel (i,j) belonging to one of the neighboring blocks passes through the missing area, the counter for that particular direction is incremented by the amount of G. Since the employed edge detector is sensitive to the image noise, the values of c_ms, $m = 1,\ldots,8$ are compared to a threshold. If any of them is less than the threshold, it is set to zero.

There are eight pixels in the clique of each pixel, and eight directions for the detected edges. Each pixel in the clique of a pixel corresponds to a direction. In our proposed method, $w_{i,j\to k,l}$ is selected based on the edge counter of the direction corresponding to (i,j) and (k,l), i.e.,

$$w_{i,j\to k,l} = \beta c_m \qquad (10)$$

where β is a constant and c_m is the counter corresponding to direction m, and direction m corresponds to the direction formed by (i,j) and (k,l). Finally, the second stage of the proposed error-concealment method can be summarized as follows. 1) Determine the edges in the neighboring blocks and assign them to eight equally spaced directions. Compute the counter for each direction. 2) Use (10) to find a set of weights for each missing block. 3) Use (9) to obtain an estimate of each missing pixel employing the weights obtained in the previous step. 4) Iteratively reestimate the missing pixels using (9) until convergence. Note that since the cost function is convex, convergence is guaranteed.

For intra-coded blocks, the missing pixel values are initially set to zero and then the MAP estimator, using the adaptive MRF and the data of the neighboring blocks, is applied. For missing inter-coded blocks, an initial estimate are obtained using information from the previous frame. Estimates of the prediction errors are found using the adaptive MRF model along with the prediction error signals of the neighboring blocks. The estimated values are then added to the initial estimates. Since the prediction error signal consists mostly of high-frequency components, the MAP estimation stage (i.e., the second stage) will improve the video reconstruction quality, especially around the edges.

IV. Computational Complexity

The numbers provided below for computational complexity correspond to a block and subblock of sizes 16 × 16 and 8 × 8, respectively. The computational load of the first stage of the proposed method consists of those computations required in 1) estimating the motion, and 2) computing the error of (6). For motion estimation, we used a spiral search method using an area of 16 × 16. This requires approximately 197 000 operations. If the search for the displacement of each of the subblocks is restricted to the set of candidate motion vectors explained in Section III, the required number of operation will reduce to 6100. The number of operations required to find the total error of (6) for four blocks is approximately 380.

For the second stage, the computational load consists of those computations required in adapting the weights of the MRF model, which are approximately 18 400 operations for a missing block, assuming four available neighboring blocks. The estimation of missing pixels using (9) is an iterative procedure which, for each iteration, requires approximately 30 operations for each missing pixel, or 16 × 16 × 30 operations for each missing block. On average, 80 iterations are required for the algorithm to converge for a block.

Clearly, the computational load of our error-concealment method is quite reasonable. Our simulation experiments confirm that the run time of our method is indeed acceptable. In fact, real-time decoding (e.g., 10 frames/s for QCIF video sequences) is still possible on a Pentium 300 MHz PC.

V. Experimental Results

Although the method proposed in this paper is general and can be applied to any block-based video compression method, H.263 is used as our video coding framework. QCIF (176 × 144) video sequences at a temporal resolution of 10 frames/s are

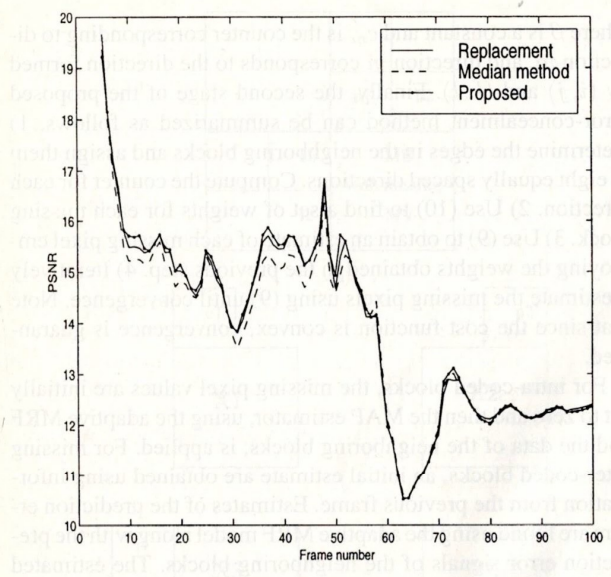


Fig. 3. PSNR values for image sequence Foreman with 10% GOB missing for different concealment methods.

coded at 64 kbps and then decoded in the presence of slice/GOB errors. The size of the blocks is 16×16, that of the subblock is 8×8.

To simulate the channel errors, the following tasks are performed. Coded video information is first grouped into packets, where each video packet consists of the coded data of a GOB or a slice. The video packets are then multiplexed with audio information according to the H.223 standard. We used an H.223 multiplexing simulator which receives video packets, simulates audio traffic, applies errors to the multiplexed bit stream according to an error pattern stored in a file, and outputs the packets [12]. The error pattern that we employed corresponds to a mobile channel [13]. Burst errors will most likely not corrupt two consecutive video packet, since audio packets are inserted between them. The erroneous bit stream is decoded such that the effect of errors will appear as missing slices/GOB's.

For inter-coded blocks, our error concealment consists of obtaining an initial estimate of the missing block using information from the previous frame, and finding an estimate of the prediction error using the adaptive MRF model. We compare the performance of the above method with two other methods: 1) a replacement method, where a missing block is replaced with the same block in the previous frame; and 2) a median method, where the motion vector of a missing block is set to the median of motion vectors of blocks to the left, above and above-right of it, and the estimated motion vector is used to obtain a motion compensation block which serves as the concealment of the missing block. Here, we consider only the case where a GOB is placed in each of the video packets. Shown in Fig. 3 are the concealment PSNR values for the three methods mentioned above for the video sequence Foreman with a 10% packet (GOB) loss rate. As can be seen, for video sequences with a large amount of motion like Foreman, the performance of the proposed method and the median method are close to each other, and both are better than the replacement method. Although the performance



Fig. 4. An inter-coded frame of the sequence Foreman concealed by the (a) replacement, (b) median, and (c) proposed methods.

of the above methods is comparable in terms of PSNR, the video sequences obtained using the proposed method are more visually appealing than the ones obtained using the other two methods. Fig. 4(a), (b), and (c) shows the reconstructed video frame (inter-coded) of the video sequence Foreman. As can be seen in the images, the replacement method does not generate good results, especially around the nose area. Moreover, the concealment result of the proposed method is clearly better than that of the other two methods.

For intra-coded blocks, we compare the performance of our method (which consists of estimating the missing block using the adaptive MRF model) to that of four other efficient methods: 1) a MAP estimator using a nonadaptive GMRF as the *a priori* model where each missing pixel is basically set to the average of the pixels around it, 2) a suboptimal version of the MAP estimator where a missing pixel is set to the median of pixels around it [8], 3) the deterministic method proposed in [4], and 4) the deterministic method proposed in [3]. Although there are other deterministic methods that are likely to outperform the above two methods, for example, the ones proposed in [6] and [7], we restrict our comparison to the above two deterministic methods. In fact, a direct comparison of our method, which is statistical, to deterministic methods is difficult because of different design approaches. Our main aim here is to compare our method to previously proposed statistical methods.

In this experiment, we employ different video sequences and different packetization schemes. In the first set of simulation experiments, we assign a slice which consists of one block, to a packet. Fig. 5(a) shows a frame of the image sequence Foreman encoded and decoded using an H.263 compliant coder. Fig. 5(b)–(g), shows (respectively) the same frame: 1) missing approximately 20% of the packets (blocks), 2) reconstructed using the nonadaptive GMRF model, 3) using the suboptimal MRF model, 4) using the method proposed in [4], 5) using the method proposed in [3], and 6) using our proposed adaptive MRF error concealment method. Clearly, our proposed method performs best in reconstruction quality, particularly in retrieving the edges and in the areas of the frame that correspond to adjacent missing blocks.

In the next set of simulation experiments, we assign the coded data of a GOB, which consists of 11 blocks, to each of the video packets. Fig. 6(a) shows a frame of the video sequence Foreman with two missing packets (GOB's), at approximately 18% loss rate. Fig. 6(b) and (c) shows the error- concealment result obtained using the nonadaptive GMRF model and suboptimal MRF models, respectively. Fig. 6(d) and (e) shows the result obtained using the methods proposed in [4] and [3], respectively. Fig. 6(f) shows the result obtained using our adaptive

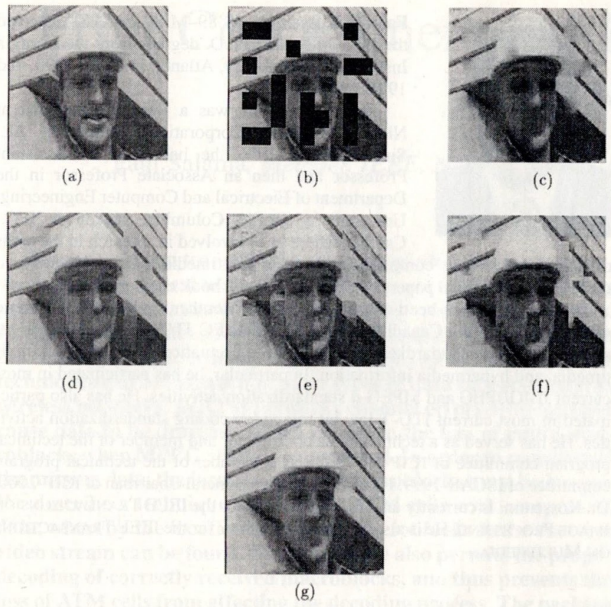


Fig. 5. A frame from the video sequence Foreman: (a) original; (b) missing blocks; reconstructed using (c) a nonadaptive GMRF model; (d) a suboptimal MRF model; (e) the method proposed in [4]; (f) the method proposed in [3]; and (g) our adaptive MRF model.

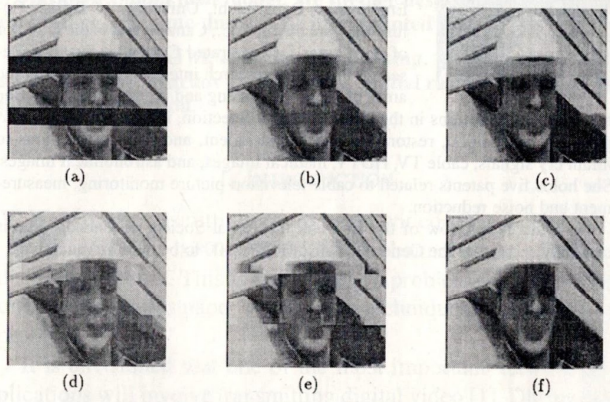


Fig. 6. A frame from the video sequence Foreman: (a) with missing GOB's, reconstructed using (b) a nonadaptive GMRF model; (c) a suboptimal MRF model; (d) the method proposed in [4]; (e) the method proposed in [3]; and (f) our adaptive MRF model.

MRF model. By comparing the figures, the superior performance of our method becomes obvious. This performance advantage is demonstrated in the blocks that contain edges. For a quantitative evaluation, Table I provides the PSNR values of the above concealment methods (for both packetization cases) for the video sequence Foreman. The table demonstrates that our method outperforms the other methods by at least 2 dB.

Finally, we compare the computational complexity of our method in terms of required number of additions and multiplications to the methods proposed in [4] and [3]. The total number of additions and multiplications required for restoring a 16 × 16 block are approximately 4500 and 20 000 using the method proposed in [4] and our method, respectively. The method proposed in [3] requires approximately 650 000 additions and multiplications to restore a 16 × 16 block. Therefore, the number of computations of our method is 4.4:1 larger than that of [4] and 1:0.03 less than those of [3]. However, our method outperforms [4] substantially in terms of the quality of the reconstructed images. This can be seen in Figs. 5 and 6. This quality improvement justifies, in most applications, the additional computational complexity.

TABLE I
PSNR (dB) COMPARISON OF DIFFERENT METHODS FOR THE VIDEO SEQUENCE FOREMAN

Method	No loss	20% Block loss	GOB missing
GMRF	32.1	26.3	25.3
Suboptimal MRF	32.1	25.4	23.1
Method proposed in [4]	32.1	24.3	23.8
Method proposed in [3]	32.1	25.2	24.1
Adaptive MRF	32.1	28.6	27.2

VI. CONCLUSION

This paper introduces a new method of error concealment for block-based coded video communications over error-prone channels. The proposed method employs an adaptive MRF as the image *a priori* model in a MAP estimation paradigm. The adaptation enables the estimation procedure to incorporate more information without increasing the order of the MRF. The proposed concealment method is able to restore missing blocks located in smooth and low-frequency areas, as well as in high-frequency and edge portions of a video frame. Our concealment method achieves very good computation–performance tradeoffs, and outperforms previously proposed MRF-based concealment methods.

ACKNOWLEDGMENT

The authors would like to thank the anonymous reviewers for their insightful comments and constructive suggestions. The authors would also like to gratefully acknowledge the help and support provided by G. Cote, their colleague in the Signal Processing and Multimedia Group at the University of British Columbia.

REFERENCES

[1] M. Ghanbari and V. Seferidis, "Cell loss concealment in ATM video codecs," *IEEE Trans. Circuit System Video Technol.*, vol. 3, pp. 238–247, June 1993.
[2] W. M. Lam, A. R. Reibman, and B. Liu, "Recovery of lost or erroneously received motion vectors," in *Proc. Int. Conf. Acoust., Speech, Signal Processing*, vol. V, 1993, pp. 417–420.
[3] Y. Wang, Q. F. Zhu, and L. Shaw, "Maximally smooth image recovery in transform coding," *IEEE Trans. Commun.*, vol. 41, pp. 1544–1551, Oct. 1993.
[4] S. S. Hemami and T. H. Y. Meng, "Transform coded image reconstruction exploiting interblock correlations," *IEEE Trans. Image Processing*, vol. 4, pp. 1023–1027, July 1995.
[5] H. Sun and W. Kwok, "Concealment of damaged block transform coded images using projection onto convex sets," *IEEE Trans. Image Processing*, vol. 4, pp. 470–477, Apr. 1995.
[6] W. Kwok and H. Sun, "Multi-directional interpolation for spatial error concealment," *IEEE Trans. Consumer Electron.*, vol. 39, pp. 455–460, Aug. 1993.
[7] W. Zeng and B. Liu, "Geometric-structure-based error concealment with novel applications in block-based low-bit-rate coding," *IEEE Trans. Circuits Syst. Video Technol.*, vol. 9, pp. 648–665, June 1999.

[8] P. Salama, N. Shroff, E. J. Coyle, and E. J. Delp, "Error concealment in encoded video streams," in *Signal Recovery Techniques for Image and Video Compression and Transmission*, N. P. Galatsanos and A. K. Katsaggelos, Eds. Boston, MA: Kluwer Academic, 1998.

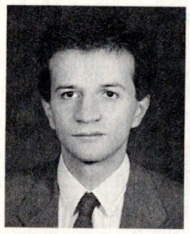
[9] R. Talluri, "Error resilient video coding in the MPEG-4 standard," *IEEE Commun. Mag.*, vol. 26, pp. 112–119, June 1998.

[10] S. Geman and D. Geman, "Stochastic relaxation, Gibbs distribution, and the Bayesian restoration of images," *IEEE Trans. Pattern Anal. Machine Intell.*, vol. 11, pp. 689–691, 1984.

[11] S. Shirani, F. Kossentini, and R. Ward, "Reconstruction of motion vector missing macroblocks in H.263 encoded video transmission over lossy networks," in *Proc. Int. Conf. Image Processing*, vol. III, Oct. 1998, pp. 487–491.

[12] G. Sullivan, "A Simple Video Packet Mux Simulator Program for Video Streams in H.263/M Using AL3 Mux of H.223 Annex B," ITU-T Study Group 15, Video Coding Expert Group, Doc. Q15-F-16, Nov. 1996.

[13] Ericsson Sweden, "WCDMA Error Patterns at 64 kb/s," ITU-T Study Group 16, Multimedia Terminals and Systems Expert Group, Cannes, France, June 1998.



Shahram Shirani (S'88–M'89) received the B.Sc. degree in electrical engineering from Esfahan University of Technology, Esfahan, Iran, in 1989 and the M.Sc. degree in biomedical engineering from Amirkabir University of Technology, Tehran, Iran in 1994. Currently, he is pursuing the Ph.D. degree in the Department of Electrical and Computer Engineering, University of British Columbia, Vancouver, B.C., Canada.

From 1994 to 1996, he was with the Department of Electrical Engineering, University of Tehran. His research interests include image and video compression, video communications, signal processing and ultrasonic imaging.



Faouzi Kossentini (S'89–M'89–SM'98) received the B.S., M.S., and Ph.D. degrees from the Georgia Institute of Technology, Atlanta, in 1989, 1990, and 1994, respectively.

During 1995, he was a Research Scientist at Nichols Research Corporation, Huntsville, AL. Since January 1996, he has been an Assistant Professor and then an Associate Professor in the Department of Electrical and Computer Engineering, University of British Columbia, vancouver, B.C., Canada, where he is involved in research in the areas of signal processing, communications, and multimedia. He has coauthored more than 100 journal papers, conference papers, book chapters and patents.

Dr. Kossentini has been active as a Voting Member, and recently as head of delegation, of the Canadian delegate to ISO/IEC JTC1/SC29, which is responsible for the standardization of coded representation of audiovisual, multimedia, and hypermedia information. In particular, he has participated in most current JBIG/JPEG and MPEG-4 standardization activities. He has also participated in most current ITU-T low bit rate video coding standardization activities. He has served as a technical area coordinator and member of the technical program committee of ICIP-1997, and as a Member of the technical program committee of ISCAS-1999. He is also the Vice General Chairman of ICIP-2000. Dr. Kossentini is currently an Associate Editor for the IEEE TRANSACTIONS ON IMAGE PROCESSING. He is also an Associate Editor for the IEEE TRANSACTIONS ON MULTIMEDIA.



Rabab Ward (F'98) received the B.Sc. degree in electrical engineering from University of Cairo, Egypt, in 1966 and the M.Sc. and the Ph.D. in electrical and computer engineering from University of California, Berkeley, in 1969 and 1972, respectively.

She is a Professor in the Electrical and Computer Engineering Department, University of British Columbia, Vancouver, B.C., Canada, and is the Director of the Center for Integrated Computer Systems Research there. Her research interests are mainly in the areas of signal processing and image processing. She has made contributions in the areas of signal detection, image encoding, compression, recognition, restoration and enhancement, and their applications to infant cry signals, cable TV, HDTV, medical images, and astronomical images. She holds five patents related to cable television picture monitoring, measurement and noise reduction.

Dr. Ward is a fellow of the EIC and the Royal Society of Canada. She is currently serving as the General Chair of ICIP'2000 to be held in Vancouver.

Wert
Bookbinding
Grantville, PA
JULY-DEC 2000
"We're Quality Bound"

APPENDIX STOCKHAMMER01

screenshot-catalog.libraries.psu.edu-2023.12.18-12_34_43
https://catalog.libraries.psu.edu/catalog/1397806
18.12.2023

MARC View

LEADER 04464nas a22007211a 4500			
001 1397806			
003 SIRSI			
005 20151215012754.0			
008 910515c19919999xx qu 0 0eng d			
010			a| 91642188 z| sn90001281
019			a| MARS
022	0		a| 1051-8215
030			a| ITCTEM
032			a| 006329 b| USPS
035			a| LIAS1562226
035			a| (CStRLIN)MDJGAEF1049-S
035			a| (OCoLC)24382124
040			d| UtOrBLW
050	0	0	a| TK6630.A1 b| I37
245	0	0	a| IEEE transactions on circuits and systems for video technology.
246	3	0	a| Circuits and systems for video technology
264		1	a| New York, NY : b| Institute of Electrical and Electronics Engineers, c| [1991-]
264		4	c| ©1991-
300			a| volumes : b| illustrations ; c| 28 cm
310			a| Quarterly.
336			a| text b| txt 2| rdacontent
337			a| unmediated b| n 2| rdamedia
338			a| volume b| nc 2| rdacarrier
362	0		a| Vol. 1, no. 1 (Mar. 1991)-
500			a| Title from cover.
550			a| "A publication of the Circuits and Systems Society.
650		0	a| High definition television v| Periodicals.
650		0	a| Digital television v| Periodicals.
650		0	a| Image processing x| Digital techniques v| Periodicals.
650		0	a| Resolution (Optics) v| Periodicals.
710	2		a| IEEE Circuits and Systems Society.
710	2		a| Institute of Electrical and Electronics Engineers. t| IEEE Xplore.
533			a| Microfiche. b| [New York, N.Y.? c| IEEE], e| microfiches ; 11 x 15 cm.
949			a| Microfilm w| ASIS c| 1 i| 1397806-1001 d| 11/7/2000 l| MICROS-HB m| HARRISBURG r| Y s| Y t| MICROFORM u| 4/13/2001
949			a| TK6679.I33 v.1 1991 w| LCPER c| 1 i| 000051829223 l| CATO-2 m| UP-ANNEX r| Y s| Y t| PERIODICAL u| 4/2/2003 z| 7757
949			a| TK6679.I33 v.2 1992 w| LCPER c| 1 i| 000051829230 l| CATO-2 m| UP-ANNEX r| Y s| Y t| PERIODICAL u| 4/2/2003 z| 7757
949			a| TK6679.I33 v.3 1993 w| LCPER c| 1 i| 000051829247 l| CATO-2 m| UP-ANNEX r| Y s| Y t| PERIODICAL u| 4/2/2003 z| 7757

949			a| TK6679.I33 v.4 1994 w| LCPER c| 1 i| 000051829254 l| CATO-2 m| UP-ANNEX r| Y s| Y t| PERIODICAL u| 4/2/2003 z| 7757
949			a| TK6679.I33 v.5-6 1995-1996 w| LCPER c| 1 i| 000051829261 d| 10/13/2023 e| 10/13/2023 k| CHECKEDOUT l| CATO-2 m| UP-ANNEX n| 1 r| M s| Y t| PERIODICAL u| 4/2/2003 z| 7757
949			a| TK6679.I33 v.7 1997 w| LCPER c| 1 i| 000051829278 l| CATO-2 m| UP-ANNEX r| Y s| Y t| PERIODICAL u| 4/2/2003 z| 7757
949			a| TK6679.I33 v.8 1998 w| LCPER c| 1 i| 000051829285 l| CATO-2 m| UP-ANNEX r| Y s| Y t| PERIODICAL u| 4/2/2003 z| 7757
949			a| TK6679.I33 v.9 1999 w| LCPER c| 1 i| 000051829292 l| CATO-2 m| UP-ANNEX r| Y s| Y t| PERIODICAL u| 4/2/2003 z| 7757
949			a| TK6679.I33 v.10 no.1-4 2000 w| LCPER c| 1 i| 000048234948 d| 11/7/2000 l| CATO-2 m| UP-ANNEX r| Y s| Y t| PERIODICAL u| 4/13/2001 z| 7757
949			a| TK6679.I33 v.10 no.5-8 2000 w| LCPER c| 1 i| 000048234931 l| CATO-2 m| UP-ANNEX r| Y s| Y t| PERIODICAL u| 10/2/2001 z| 7757
949			a| TK6679.I33 v.11 no.1-6 2001 w| LCPER c| 1 i| 000048427524 l| CATO-2 m| UP-ANNEX r| Y s| Y t| PERIODICAL u| 11/5/2002 z| 7757
949			a| TK6679.I33 v.11 no.7-12 2001 w| LCPER c| 1 i| 000048427517 l| CATO-2 m| UP-ANNEX r| Y s| Y t| PERIODICAL u| 11/5/2002 z| 7757
949			a| TK6679.I33 v.12 no.1-6 2002 w| LCPER c| 1 i| 000052496431 l| CATO-2 m| UP-ANNEX r| Y s| Y t| PERIODICAL u| 6/16/2003 z| 7757
949			a| TK6679.I33 v.12 no.7-12 2002 w| LCPER c| 1 i| 000052496424 l| CATO-2 m| UP-ANNEX r| Y s| Y t| PERIODICAL u| 6/16/2003 z| 7757
949			a| TK6679.I33 v.13 no.1-6 2003 w| LCPER c| 1 i| 000052816321 l| CATO-2 m| UP-ANNEX r| Y s| Y t| PERIODICAL u| 4/1/2004 z| 7757
949			a| TK6679.I33 v.13 no.7-12 2003 w| LCPER c| 1 i| 000052816314 l| CATO-2 m| UP-ANNEX r| Y s| Y t| PERIODICAL u| 4/1/2004 z| 7757
949			a| TK6679.I33 v.14 no.1-4 2004 w| LCPER c| 1 i| 000055002318 l| CATO-2 m| UP-ANNEX r| Y s| Y t| PERIODICAL u| 6/15/2005 z| 7757
949			a| TK6679.I33 v.14 no.5-8 2004 w| LCPER c| 1 i| 000055013178 l| CATO-2 m| UP-ANNEX r| Y s| Y t| PERIODICAL u| 6/15/2005 z| 7757
949			a| TK6679.I33 v.14 no.9-12 2004 w| LCPER c| 1 i| 000055002301 l| CATO-2 m| UP-ANNEX r| Y s| Y t| PERIODICAL u| 6/15/2005 z| 7757
949			a| TK6679.I33 v.15 no.1-4 2005 w| LCPER c| 1 i| 000055120340 l| CATO-2 m| UP-ANNEX r| Y s| Y t| PERIODICAL u| 6/8/2006 z| 7757
949			a| TK6679.I33 v.15 no.5-8 2005 w| LCPER c| 1 i| 000055120609 l| CATO-2 m| UP-ANNEX r| Y s| Y t| PERIODICAL u| 6/8/2006 z| 7757
949			a| TK6679.I33 v.15 no.9-12 2005 w| LCPER c| 1 i| 000055120333 l| CATO-2 m| UP-ANNEX r| Y s| Y t| PERIODICAL u| 6/8/2006 z| 7757
949			a| TK6679.I33 v.16 no.1-6 2006 w| LC c| 1 i| 000061732261 l| CATO-2 m| UP-ANNEX r| Y s| Y t| PERIODICAL u| 9/18/2007 z| 7757
949			a| TK6679.I33 v.16 no.7-12 2006 w| LC c| 1 i| 000061732278 l| CATO-2 m| UP-ANNEX r| Y s| Y t| PERIODICAL u| 9/18/2007 z| 7757
852	0	1	a| PSt b| UP-ANNEX c| ANNEX h| TK6679 i| .I33
866		0	8| 0 a| v.1(1991)-v.16(2006)
852	8		a| PSt b| HARRISBURG c| MICROS-HB h| Microfiche
866		0	8| 0 a| v.1(1991)-v.9(1999)

PennState

Copyright @2019 The Pennsylvania State University. All rights reserved. Except where otherwise noted, this work is subject to a Creative Commons Attribution 4.0 license. Details and exceptions.

Legal Statements | PSU Hotlines

PENN STATE UNIVERSITY LIBRARIES

Libraries Home (814) 865-6368
Libraries Intranet (Staff Only)
Accessibility Help
Website Feedback
Policies and Guidelines
Staff Directory

screenshot-catalog.libraries.psu.edu-2023.12.18-12_34_43
https://catalog.libraries.psu.edu/catalog/1397806
18.12.2023

IEEE transactions on circuits and systems for video technology

Additional Titles:	Circuits and systems for video technology
Published:	New York, NY : Institute of Electrical and Electronics Engineers, [1991-]
Copyright Date:	©1991-
Physical Description:	volumes : illustrations ; 28 cm
Additional Creators:	IEEE Circuits and Systems Society and Institute of Electrical and Electronics Engineers

Availability

Browse Nearby on Shelf I Want It

Penn State Harrisburg (1 item)

Call number	Material	Location
Harrisburg - Microforms - 2nd Floor - In-Library Use: Holdings Summary v.1(1991)-v.9(1999)		
Microfilm	Microfilm, Microfiche, etc.	Harrisburg - Microforms - 2nd Floor - In-Library Use

Library Storage (24 items)

Call number	Material	Location
Annexed Material: Holdings Summary v.1(1991)-v.16(2006)		
TK6679.I33 v.1 1991	Bound Journal	Annexed Material
TK6679.I33 v.2 1992	Bound Journal	Annexed Material
TK6679.I33 v.3 1993	Bound Journal	Annexed Material
TK6679.I33 v.4 1994	Bound Journal	Annexed Material
TK6679.I33 v.5-6 1995-1996	Bound Journal	Annexed Material
TK6679.I33 v.7 1997	Bound Journal	Annexed Material
TK6679.I33 v.8 1998	Bound Journal	Annexed Material
TK6679.I33 v.9 1999	Bound Journal	Annexed Material
TK6679.I33 v.10 no.1-4 2000	Bound Journal	Annexed Material
TK6679.I33 v.10 no.5-8 2000	Bound Journal	Annexed Material
TK6679.I33 v.11 no.1-6 2001	Bound Journal	Annexed Material

TK6679.I33 v.11 no.7-12 2001	Bound Journal	Annexed Material
TK6679.I33 v.12 no.1-6 2002	Bound Journal	Annexed Material
TK6679.I33 v.12 no.7-12 2002	Bound Journal	Annexed Material
TK6679.I33 v.13 no.1-6 2003	Bound Journal	Checked out
TK6679.I33 v.13 no.7-12 2003	Bound Journal	Checked out
TK6679.I33 v.14 no.1-4 2004	Bound Journal	Annexed Material
TK6679.I33 v.14 no.5-8 2004	Bound Journal	Annexed Material
TK6679.I33 v.14 no.9-12 2004	Bound Journal	Annexed Material
TK6679.I33 v.15 no.1-4 2005	Bound Journal	Annexed Material
TK6679.I33 v.15 no.5-8 2005	Bound Journal	Annexed Material
TK6679.I33 v.15 no.9-12 2005	Bound Journal	Annexed Material
TK6679.I33 v.16 no.1-6 2006	Bound Journal	Annexed Material
TK6679.I33 v.16 no.7-12 2006	Bound Journal	Annexed Material

Dates of Publication and/or Sequential Designation:
Vol. 1, no. 1 (Mar. 1991)-

Subject(s):
High definition television—Periodicals
Digital television—Periodicals
Image processing—Digital techniques—Periodicals
Resolution (Optics)—Periodicals

ISSN:
1051-8215

Publication Frequency:
Quarterly.

Note:
Title from cover.

Reproduction Note:
Microfiche. [New York, N.Y.? IEEE], microfiches ; 11 x 15 cm.

Issuing Body:
"A publication of the Circuits and Systems Society.

View MARC record | catkey: 1397806

PennState

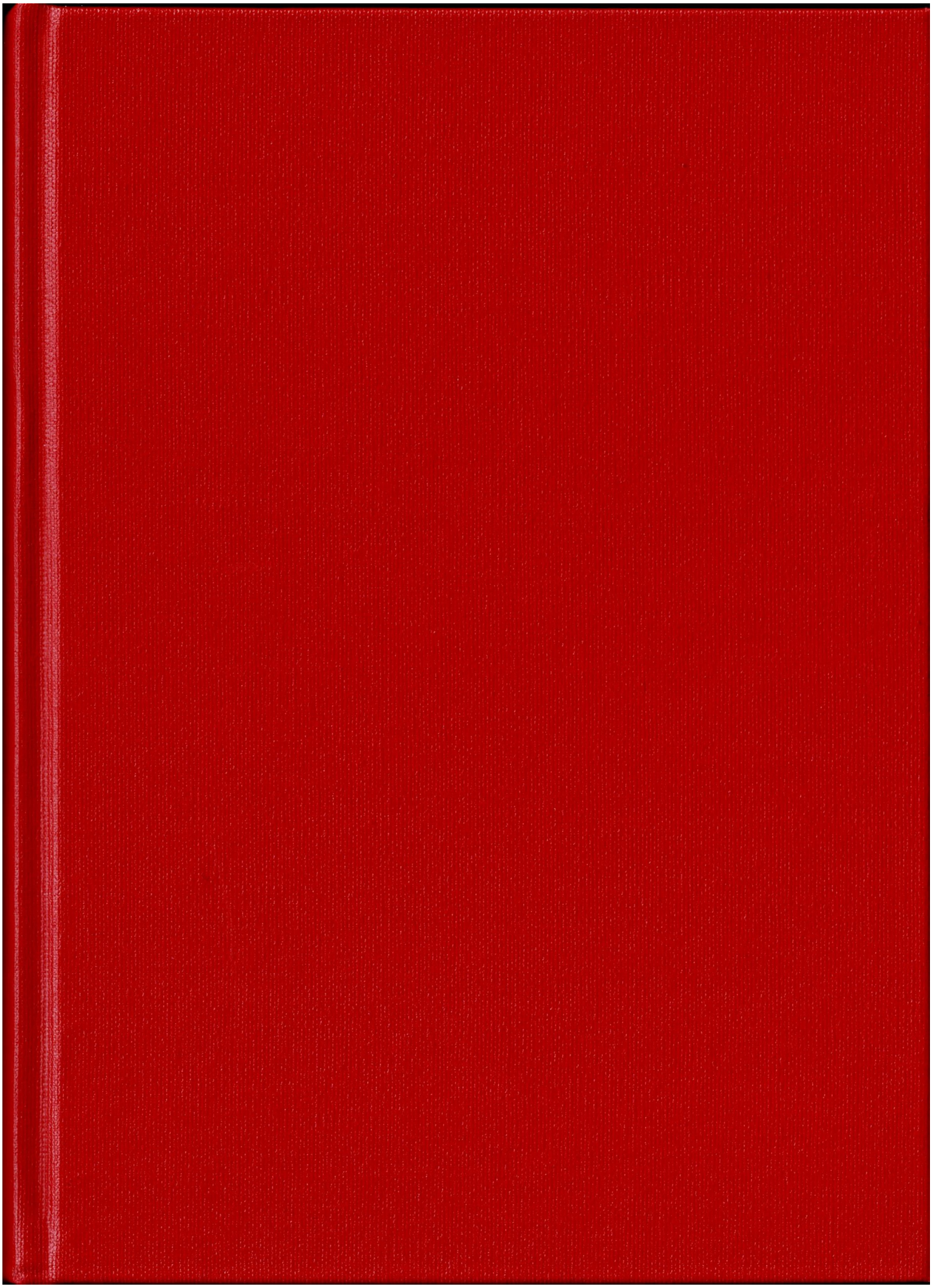
Copyright @2019 The Pennsylvania State University. All rights reserved. Except where otherwise noted, this work is subject to a Creative Commons Attribution 4.0 license. Details and exceptions.

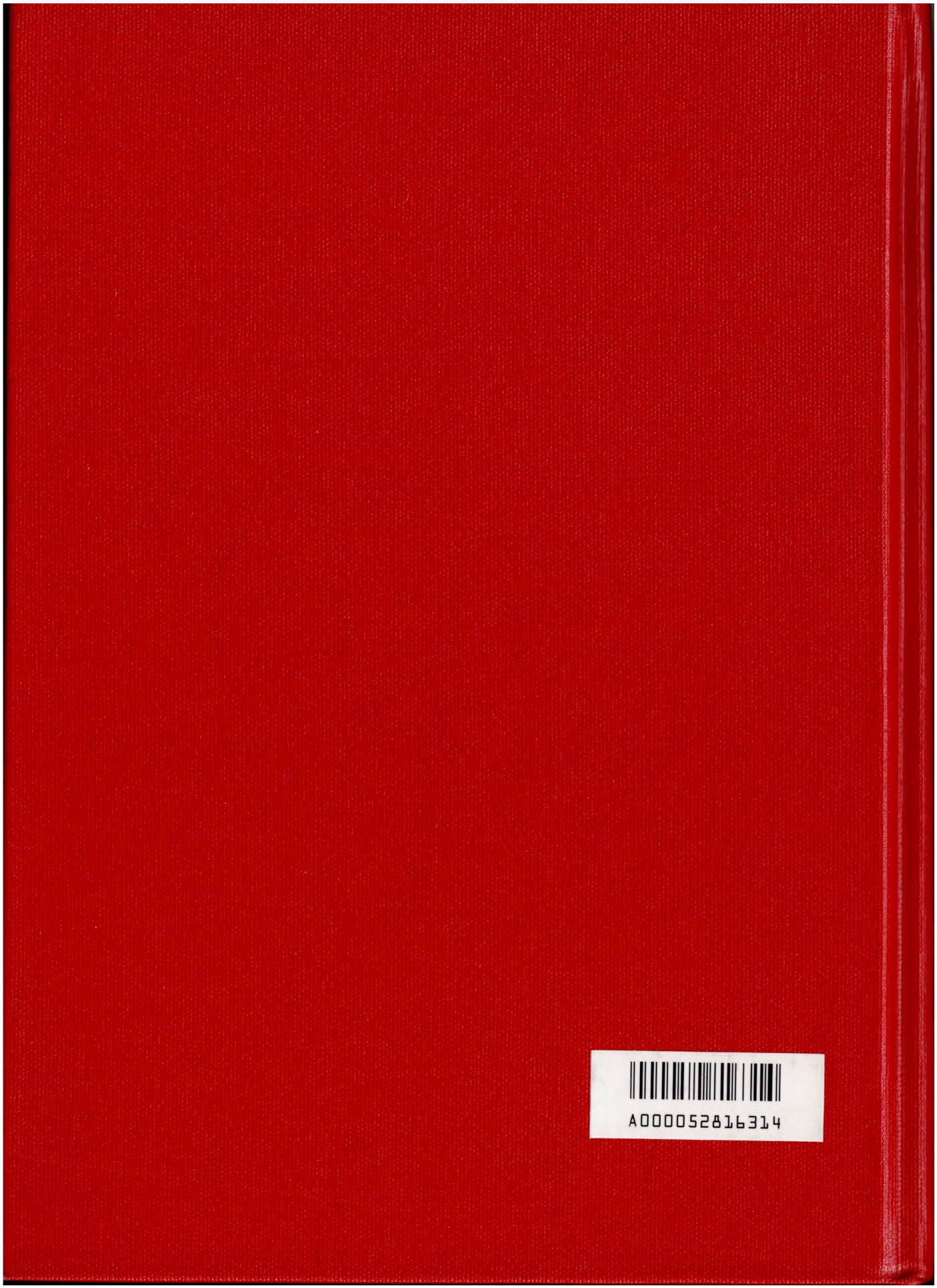
Legal Statements | PSU Hotlines

PENN STATE UNIVERSITY LIBRARIES

Libraries Home (814) 865-6368
Libraries Intranet (Staff Only)
Accessibility Help
Website Feedback
Policies and Guidelines
Staff Directory

APPENDIX STOCKHAMMER02




A000052816314

SHELVED IN
BOUND
PERIODICAL
COLLECTION

ENGINEERING LIBRARY

Engin

IEEE TRANSACTIONS ON

CIRCUITS AND SYSTEMS FOR VIDEO TECHNOLOGY

A PUBLICATION OF THE IEEE CIRCUITS AND SYSTEMS SOCIETY

WWW.IEEE-CAS.ORG



RECEIVED
AUG 6 2003
PENNSYLVANIA STATE UNIVERSITY LIBRARIES

JULY 2003 VOLUME 13 NUMBER 7 ITCTEM (ISSN 1051-8215)

SPECIAL ISSUE ON THE H.264/AVC VIDEO CODING STANDARD

GUEST EDITORIAL

Introduction to the Special Issue on the H.264/AVC Video Coding Standard . . . *A. Luthra, G. J. Sullivan, and T. Wiegand* 557

PAPERS

Overview of the H.264/AVC Video Coding Standard . . . . . *T. Wiegand, G. J. Sullivan, G. Bjøntegaard, and A. Luthra* 560
Motion- and Aliasing-Compensated Prediction for Hybrid Video Coding . . . . . *T. Wedi and H. G. Musmann* 577
Generalized B Pictures and the Draft H.264/AVC Video-Compression Standard . . . . . *M. Flierl and B. Girod* 587
Low-Complexity Transform and Quantization in H.264/AVC . . . . . *H. S. Malvar, A. Hallapuro, M. Karczewicz, and L. Kerofsky* 598
Variable Block-Size Transforms for H.264/AVC . . . . . *M. Wien* 604
Adaptive Deblocking Filter . . . . . *P. List, A. Joch, J. Lainema, G. Bjøntegaard, and M. Karczewicz* 614
Context-Based Adaptive Binary Arithmetic Coding in the H.264/AVC Video Compression Standard . . . . . *D. Marpe, H. Schwarz, and T. Wiegand* 620
The SP- and SI-Frames Design for H.264/AVC . . . . . *M. Karczewicz and R. Kurceren* 637
H.264/AVC Over IP . . . . . *S. Wenger* 645
H.264/AVC in Wireless Environments . . . . . *T. Stockhammer, M. M. Hannuksela, and T. Wiegand* 657
A Generalized Hypothetical Reference Decoder for H.264/AVC . . . *J. Ribas-Corbera, P. A. Chou, and S. L. Regunathan* 674
Rate-Constrained Coder Control and Comparison of Video Coding Standards . . . . . *T. Wiegand, H. Schwarz, A. Joch, F. Kossentini, and G. J. Sullivan* 688
H.264/AVC Baseline Profile Decoder Complexity Analysis . . . . . *M. Horowitz, A. Joch, F. Kossentini, and A. Hallapuro* 704
Complexity of Optimized H.26L Video Decoder Implementation . . . *V. Lappalainen, A. Hallapuro, and T. D. Hämäläinen* 717

COMMENTS AND CORRECTIONS

Corrections to "Genetic Algorithm Optimization of Multidimensional Grayscale Soft Morphological Filters With Applications in Film Archive Restoration . . . . . *M. S. Hamid, N. R. Harvey, and S. Marshall* 726

CALLS FOR PAPERS

ISCAS 2004 727
Special Issue on Integrated Multimedia Platforms 728

IEEE CIRCUITS AND SYSTEMS SOCIETY

The Circuits and Systems Society is an association of IEEE members with professional interest in the field of circuits and systems theory. All members of the IEEE are eligible for membership in the Society and will receive this TRANSACTIONS upon payment of the annual Society membership fee of $12.00, plus an annual subscription fee of $18.00. For information on joining, write to the IEEE at the address below. *Member copies of Transactions/Journals are for personal use only.*

IEEE TRANSACTIONS ON CIRCUITS AND SYSTEMS FOR VIDEO TECHNOLOGY

Editor-in-Chief
THOMAS SIKORA
Inst. for Telecommunications
Communication Systems Dept.
Technical Univ. Berlin
Sekr. EN-1, Einsteinufer 17
10587 Berlin, Germany
Phone: +1 49 30 314 25799
Fax: +1 49 30 314 22514
E-mail: sikora@nue.tu-berlin.de
http://www.nue.tu-berlin.de

Past Editor-in-Chief
WEIPING LI
WebCast Technologies, Inc.
1153 Bordeaux Dr., Ste. 205
Sunnyvale, CA 94089
Phone: +1 408 541 4150
Fax: +1 408 745 0249
E-mail: li@webcasttech.com

Associate Editors

ISHFAQ AHMAD
Dept. Comput. Sci. & Eng.
Univ. Texas at Arlington
248 D/E Nedderman Hall
416 Yates St., Box 19015
Arlington, TX 76019-0015
iahmad@cse.uta.edu

KIYOHARU AIZAWA
Dept. Elect. Eng.
Univ. Tokyo
7-3-1 Hongo, Bunkyo-ku
Tokyo 113 Japan
aizawa@ee.t.u-tokyo.ac.jp

OSAMA K. AL-SHAYKH
PacketVideo Technologies
10350 Science Ctr. Dr., Ste. 140
San Diego, CA 92121
osama@packetvideo.com

JOHN F. ARNOLD
Schl. Elect. Eng.
Univ. College, UNSW
Australian Defence Force Academy
Canberra ACT 2600, Australia
j.arnold@adfa.edu.au

RAJARATHNAM CHANDRAMOULI
Dept. Elect. Comput. Eng.
207 Burchard Building
Stevens Inst. Technol.
Hoboken, NJ 07030
rchandr1@stevens-tech.edu

CHANG WEN CHEN
Dept. Elect. Comput. Eng.
Florida Inst. of Technol.
Melbourne, FL 32091
cchen@fit.edu

LIANG-GEE CHEN
Dept. Elect. Eng.
National Taiwan Univ.
Taipei, Taiwan 10764 R.O.C.
lgchen@cc.ee.ntu.edu.tw

SHERMAN CHEN
Broadband Systems Engineering
Broadcom Corp.
16215 Alton Parkway
P.O. Box 57013
Irvine, CA 92619-7013
schen@broadcom.com

LEONARDO CHIARIGLIONE
Multimedia & Video Services
CSELT
Via G. Reiss Romoli, 274
Torino I-10148 Italy
leonardo.chiariglione@cselt.it

HAMID GHARAVI
NIST
U.S. Dept. Commerce
100 Bureau Dr., Stop 8920
Gaithersburg, MD 20899-8920
gharavi@antd.nist.gov

JENQ-NENG HWANG
Dept. Elect. Eng.
Univ. Washington
Seattle, WA 98195
hwang@ee.washington.edu

EBROUL IZQUIERDO
Elect. Eng. Dept.
Queen Mary, Univ. of London
London E1 4NS, UK
ebroul.izquierdo@elec.qmul.ac.uk

ROB KOENEN
InterTrust Technologies Corp.
4750 Pattrick Henry Dr.
Santa Clara, CA 95054
rob.koenen@ieee.org

ALEX KOT
Schl. Elect. Electron. Eng.
Nanyang Technol. Univ.
S1, Nanyang Ave.
Singapore 639798
eackot@ntu.edu.sg

S. Y. KUNG
Dept. Elect. Eng.
Princeton Univ.
Princeton, NJ 08544
kung@princeton.edu

MURAT KUNT
Dept. Elect. Eng.
Swiss Federal Inst. Technol.
Lausanne CH-1015 Switzerland
kunt@epfl.ch

ROSA LANCINI
CEFRIEL
Via Fucini, 2
Milano 20133 Italy
rosa@cefriel.it

SANG UK LEE
School Elect. Eng.
Seoul National Univ.
Kwanak, P.O. Box 34
Seoul 151-742 Korea
sanguk@sting.snu.ac.kr

JENS-RAINER OHM
Inst. Commun. Eng.
Aachen Univ. Technol.
Melatener Str. 23
Aachen D-52072, Germany
ohm@ient.rwth-aachen.de

LEVENT ONURAL
Elect. & Electron. Eng. Dept.
Bilkent Univ.
TR-06533 Ankara, Turkey
l.onural@ieee.org

SETHURAMAN PANCHANATHAN
Dept. Comput. Sci. Eng.
Arizona State Univ.
Tempe, AZ 85287-5406
panch@asu.edu

FERNANDO PEREIRA
Dept. Elect. Comput. Eng.
Instituto Superior Tecnico
Av. Rovisco Pais
Lisboa Codex 1096 Portugal
fp@lx.it.pt

ERIC PETAJAN
face2face animation, inc.
2 Kent Place Blvd.
Summit, NJ 07901
eric@f2f-inc.com

ATUL PURI
Apple Computer
2 Infinite Loops
MS 302-3KS
Cupertino, CA 95014
apuri@apple.com
apuri@ieee.org

HARRY SHUM
Microsoft Research Asia
3/F Beijing Sigma Center
Beijing 100080, China
hshum@microsoft.com

ROBERT L. STEVENSON
Dept. Elect. Eng.
Univ. Notre Dame
Notre Dame, IN 46556
Stevenson.1@nd.edu

MICHAEL G. STRINTZIS
Elect. Comput. Eng. Dept.
Univ. Thessaloniki
Thessaloniki 540 06 Greece
strintzi@eng.auth.gr

HUIFANG SUN
Mitsubishi Electric Research Labs
558 Central Ave.
New Providence, NJ 07974
hsun@merl.com

ALI TABATABAI
Sony Electronics
3300 Zanker Rd., MD SJ2C4
San Jose CA 95134
ali.tabatabai@am.sony.com

QI TIAN
Kent Ridge Digital Labs
21 Heng Mui Keng Terrace
Singapore 119613
tian@lit.org.sg

KOU-HU TZOU
Divio, Inc.
441 DeGuigne Drive
Sunnyvale, CA 94085
ktzou@divio.com

HIROSHI WATANABE
Visual Commun. Lab. 922A
NTT Human Interface Labs.
1-1 Hikarinooka
Yokosuka 239 Japan
hiroshi@giti.waseda.ac.jp

ZIXIANG XIONG
Dept. Elect. Eng.
Texas A&M Univ.
College Station, TX 77843
zx@lena.tamu.edu

THE INSTITUTE OF ELECTRICAL AND ELECTRONICS ENGINEERS, INC.

Officers

MICHAEL S. ADLER, *President*
ARTHUR W. WINSTON, *President-Elect*
LEVENT ONURAL, *Secretary*
PEDRO A. RAY, *Treasurer*
RAYMOND D. FINDLAY, *Past President*
JAMES M. TIEN, *Vice President, Educational Activities*
MICHAEL R. LIGHTNER, *Vice President, Publication Services and Products*
W. CLEON ANDERSON, *Vice President, Regional Activities*
GERALD H. PETERSON, *President, IEEE Standards Association*
LEAH H. JAMIESON, *Vice President, Technical Activities*
JAMES V. LEONARD, *President, IEEE-USA*
CARY Y. YANG, *Director, Division I—Circuits and Devices*

Executive Staff

DANIEL J. SENESE, *Executive Director*
DONALD CURTIS, *Human Resources*
ANTHONY DURNIAK, *Publications Activities*
JUDITH GORMAN, *Standards Activities*
CECELIA JANKOWSKI, *Regional Activities*
BARBARA COBURN STOLER, *Educational Activities*
MATTHEW LOEB, *Corporate Strategy & Communications*
RICHARD D. SCHWARTZ, *Business Administration*
W. THOMAS SUTTLE, *IEEE-USA*
MARY WARD-CALLAN, *Technical Activities*
JOHN WITSKEN, *Information Technology*

IEEE Periodicals

Transactions/Journals Department

Staff Director: FRAN ZAPPULLA
Editorial Director: DAWN MELLEY *Production Director*: ROBERT SMREK
Managing Editor: MONA MITTRA *Senior Editor*: JILL A. SINAY

IEEE TRANSACTIONS ON CIRCUITS AND SYSTEMS FOR VIDEO TECHNOLOGY (ISSN 1051-8215) is published monthly by the Institute of Electrical and Electronics Engineers, Inc. Responsibility for the contents rests upon the authors and not upon the IEEE, the Society/Council, or its members. **IEEE Corporate Office:** 3 Park Avenue, 17th Floor, New York, NY 10016-5997. **IEEE Operations Center:** 445 Hoes Lane, P.O. Box 1331, Piscataway, NJ 08855-1331. **NJ Telephone:** +1 732 981 0060. **Price/Publication Information:** Individual copies: IEEE Members $10.00 (first copy only), nonmembers $20.00 per copy. (Note: Add $4.00 postage and handling charge to any order from $1.00 to $50.00, including prepaid orders.) Member and nonmember subscription prices available upon request. Available in microfiche and microfilm.

Copyright and Reprint Permissions: Abstracting is permitted with credit to the source. Libraries are permitted to photocopy for private use of patrons, provided the per-copy fee indicated in the code at the bottom of the first page is paid through the Copyright Clearance Center, 222 Rosewood Drive, Danvers, MA 01923. For all other copying, reprint, or republication permission, write to Copyrights and Permissions Department, IEEE Publications Administration, 445 Hoes Lane, P.O. Box 1331, Piscataway, NJ 08855-1331. Copyright © 2003 by The Institute of Electrical and Electronics Engineers, Inc. All rights reserved.

Periodicals Postage Paid at New York, NY and at additional mailing offices. **Postmaster:** Send address changes to IEEE TRANSACTIONS ON CIRCUITS AND SYSTEMS FOR VIDEO TECHNOLOGY, IEEE, 445 Hoes Lane, P.O. Box 1331, Piscataway, NJ 08855-1331. GST Registration No. 125634188. Printed in U.S.A.